

**A Further Step toward H<sub>2</sub> in Automobile:  
Development of an Efficient Bi-functional  
Catalyst for Single Stage Water Gas Shift**

**Khalid Ghazi Azzam**

**A Further Step toward H<sub>2</sub> in Automobile:  
Development of an Efficient Bi-Functional  
Catalyst for Single Stage Water Gas Shift**

**by**

**Khalid Ghazi Azzam**



To my parents, brothers, and sisters  
To my beloved wife (Ola)

## Promotion committee

|                                     |                     |
|-------------------------------------|---------------------|
| Prof. dr. P.J. Gellings, Chairman   | Universiteit Twente |
| Prof. dr. ir. L. Lefferts, Promotor | Universiteit Twente |
| Dr. K. Seshan, assistent-promotor   | Universiteit Twente |
| Prof.dr. F. Kapteijn                | TU Delft            |
| Prof.dr.ir. J.A.M. Kuipers          | Universiteit Twente |
| Prof.dr.ing. D.H.A Blank            | Universiteit Twente |
| Dr. P. Berben                       | BASF                |
| Dr.ir. J.E. ten Elshof              | Universiteit Twente |

The research described in this thesis was carried out in the Catalytic Processes and Materials (CPM) group at the University of Twente and has been financially supported by STW (Dutch Technology Foundation), Project number 790.36.030.

**ISBN: 978-90-365-2644-9**

No part of this work may be reproduced by print, photocopy or any other means without the permission in writing from the author.

© *Khalid Ghazi Azzam, Enschede, The Netherlands, 2008.*

[azzamkhalid@gmail.com](mailto:azzamkhalid@gmail.com)

Printed by Wm Veenstra

Postbus 40199, 8004 DD Zwolle, The Netherlands

**A FURTHER STEP TOWARD H<sub>2</sub> IN  
AUTOMOBILE: DEVELOPMENT OF AN  
EFFICIENT BI-FUNCTIONAL CATALYST  
FOR SINGLE STAGE WATER GAS SHIFT**

**PROEFSCHRIFT**

*ter verkrijging van*  
de graad van doctor aan de Universiteit Twente,  
op gezag van de rector magnificus,  
*prof.dr. W.H.M. Zijm,*  
volgens besluit van het College voor Promoties  
in het openbaar te verdedigen  
op vrijdag 09 Mei 2008 om 15.00 uur

door

**Khalid Ghazi Azzam**  
geboren op 02 Juni 1976  
te Makhraba (Jordan)

This dissertation has been approved by the promoter

**Prof.dr.ir. L. Lefferts**

And the assistant promoter

**Dr. K. Seshan**

## Table of Contents

|  | <b>Page</b> |
|--|-------------|
| <b>Summary</b>   | 1           |
| <b>Samenvatting</b>  | 5           |
| <br>   |             |
| <b>Chapter 1</b>   |             |
| <b>General introduction</b>  | 9           |
| 1.1 Introduction   | 9           |
| 1.2 Fuel cells   | 10          |
| 1.3 Routes of H <sub>2</sub> production                                | 11          |
| 1.3.1 Steam reforming  | 11          |
| 1.3.2 Catalytic partial oxidation                                      | 12          |
| 1.3.3 CO <sub>2</sub> reforming  | 13          |
| 1.3.4 Auto-thermal reforming   | 13          |
| 1.4 Water Gas Shift Reaction: background and state of art              | 13          |
| 1.5 Thesis outlines  | 17          |
| 1.6 References   | 19          |
| <br>   |             |
| <b>Chapter 2</b>   |             |
| <b>Role of the support on WGS reaction sequences</b>                   | 22          |
| Abstract   | 22          |
| 2.1 Introduction   | 23          |
| 2.2 Experimental   | 26          |
| 2.2.1 Catalyst preparation   | 26          |
| 2.2.2 Characterization   | 26          |
| 2.2.3 Pulse experiments  | 27          |
| 2.2.4 FTIR studies   | 28          |
| 2.3 Results  | 28          |
| 2.3.1 Pt/CeO <sub>2</sub>  | 28          |
| 2.3.2 Pt/TiO <sub>2</sub>  | 32          |
| 2.3.3 Pt/ZrO <sub>2</sub>  | 34          |
| 2.4 Discussion   | 35          |
| 2.5 Conclusions  | 43          |
| 2.6 References   | 44          |
| <br>   |             |
| <b>Chapter 3</b>   |             |
| <b>Role of support and promoter on catalyst activity and stability</b> | 47          |
| Abstract   | 47          |
| 3.1 Introduction   | 48          |
| 3.2 Experimental   | 50          |
| 3.2.1 Catalyst preparation   | 50          |
| 3.2.2 Characterization   | 51          |
| 3.2.3 Catalytic tests  | 52          |
| 3.2.4 Pulse experiments  | 52          |

|   |   |     |
|---|---|-----|
| 3.3   | Results and Discussion                          | 53  |
| 3.3.1   | Catalytic performance                           | 53  |
| 3.3.2   | Catalysts deactivation                          | 55  |
| 3.3.3   | Development of a stable and efficient catalyst  | 60  |
| 3.4   | Conclusions                                     | 64  |
| 3.5   | References                                      | 66  |
| <br>  |   |     |
| <b>Chapter 4</b>  |   |     |
| <b>Deactivation mechanism of Pt/TiO<sub>2</sub> catalyst in Water Gas Shift reaction</b>                          |   | 69  |
|   | Abstract  | 69  |
| 4.1   | Introduction                                    | 70  |
| 4.2   | Experimental                                    | 71  |
| 4.2.1   | Catalyst preparation                            | 71  |
| 4.2.2   | Characterization                                | 72  |
| 4.2.3   | Catalytic tests                                 | 72  |
| 4.3   | Results and Discussion                          | 73  |
| 4.4   | Conclusions                                     | 83  |
| 4.5   | References                                      | 84  |
| <br>  |   |     |
| <b>Chapter 5</b>  |   |     |
| <b>Optimization and characterization of Pt-Re/TiO<sub>2</sub> for Water Gas Shift</b>                             |   | 86  |
|   | Abstract  | 86  |
| 5.1   | Introduction                                    | 87  |
| 5.2   | Experimental                                    | 88  |
| 5.2.1   | Catalyst preparation                            | 88  |
| 5.2.1.1   | Effect of preparation strategy                  | 88  |
| 5.2.1.2   | Effect of Pt/Re molar ratios                    | 89  |
| 5.2.1.3   | Effect of Pt and Re loadings                    | 90  |
| 5.2.2   | Catalysts characterization                      | 90  |
| 5.2.3   | Catalytic tests                                 | 91  |
| 5.3   | Results and Discussion                          | 92  |
| 5.3.1   | Catalyst optimization                           | 92  |
| 5.3.1.1   | Effect of preparation strategy                  | 92  |
| 5.3.1.2   | Effect of Pt/Re molar ratios                    | 95  |
| 5.3.1.3   | Effect of Pt and Re loading                     | 96  |
| 5.3.2   | Catalyst Characterization                       | 99  |
| 5.3.2.1   | H <sub>2</sub> Temperature programmed reduction | 99  |
| 5.3.2.2   | CO-temperature programmed desorption            | 102 |
| 5.3.2.3   | IR spectra of CO adsorption                     | 102 |
| 5.3.2.4   | IR spectra of in situ WGS reaction              | 104 |
| 5.4   | Conclusions                                     | 108 |
| 5.5   | References                                      | 109 |
| <br>  |   |     |
| <b>Chapter 6</b>  |   |     |
| <b>Role of Re in Pt-Re/TiO<sub>2</sub> catalyst for Water Gas Shift reaction: A mechanistic and kinetic study</b> |   | 111 |

|   |  |     |
|---|--|-----|
|   | Abstract   | 111 |
| 6.1   | Introduction   | 112 |
| 6.2   | Experimental   | 114 |
| 6.2.1   | Catalyst preparation   | 114 |
| 6.2.2   | Characterization   | 114 |
| 6.2.3   | Pulse experiments  | 115 |
| 6.2.4   | Catalytic tests  | 115 |
| 6.3   | Results  | 116 |
| 6.3.1   | Catalysts characterization and WGS reaction performance                  | 116 |
| 6.3.2   | Transient pulse experiments over Pt-Re/TiO <sub>2</sub> catalytic system | 117 |
| 6.3.3   | Transient pulse experiments over Pt/C and Pt-Re/C catalytic system       | 121 |
| 6.3.4   | Kinetic studies for Pt-Re/TiO <sub>2</sub> catalytic system              | 123 |
| 6.4   | Discussion   | 125 |
| 6.5   | Conclusions  | 133 |
| 6.6   | References   | 134 |
|   | Appendix A   | 137 |
|   | Appendix B   | 138 |
| <b>Chapter 7</b>                                    |  |     |
| <b>Outlooks and recommendations for future work</b> |  | 142 |
| 7.1   | Water Gas Shift reaction mechanism                                       | 142 |
| 7.2   | Development of an efficient catalyst for WGS                             | 144 |
| 7.3   | Optimization of Pt-Re/TiO <sub>2</sub> catalyst                          | 145 |
| 7.4   | References   | 146 |
|   | Acknowledgment   | 147 |
|   | Publications   | 149 |

## Summary

The suitability of polymer electrolyte fuel (PEM) cells for stationary and vehicular applications initiated research in all areas of fuel processor (*i.e.* reformer, water-gas-shift, preferential oxidation of CO (PROX)) catalysts for hydrogen generation. Water gas shift (WGS) reaction is an essential part of these processors because of its role in CO purification, which poisons the Pt electrodes of PEM, and its role in generating additional hydrogen. The WGS reaction is well established in conventional large steady-state operations, such as ammonia plants, but it has found new purpose and challenges to fit the requirements for energy power generation through fuel cell. More active catalysts are necessary as large volumes of shift reactors are usually required which would be responsible for about 50% of the volume of the whole fuel processor. Therefore, replacing the conventionally two stages WGS, *i.e.* the high temperature shift and the low temperature shift, with a single stage WGS shift seems to be promising for reducing the total volume of fuel processor. In this dissertation, a development of active, selective, and stable single stage water-gas-shift (WGS) catalyst for H<sub>2</sub> production for fuel cell applications has been investigated. Such efficient catalysts could be used in a H<sub>2</sub> selective catalytic membrane reactor in order to overcome thermodynamic limitations when temperature is chosen relatively high for improving reaction rate.

In chapter 2, the objective of the study was to understand the influence of the catalyst-oxide support on the WGS sequences. We have used *in situ* FTIR spectroscopy and transient kinetic studies to follow the elementary reactions that occur at 300°C over different catalysts (Pt/CeO<sub>2</sub>, Pt/TiO<sub>2</sub>, and Pt/ZrO<sub>2</sub>) that have comparable Pt particle size and different red-ox properties of the oxide supports. In all cases, platinum adsorbs/activates CO and the oxide supports activate H<sub>2</sub>O (bi-functional catalysts). In addition to the two WGS routes discussed in literature, *i.e.*, red-ox and associative formate routes, we propose an extra route, called an associative formate with red-ox regeneration of the oxide support, that may be involved in the complex WGS reaction scheme. We have found that WGS reaction follows the associative formate on Pt/CeO<sub>2</sub>.

In the case of Pt/ZrO<sub>2</sub>, the WGS reaction follows the associative formate with red-ox regeneration. And differently, both the red-ox and the associative formate with red-ox regeneration contribute in WGS over Pt/TiO<sub>2</sub> catalyst. The presented results indicate that the oxide support has crucial effect on WGS pathways and seems to be the key factor of catalyst performance.

The influence of oxide supports and promoters on catalyst activity, selectivity, and stability was discussed in chapter 3. Various oxide supports (including mixed oxides) that differ in term of reducibility or oxygen mobility supporting platinum have been examined as Pt-based supports. We have found that the nature of oxide supports has a crucial effect on the performance of Pt based catalyst in WGS reaction. Supports not only determine the activity of the catalyst, but also influence their stability (deactivation mechanism). Among the catalysts studied, Pt/TiO<sub>2</sub> was the most active catalyst. Using mixed-oxides as catalyst supports did not improve the activity despite the better red-ox properties of mixed-oxides compared with the single-oxide supports. Pt/ZrO<sub>2</sub> was stable during WGS reaction but has low activity. Pt/CeO<sub>2</sub> deactivated with time due to formation of stable carbonate on ceria surface. For Pt/TiO<sub>2</sub> catalyst, sintering of Pt was found to be the cause of deactivation (details are described in chapter 4). The catalyst could be stabilized by adding a second metal (Re), which prevents Pt sintering. In addition, Pt-Re/TiO<sub>2</sub> catalyst was more active than Pt/TiO<sub>2</sub>. This developed catalyst (Pt-Re/TiO<sub>2</sub>) is promising for single stage WGS reaction.

In chapter 4, we used kinetic (steady state and transient) and in situ FTIR spectroscopic methods to study the fresh, used, and reactivated Pt/TiO<sub>2</sub> to understand the deactivation mechanism during WGS reaction. We have studied all possible causes of deactivation including carbon deposition, Pt sintering, strong metal support interaction (SMSI), loss of TiO<sub>2</sub> surface area, and stable reaction intermediates (*e.g.* carbonate or formate). The loss of Pt surface area was the cause of Pt/TiO<sub>2</sub> deactivation, exclusively. This Pt sintering occurred mainly due to the presence of traces of formaldehyde formed under WGS reaction conditions by reaction of H<sub>2</sub> and CO.

Chapter 5 consists of two parts. In the first part, an optimization study was carried out to check the influence of preparation strategies, Pt/Re molar ratios, and metals content on the catalytic performance of Pt-Re/TiO<sub>2</sub> catalyst (activity and stability) in WGS. Results indicated that sequential impregnation of Re precursor prior to Pt precursor without intermediate pretreatment is the optimum preparation strategy. The Pt/Re ratio of unity with 0.5wt% Pt content showed excellent activity and stability, at moderate temperature (300°C), in WGS reaction. In the second part, different characterization techniques, including CO chemisorption, H<sub>2</sub>-TPR, CO-TPD, and *in situ* FTIR CO adsorption at 300°C, are used in order to examine the Pt and Re interactions and/or alloy formation, if there is. We compared the bimetallic Pt-Re catalysts with its monometallic one (Pt/TiO<sub>2</sub>). The characterization results gave no evidence of strong interaction between Pt and Re (no alloy formation). On the other hand, during WGS reaction at 300°C, stronger interaction was observed by the *in situ* FTIR results. This stronger interaction that happened during WGS shift might be to possible interaction or alloy formation on the peripheries of Pt and ReO<sub>x</sub> particles that occurs during the red-ox cycles of ReO<sub>x</sub>. This interaction also explains the high degree of stability of this catalyst.

In chapter 6, we have proven the role of red-ox cycles of ReO<sub>x</sub> in enhancing the catalytic activity of Pt-Re/TiO<sub>2</sub> catalyst by studying the kinetics and reaction mechanism of WGS. We used transient kinetic studies and *in situ* FTIR spectroscopy to follow the reaction sequences that occur during WGS reaction over this catalyst. Results pointed to contributions of an associative formate route with red-ox regeneration and two classical red-ox routes involving TiO<sub>2</sub> and ReO<sub>x</sub>, respectively. Under WGS reaction condition, rhenium is present at least partly as ReO<sub>x</sub> providing an additional red-ox route for WGS reaction in which ReO<sub>x</sub> is reduced by CO generating CO<sub>2</sub> and re-oxidized by H<sub>2</sub>O forming H<sub>2</sub>.

The overall reaction rate, based on steady state kinetics at 300°C, was given by

$$r_{H_2} = 0.075 \cdot e^{\frac{31kJ.mol^{-1}}{RT}} \cdot p_{H_2O} \cdot p_{H_2}^{-0.5} (1 - \beta)$$
, where  $\beta$  is the approach to equilibrium. Results obtained in the study indicated that the reaction between CO adsorbed on Pt and OH groups on titania is the rate determining step. Hydrogen inhibits the WGS rate by

suppressing the formation of OH groups. Therefore, removing H<sub>2</sub> from the reaction mixture by using a hydrogen-selective-membrane reactor is promising strategy for practical applications.

## Samenvatting

De toepasbaarheid van polymere elektrolyte brandstofcellen (PEM) in stationaire en transporttoepassingen heeft geleid tot onderzoeksinitiatieven in allerlei aspecten van de brandstofcelkatalysator-processors voor waterstofproductie (bijvoorbeeld reformer, water gas shift of selectieve oxidatie van CO (PROX)). De water gas shift (WGS) reactie is een belangrijk onderdeel van deze processors. Door koolmonoxidezuivering, wordt vergiftiging van de platina electrodes van de PEM vermeden. Daarnaast wordt door de WGS additioneel waterstof gegenereerd. De WGS reactie wordt al veel toegepast in conventionele productie op grote schaal, bijvoorbeeld in ammoniakfabrieken. In de energieproductie via brandstofcellen heeft het een nieuwe toepassing met bijbehorende uitdagingen gevonden. In een huidige brandstofprocessor bestaat ca 50% van het totaalvolume uit katalysator. Voor de reductie van het brandstofprocessorvolume is het vervangen van de conventionele tweestaps WGS (namelijk de *High temperature shift* en de *Low temperature shift*) door een enkelstaps WGS een veelbelovende optie. Hiervoor is de ontwikkeling van actievere katalysatoren nodig. In dit promotieonderzoek is de ontwikkeling van een actieve, selectieve en stabiele enkelstaps WGS katalysator voor de productie van waterstof onderzocht. Deze efficiënte katalysator kan gebruikt worden in een H<sub>2</sub>-selectieve katalytische membraanreactor, om de thermodynamische begrenzings van relatief hogere temperaturen te vermijden en om de reactiesnelheid te verhogen.

Het doel van het onderzoek in hoofdstuk 2 was het begrijpen van de invloed van oxidische dragermaterialen van de katalysator op de WGS reactiestappen. Hiervoor werd gebruik gemaakt van *in situ* FTIR spectroscopie en transient kinetische onderzoeken om de elementaire reacties te volgen die optreden bij 300°C. Voor dit onderzoek werden verschillende katalysatoren (Pt/CeO<sub>2</sub>, Pt/TiO<sub>2</sub> en Pt/ZrO<sub>2</sub>) met vergelijkbare Pt deeltjesgrootte en verschillende redoxeigenschappen van de oxidedrager gebruikt. In alle gevallen adsorbeert/activeert platina CO en activeert de oxidedrager H<sub>2</sub>O (bifunctionele katalysator). Naast de twee WGS routes beschreven in de literatuur, te weten de redox route en de associatieve formaat route, stellen wij een extra route voor, genaamd een associatieve formaat route met redox regeneratie van de oxidedrager, welke betrokken

kan zijn in het complexe WGS reactieschema. Op Pt/CeO<sub>2</sub> volgt WGS reactie de associatieve formaat route volgt op. In geval van Pt/ZrO<sub>2</sub> volgt de WGS reactie de associatieve formaat route met redox regeneratie. Bij WGS op een Pt/TiO<sub>2</sub> katalysator zijn zowel de redox route als de associatieve formaat route met redox regeneratie relevant. De hier gepresenteerde resultaten geven aan dat de oxidedrager een cruciale rol speelt in het WGS mechanisme en bepalend is voor de prestaties van de katalysator.

In hoofdstuk 3 wordt de invloed van oxidedragers en promotors op katalysatoractiviteit, selectiviteit en stabiliteit besproken. In reduceerbaarheid of zuurstofmobilititeit verschillende oxidedragers (inclusief gemengde oxides), zijn onderzocht als dragermateriaal voor Pt..De aard van de oxidedrager heeft een cruciaal effect heeft op de prestatie van de Pt gebaseerde katalysator in de WGS reactie. Dragere bepalen niet alleen de activiteit van de katalysator, maar beïnvloeden ook hun stabiliteit (deactiveringsmechanisme). Pt/TiO<sub>2</sub> was meest actieve van de onderzochte katalysatoren. Het gebruik van gemengde oxides als katalysatordrager verbeterde de activiteit niet, ondanks de verbeterde redoxeigenschappen van gemengde oxides van deze materialen. Pt/ZrO<sub>2</sub> is stabiel gedurende de WGS reactie, maar heeft een lage activiteit. Pt/CeO<sub>2</sub> deactiveerde in de loop van de tijd door vorming van stabiel carbonaat op het ceriumoppervlak. Voor Pt/TiO<sub>2</sub> was sintering van Pt de oorzaak van de deactivering (zie hoofdstuk 4 voor details). De katalysator kan gestabiliseerd worden door het toevoegen van een tweede metaal (Re) dat Pt sintering voorkomt. Bovendien was de Pt-Re/TiO<sub>2</sub> katalysator actiever dan Pt/TiO<sub>2</sub>. De Pt-Re/TiO<sub>2</sub> katalysator is veelbelovend voor de éénstaps WGS reactie.

In hoofdstuk 4 zijn verse, gebruikte en gereactiveerde Pt/TiO<sub>2</sub> in kinetische experimenten (steady state en transient) en *in situ* FTIR spectroscopie bestudeerd, met als doel het begrijpen van het deactiveringsmechanisme tijdens de WGS reactie. Mogelijke oorzaken van deactivering zijn onderzocht, waaronder: afzetting van koolstof, sinteren van platina, sterke metaal interactie met de drager (SMSI), verlies van actief TiO<sub>2</sub> oppervlak en de vorming van stabiele tussenproducten (b.v. carbonaat of formaat). Het verlies van actief Pt oppervlak (door sinteren), vormt de enige oorzaak van Pt/TiO<sub>2</sub> deactivering. Het

sinteren van Pt wordt voornamelijk veroorzaakt door vorming van sporen formaldehyde bij WGS reactiecondities.

In het eerste gedeelte van hoofdstuk 5 worden de molaire verhouding tussen Pt/Re, het metaal gehalte en de bereidingstechniek van de Pt-Re/TiO<sub>2</sub> katalysator geoptimaliseerd. Hierbij werd een maximale activiteit en stabiliteit nagestreefd.. Uit de resultaten blijkt dat het achtereenvolgens impregneren van de Re precursor en de Pt precursor, zonder tussenbehandeling, de optimale bereidingswijze is. Een Pt/Re verhouding van 1:1 bij een belading van 0.5% van beide metalen levert een uitstekende activiteit en stabiliteit tijdens de WGS reactie bij een temperatuur van 300°C. In het tweede gedeelte van hoofdstuk 5 worden diverse karakteriseringstechnieken (CO chemisorptie, H<sub>2</sub>-TPR, CO-TPD, and *in situ* FTIR CO adsorptie bij 300°C) gebruikt om de interacties tussen Pt en Re, evenals de eventuele vorming van een legering te bepalen. De bimetallische Pt-Re katalysator is vergeleken met de monometallische variant (Pt/TiO<sub>2</sub>). Uit de resultaten van de karakterisering blijkt dat er geen legering tussen Pt en Re gevormd wordt. Uit de *in situ* FTIR resultaten blijkt echter wel dat er een duidelijke interactie tijdens de WGS reactie bij 300°C waar te nemen is. Dit is mogelijk te verklaren door interactie of het vormen van een legering aan de buitenkant van Pt en ReO<sub>x</sub> deeltjes tijdens de redox cycli van ReO<sub>x</sub>. Deze interactie kan een verklaring zijn voor de hoge stabiliteit van deze katalysator.

In hoofdstuk 6 wordt, middels bestudering van de kinetiek en het reactiemechanisme van de WGS, de rol van de ReO<sub>x</sub> redox cycli in het verbeteren van de Pt-Re/TiO<sub>2</sub> katalysator activiteit aangetoond. De volgorde van reacties op deze katalysator tijdens de WGS reactie wordt gevolgd met behulp van transient kinetische onderzoeken en *in situ* FTIR spectroscopie. Uit de resultaten blijken bijdragen van een associatieve formaat route met red-ox regeneratie en twee klassieke red-ox routes met respectievelijk TiO<sub>2</sub> en ReO<sub>x</sub>. Bij WGS reactiecondities is Re, voor een gedeelte in de vorm van ReO<sub>x</sub> aanwezig. Dit vormt een alternatieve red-ox route waarbij ReO<sub>x</sub> door CO gereduceerd wordt onder vorming van CO<sub>2</sub> en reoxidatie plaats vindt door H<sub>2</sub>O onder vorming van H<sub>2</sub>.

De totale reactiesnelheid, gebaseerd op steady state kinitiek bij 300°C, wordt beschreven

door:  $r_{H_2} = 0.075 \cdot e^{\frac{31kJ \cdot mol^{-1}}{RT}} \cdot p_{H_2O} \cdot p_{H_2}^{-0.5} (1 - \beta)$ , waarin  $\beta$  aangeeft in welke mate evenwicht

wordt benaderd. Uit de resultaten blijkt dat de reactie van CO geadsorbeerd op Pt, met OH groepen op Ti de snelheidsbepalende stap is. Waterstof belemmert de WGS snelheid door het tegenhouden van de vorming van OH groepen. Hieruit blijkt dat het verwijderen van H<sub>2</sub> uit het reactiemengsel, door gebruik te maken van een waterstofselectieve membraanreactor, een veelbelovende strategie voor praktische toepassingen is.

# Chapter 1

## General Introduction

---

### 1.1 Introduction

Hydrogen is one of the most important industrial chemicals because of its multi-industrial applications. The annual world production of H<sub>2</sub> was about  $5 \times 10^{11}$  Nm<sup>3</sup> in 2005 [1]. The production of H<sub>2</sub> has gained importance in recent years due to the increased demand in conventional applications, *e.g.*, ammonia production, hydrocarbon synthesis *via* Fischer Tropsch process, and petroleum refining processes (hydrotreating and hydrocracking) [2-4]. Moreover, the characteristics of H<sub>2</sub> as a clean energy carrier and the growing environmental concerns and stringent emission norms make it very suitable as future fuel for fuel cells in mobile and stationary applications.

Rapid developments of the proton-exchange membrane (PEM) fuel cell technology in recent years have initiated research in all areas of fuel processor catalysts for hydrogen generation. The main target is to develop active, selective, and stable catalytic systems in order to reduce the size and increase the efficiency of fuel processor. The overall efficiency in producing hydrogen with extreme low CO content, which is vital for the PEM fuel cell performance, is dependent on the efficiency of the catalysts in each segment (reformers, water gas shift, and preferential oxidation or methanation of CO) of the fuel processor. The CO concentration in the H<sub>2</sub> stream to fuel cell must be reduced to less than 50 ppm to avoid poisoning the Pt electrodes because CO adsorbs more strongly than hydrogen.

## 1.2 Fuel cells

Fuel cells are clean and efficient sources of electrical power for small and large, mobile and stationary applications. They are devices that directly convert the chemical energy of the fuel (gas or liquid) into electrical energy while avoiding the mechanical and thermodynamic limitations of the traditional internal combustion engines. Fuel cells are considered as a promising engines for automobile applications [3] because of (i) the higher efficiency of the fuel cells compared to the traditional internal combustion engines (65% versus 35%, respectively) and (ii) they emit no CO<sub>x</sub>, NO<sub>x</sub>, or HC gas exhaust,

There are a variety of fuel cells depending on the applications [1,5]. These are proton-exchange membrane (PEM) fuel cell operating at ~ 80°C, alkaline fuel cells (AFC) operating at ~ 100°C, phosphoric acid fuel cells (PAFC) for ~ 200°C operation, molten carbonate fuel cells (MCFC) at ~ 650°C, and solid oxide fuel cells (SOFC) for high temperature operation of 800 – 1100°C. The characteristics of PEM, such as low operating temperature, low weight, and suitability for discontinuous operations, make it very suitable for mobile power applications. The ideal fuel for PEM fuel cells is pure hydrogen containing less than 50 ppm carbon monoxide (CO poisons the Pt electrodes of fuel cells). Basically, hydrogen is electrochemically oxidized to hydrogen ions at the anode. The hydrogen ions pass through a proton conductive membrane to the cathode where they react with reduced oxygen from air forming water. During this reaction, electrons are transferred *via* external circuit providing power (see Fig. 1).

Size, weight, safety, cost, and technical limitations make it difficult to store hydrogen in sufficient quantity and density. Therefore, generation of H<sub>2</sub> on site and on demand by reforming fuels such as natural gas, gasoline, propane (LPG) or methanol could be a practical option.



as pure gas or as syngas for the production of other chemicals (*e.g.* ammonia or methanol) for many decades [7].



Steam reforming of methane is highly endothermic reaction ( $\Delta H = 206$  kJ/mol) and is carried out in fired tubes at temperature above 850°C and at 15-30 bar pressure. The natural gas reacts with steam on a Ni based catalyst at residence time of several seconds to produce syngas. Because Ni based catalysts are very active for decomposition of CH<sub>4</sub> to carbon and hydrogen, steam excess is introduced to prevent carbon deposition and the feed H<sub>2</sub>O/CH<sub>4</sub> mole ratio is typically 2 – 5 depending on the end use. Excess of H<sub>2</sub>O shift the water-gas-shift equilibrium (reaction (3)) resulting in high H<sub>2</sub>/CO ratio (ratio of 3) [7, 8].



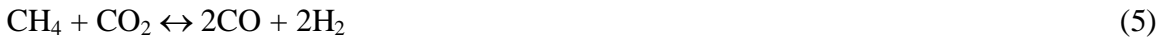
### 1.3.2 Catalytic Partial Oxidation (CPO)

Catalytic partial oxidation (CPO) of CH<sub>4</sub> to syngas (reaction 4) is an attractive method compared to that of SR to produce syngas. The most significant aspect of this process is the replacement of the highly endothermic SR reaction by exothermic partial oxidation process ( $\Delta H = -36$ kJ/mol). Rh-supported catalysts are commonly used in CPO [9]. Compared with the steam reforming process, oxidation process is much faster, energy efficient, compact and simple. High reaction temperature is the main drawback of the process. The CPO process results in a lower H<sub>2</sub>/CO ratio than SR (ratio of 2), implying that more CO must be further converted via the WGS reaction (Eq. 3) to increase the H<sub>2</sub> yield. The small reactor size and high throughput of CPO make it interesting to apply this process to produce H<sub>2</sub> for fuel cells.



### 1.3.3 CO<sub>2</sub> reforming (or Dry Reforming)

Carbon dioxide reforming or dry reforming of methane (reaction (5)) is an endothermic reaction ( $\Delta H = 247\text{kJ/mol}$ ). This process shows a growing interest from both industrial and environmental viewpoints [10]. From an environmental viewpoint, CO<sub>2</sub> and CH<sub>4</sub> are undesirable greenhouse gases and both are consumed by this reaction. However, the high endothermicity of the process and the related heat input required makes it a net CO<sub>2</sub> producing process and hence from an environmental point of view less attractive. The lower H<sub>2</sub>/CO ratio than SR is suitable for the production of oxygenated compounds [11]. The low H<sub>2</sub>/CO ratio makes this process not particular suitable for the production of H<sub>2</sub> for fuel cell applications.



### 1.3.4 Auto-thermal reforming (ATR)

The process of ATR uses methane or liquid hydrocarbons as fuel that undergoes reaction with air and steam/CO<sub>2</sub> in a single reactor. Since the ATR process consists of the combination of CPO (Eq.4) and SR (Eq.2), the balance of the specific heat for each reaction becomes a very distinctive characteristic of this process. This makes the whole process relatively more energy efficient since the heat produced in CPO can be used directly in SR. With ATR technologies, conventional SR plants can be improved, reducing size and weight, lower costs, and faster starting time. The drawback of this process is that it requires an expensive oxygen plant [12].

## 1.4 Water Gas Shift Reaction: background and state of art

The water gas shift (WGS) reaction was discovered by the Italian physicist Felice Fontana in 1780. WGS is reversible and exothermic ( $\Delta H = -41\text{kJ/mol}$ ) chemical reaction (Eq.3) in which water and carbon monoxide react to form carbon dioxide and hydrogen. WGS is a crucial step in maximizing hydrogen yield after the conversion of hydrocarbons

to synthesis gas *via* steam reforming, partial oxidation, CO<sub>2</sub> reforming, or auto-thermal reforming.

The current commercial WGS technology is carried out in two stages to overcome the thermodynamic limitation for the reaction at higher temperatures and to achieve almost complete CO conversions (unconverted CO below 1000 ppm). The two steps involve a high temperature (350-500°C) shift (HTS) over Fe<sub>2</sub>O<sub>3</sub>/Cr<sub>2</sub>O<sub>3</sub> catalyst followed by a low temperature (200-250°C) shift (LTS) over a Cu/ZnO/Al<sub>2</sub>O<sub>3</sub> catalyst [3].

The exiting gas from the steam reformer, which contains 10-13 vol% CO, is cooled to about 350 – 500°C and then undergoes further processing to increase H<sub>2</sub> yield and to lower the CO concentration to about 2-3 vol% over Fe<sub>2</sub>O<sub>3</sub>/Cr<sub>2</sub>O<sub>3</sub> catalyst in adiabatic fixed bed WGS reactor operating at 350 – 500°C, 20 – 30 atm, and a GHSV of 400-1200h<sup>-1</sup> [3]. The Fe<sub>2</sub>O<sub>3</sub>/Cr<sub>2</sub>O<sub>3</sub> catalyst is not very active but is resistant to poisons or impurities (e.g. sulfur or chlorine) present in syngas and to adiabatic temperature increase. The low activity of the catalyst also implies that a relatively high temperature is needed to achieve a sufficient reaction rate. On the other hand, the high temperature limits the maximal conversion because of the unfavorable thermodynamic equilibrium. Thus, a second catalyst bed with Cu catalysts is used to convert the remaining CO almost completely at low temperature.

The gas exiting CO (2 – 3 vol%) the HTS reactor is further shifted and the CO concentration is reduced to <0.2 vol% by the LTS reactor. The gas feed from the HTS reactor is cooled down to 200°C before it enters the adiabatic low temperature fixed bed reactor containing a high activity CuO/ZnO/Al<sub>2</sub>O<sub>3</sub> catalyst. The LTS reactor operates at 180 – 230°C, 10 – 30 atm, and GHSV of about 3600h<sup>-1</sup>. The catalyst for this process consists of 30%CuO, 35-55%ZnO, and about 15-35%Al<sub>2</sub>O<sub>3</sub>. It is believed that Cu is the active site and ZnO minimizes the sintering of Cu [3]. Because of the sensitivity of LTS catalyst to sintering, the catalyst must be reduced carefully to avoid excessive temperature increase. The starting temperature is 120°C with 50%H<sub>2</sub>/N<sub>2</sub>, both temperature and H<sub>2</sub> concentration increased gradually until completing the reduction of

LTS catalyst without allowing the bed temperature to rise above 230°C [13]. The characteristics of LTS catalyst make it difficult to be used in the first bed (HTS reactor) because it cannot withstand the adiabatic increase in temperature, which would damage the catalyst. Moreover, LTS catalyst is sensitive to poisoning, for *e.g.* by sulfur. Thus, one of the important roles of HTS catalyst is to trap sulfur and chlorine impurities to protect the LTS catalyst.

The two-step WGS (HTS and LTS) which is currently practiced at industrial scale, is not an appropriate choice for H<sub>2</sub> production for small scale fuel cell applications ( $\leq 100$  kW) because of its technical complexity and the multiple stages involved [3]. In particular starting up and shutting down the engine frequently is anticipated to become extremely complicated. Other important issues are (i) Cu catalysts used in the low temperature step are known to be pyrophoric; air diffusing into the reactor after shutting down may cause fire, or at least will damage the catalyst and (ii) Fe based catalysts does not have sufficient activity.

Precious metals based catalysts are reported as promising WGS catalysts because they are robust, they can operate at higher temperatures where the kinetics is more favorable in contrast to Cu catalysts, less sensitive to poisons (Cl and S) than LTS catalysts (Cu based) and they are more active than the HTS (Fe/Cr oxide based) catalyst [3, 14]. Among those catalysts are the precious metals Ru, Os, Ir, Pt, Pd, Rh, Ag, or Au [15-38] on several supports such as ZrO<sub>2</sub> [21,26], TiO<sub>2</sub> [19,24,25], Fe<sub>2</sub>O<sub>3</sub> [27], CeO<sub>2</sub> [17,20,22,23,37,38], MgO [28], SiO<sub>2</sub> [20], Carbon [20], Ce(Zr)O<sub>2</sub> [29, 30], Ce(Al)O<sub>2</sub> [27, 31], and Ce(La)O<sub>2</sub> [32].

In general, precious metals based catalysts are considered bi-functional [15,18,23,24,30-33], where both the metal and the support have essential roles for the WGS reaction. Among the two reactants for WGS reaction, CO and H<sub>2</sub>O, the latter is more difficult to activate [33] due to its thermodynamic stability. Metals such as Cu and Fe are reported to undergo oxidation by water [7] thereby activating it. However, Pt does not interact chemically with water because the PtO<sub>x</sub> that would be formed is not thermodynamically

stable [34] at WGS temperatures. Thus for Pt based WGS catalysts a hydrophilic oxide support is essential to adsorb and activate water [15,18,23,24,30-33]. Therefore, such catalysts are bifunctional with platinum activating CO and support activating H<sub>2</sub>O. Activity of these catalysts is reported to depend on a number of factors, such as, catalyst preparation and testing conditions. In most of catalytic screening done in literature, long-term stability was not measured.

Although numerous mechanistic and kinetics studies, over precious metals based catalysts (*e.g.* Pt/CeO<sub>2</sub>), have been carried out in recent years, disagreement remains about the nature of the reaction intermediates and the role of the support. Two reaction mechanisms are mainly proposed in the literature: the “adsorptive mechanism” (involving in particular formate surface species, see Fig. 2a) [21,29,35-38] and the “regenerative mechanism” (red-ox, see Fig. 2b) [17,18,22,23,39-42].

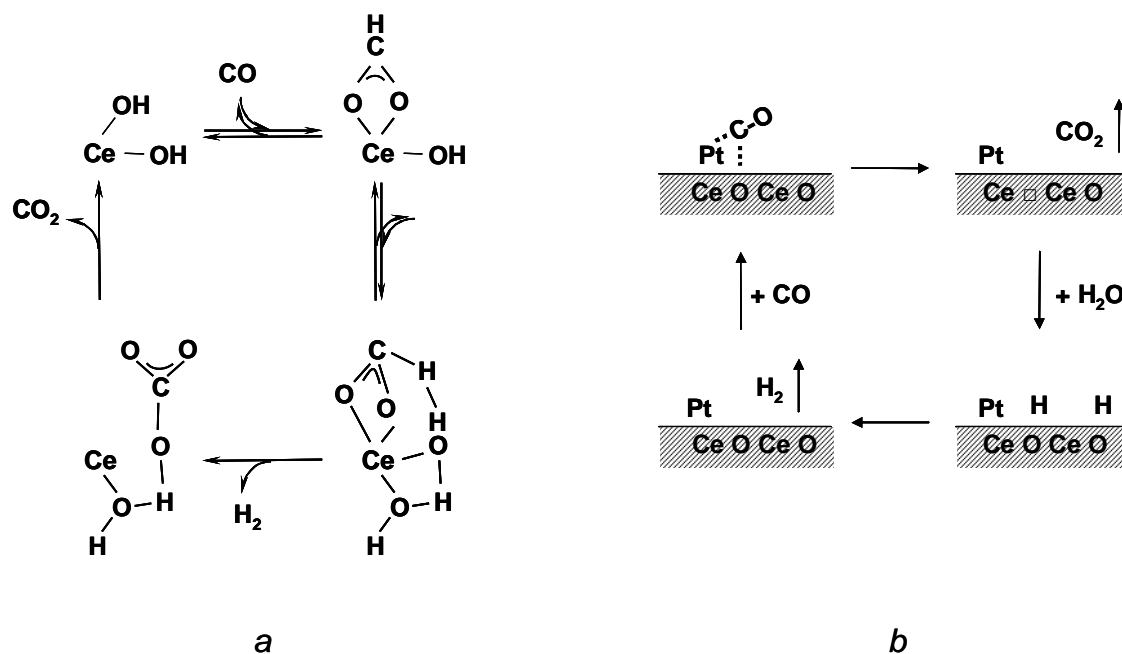


Fig. 2: Formate (a) and red-ox (b) mechanism for WGS shift reaction over Pt/CeO<sub>2</sub> catalyst

In the adsorptive (or associative) mechanism [21,29,35-38], hydroxyl groups on the support react with CO and form surface formates. The decomposition of formate species is suggested to be facilitated by presence of water in gas phase and is claimed to be rate

determining. During this step, hydroxyl groups are regenerated on the oxide surface. No oxygen is removed from the surface during the catalytic cycle and the oxide does not undergo any red-ox changes during the WGS sequence. This mechanism was supported by FTIR measurements, isotopic exchange experiments, pulse type experiments and kinetic studies of CO<sub>2</sub> hydrogenation (reverse WGS) [21,29,35-38]. The role for Pt is not clear from the studies, and even can not be elucidated from the reaction schemes proposed. However, it has been suggested without clear experimental evidence, that Pt helps in the generation of bridging OH group, which are claimed to be necessary for the formation of surface formate groups. Platinum also facilitates decomposition of formate groups in presence of H<sub>2</sub>O.

In the regenerative mechanism, water adsorbs and dissociates on a partly reduced support, releasing H<sub>2</sub> and reoxidizing the support. In parallel, CO<sub>(g)</sub> adsorbs on metallic sites to form a M-bond carbonyl species, which then reduces the support and releases CO<sub>2</sub>. This mechanism was supported by kinetic studies, TPD, TPR, steady-state isotopic transient kinetic analysis (SSITKA), and oxygen storage capacity measurements [17,18,22,23,39-42].

It is thus clear from both proposed WGS mechanisms that both active metal and oxide support are essential for the catalyst activity (bifunctional catalysts). Thus, better insight in how water and CO are activated on the catalyst may help in designing more efficient catalysts (active, stable, and selective) for WGS reaction.

## **1.5 Thesis outline**

The objective of this study is to gain insight in to the influence of oxide support on the reaction sequences, activity, selectivity and stability of Pt based catalysts in order to develop an efficient single stage WGS catalyst. From cost and practical considerations, Pt content should be less than 0.5wt% and will be operated at moderate temperature (~300°C). However, this increase in the WGS reaction temperature, results in lower CO conversion because of thermodynamic limitation. At the same time, higher temperature is favorable for reaction kinetic. In order to overcome this, the catalyst can be combined

with a H<sub>2</sub>-selective catalytic membrane reactor to separate H<sub>2</sub> and shift the equilibrium in order to achieve higher CO conversions. Because of this, a detailed WGS kinetic and reaction mechanism over the developed catalyst is covered in this dissertation.

The dissertation consists of the following seven chapters: In **chapter 1**, the state of art for the WGS reaction is briefly described. Therein, the background of the reaction including the catalysts studied and reaction mechanisms proposed in literature is summarized together with the objective of this study. In **chapter 2**, an investigation of the influence of the oxide support on mechanistic reaction sequence for Water Gas Shift (WGS) reaction over Pt/CeO<sub>2</sub>, Pt/TiO<sub>2</sub>, and Pt/ZrO<sub>2</sub> (different red-ox catalysts characteristics) catalysts is presented. **Chapter 3** focuses on the role of catalyst support and promoter on the catalyst activity and stability. In this chapter the best catalyst is chosen for further developments. In **chapter 4**, the deactivation mechanism of Pt/TiO<sub>2</sub> catalyst is discussed in details. Therein, the causes of deactivation and intermediates responsible for catalyst deactivation are investigated. **Chapter 5** consists of an optimization and characterization study of the developed Pt-Re/TiO<sub>2</sub> catalyst. This chapter focuses on finding the optimum performance of the catalyst by studying the effect preparation strategies, Pt/Re molar ratio, and Pt and Re contents. We also characterized the optimum catalyst, using CO chemisorption, CO-TPD, H<sub>2</sub>-TPR, and in situ FTIR, to understand the role of Re on influencing Pt properties. In **chapter 6**, we used transient kinetic studies and *in situ* FTIR spectroscopy to follow the reaction sequences that occur during Water Gas Shift reaction over Pt-Re/TiO<sub>2</sub> catalyst. This Chapter also discusses the overall reaction rate on this catalyst based on steady state kinetics in order to support the reaction mechanism proposed. Finally, the thesis ends with general conclusions and recommendations for future work in **chapter 7**.

## 1.6 References

- [1] B. C. R. Ewan, R.W.K. Allen, *Int. J. Hydrogen Energy* 30 (2005) 809.
- [2] D.R. Strongin, G.A. Somorjai, in: J.R. Jennings (Ed.), *Catalytic Ammonia Synthesis Fundamentals and Practice*, Plenum Press, New York, 1991, p. 1.
- [3] C.H. Bartolomew, R.J. Farrauto, in: C.H. Bartolomew, R.J. Farrauto (Eds.). *Fundamentals of industrial catalytic processes*, John Wiley & Sons, Hoboken, NJ, 2006, p. 370.
- [4] B. Bussemeier, C. D. Frohning, B. Cornils, *Hydro. Proc.* 11 (1976) 105.
- [5] G. J. K. Acres, J. C. Frosta, G. A. Hards, R. J. Pottera, T. R. Ralph, D. Thompsetta, G. T. Bursteinb, G. J. Hutchings, *Catal. Today* 38 (1997) 393.
- [6] M. A. Rosen and D. S. Scott, *Int. J. Hydrogen Energy* 23 (1998) 653.
- [7] J. R. Rostrup-Nielsen, in: J.R. Anderson and M. Boudart (Eds), *Catalysis, Science and Technology*, Springer-Verlag, Berlin, 1984, Vol 5, p. 1.
- [8] J. R. H. Ross, *Catal. Today* 100 (2005) 151.
- [9] S. Eriksson, M. Wolf, A. Schneider, J. Mantzaras, F. Raimondi, M. Boutonnet, S. Jaras, *Catal. Today* 117 (2006) 447.
- [10] M. Rezaei, S.M. Alavi, S. Sahebdehfar, P. Bai, X. Liu, Z. Yan, *Appl. Catal B* 77 (2007) 364.
- [11] J. R. H. Ross, A. N. J. van Keulen, M. E. S. Hegarty, K. Seshan, *Catal. Today* 30 (1996) 193.
- [12] J. R. Rostrup-Nielsen, J. Sehested, J. K. Nørskov, *Adv. Catal.* 47 (2002) 65.
- [13] D. R. Goodman, in: *Catalyst Handbook*, M. W. Twigg. Wolfe, London, chap. 3 p. 140-188.
- [14] W. Ruettinger, O. Ilinich, R. J. Farrauto, *J. Power Sources* 118 (2003) 61.
- [15] D. C. Grenoble, M. M. Estadt, D. F. Ollis, *J. Catal.* 67 (1981) 90.
- [16] T. Tabakova, V. Idakiev, D. Andreeva, I. Mitov, *Appl. Catal. A: General* 222 (2000) 91.
- [17] Q. Fu, H. Saltsburg, M. Flytzani-Stephanopoulos, *Science* 301 (2003) 935.
- [18] X. Wang, R. J. Gorte, *Appl. Catal. A: General* 247 (2003) 157.

- [19] Y. Sato, K. Terada, S. Hasegawa, T. Miyao, S. Naito, *Appl. Catal. A: General* 296 (2005) 80.
- [20] G. Jacobs, L. Williams, U. Graham, D. Sparks, B. Davis, *J. Phys. Chem. B* 107 (2003) 10398.
- [21] H. Iida, A. Igarashi, *Appl. Catal. A: General* 303 (2006) 48.
- [22] F. C. Meunier, D. Tibiletti, A. Goguet, D. Reid, R. Burch, *Appl. Catal. A: General* 289 (2006) 104.
- [23] T. Bunluesin, R. J. Gorte, G. W. Graham, *Appl. Catal. B: Environmental* 15 (1998) 107.
- [24] P. Panagiotopoulou, A. Christodoulakis, D. I. Kondarides, S. Boghosian, *J. Catal.* 240 (2006) 114.
- [25] H. Iida, A. Igarashi, *Appl. Catal. A* 298 (2006) 152.
- [26] E. Xue, M.O’Keeffe and J.R.H. Ross, *Stud. Surf. Science*, 130 (2000) 3813.
- [27] A. Basinska, F. Domka and A. Mickiewicz, *Appl. Catal., A*, 179 (1999) 241.
- [28] D. Wolf, M. Barré-Chassonnery, M. Hohenberger, A. van Vaan, M. Baerns, *Catal. Today*, 40 (1998) 147-156.
- [29] S. Yu Choung, M. Ferrandon, T. Karause, *Catal. Today* 99 (2005) 257.
- [30] W. Ruettinger, X. Liu, R. J. Farrauto, *Appl. Catal. B* 65 (2006) 135.
- [31] A. Haryanto, S. Fernando, S. Adhikari, *Catal. Today* 129 (2007) 269.
- [32] F.C. Meunier, D. Reida, A. Goguet, S. Shekhtman, C. Hardacre, R. Burch, W. Deng, M. Flytzani-Stephanopoulos, *J. Catal.* 247 (2007) 277.
- [33] M. A. Henderson, *Surf. Sci. Rep.* 46 (2002) 1.
- [34] K. Takanae, K. Aika, K. Seshan and L. Lefferts, *J. Catal.* 227 (2004) 101.
- [35] G. Jacobs, U. M. Graham, E. Chenu, P. M. Patterson, A. Dozier, B. H. Davis, *J. Catal.* 229 (2005) 499.
- [36] A. Goguet, S. O. Shekhtman, R. Burch, C. Hardcare, F. C. Meunier, G. S. Yablonsky, *J. Catal.* 237 (2006) 102.
- [37] T. Shido, Y. Iwasawa, *J. Catal.* 141 (1993) 71.
- [38] E. Chenu, G. Jacobs, A. C. Crawford, R. A. Keogh, P. M. Patterson, D. E. Sparks, B.H. Davis, *Appl. Catal. B* 59 (2005) 45.
- [39] R. J. Gorte, S. Zhao, *Catal. Today* 104 (2005) 18.

- [40] S. Hilaire, X. Wang, T. Luo, R.J. Gorte, J. Wagner, *Appl. Catal. A* 215 (2001) 271.
- [41] W. Liu, M. Flytzani-Stephanopoulos, *J. Catal.* 153 (1995) 317.
- [42] C. M. Y. Yeung, F. Meunier, R. Burch, D. Thompsett, S. C. Tsang, *J. Phys. Chem. B* 110 (2006) 8540.

# Chapter 2

## Role of the support on WGS reaction sequences

---

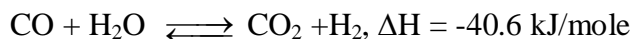
### *Abstract*

*Oxide support plays a significant role in the mechanistic reaction sequence for Water Gas Shift (WGS) reaction over Pt based catalysts. In situ FTIR spectroscopic and transient kinetic studies have been used to follow the reactions that occur. CeO<sub>2</sub>-, TiO<sub>2</sub>- and ZrO<sub>2</sub>- supported Pt catalysts have been studied at 300°C. In all cases, CO is adsorbed on Pt. The role of the support oxide is to activate water, completing the WGS reaction sequence. We have taken into consideration four different pathways that may be involved in the complex WGS reaction scheme. These are (A) red-ox route (B) associative formate route (C) associative formate route with a red-ox regeneration of the oxide support and (D) carbonate route. In the case of Pt/ZrO<sub>2</sub>, the WGS reaction follows the associative formate with red-ox regeneration (route C). On Pt/TiO<sub>2</sub>, both the red-ox (route A) and the associative formate with red-ox regeneration (route C) contribute. The associative formate (route B) is the relevant reaction pathway on Pt/CeO<sub>2</sub>.*

**Keywords:** *Water Gas Shift, Platinum, Ceria, Titania, Zirconia, Reaction mechanism, Red-Ox, Associative formate mechanism, Carbonate.*

## 2.1 Introduction

WGS is a reversible, exothermic reaction in which carbon monoxide reacts with steam to produce hydrogen and carbon dioxide.



This reaction is a crucial step in maximizing hydrogen after the conversion of hydrocarbons to synthesis gas *via* steam reforming or partial oxidation [1]. The demand for hydrogen is expected to increase in the future due to its use in fuel cell applications for power generation. This is because fuel cells are appreciably more efficient than the current internal combustion engines and they are environmentally friendly as they produce no CO<sub>x</sub>, NO<sub>x</sub>, hydrocarbons or soot emissions [2, 3].

The state-of-the-art industrial process for WGS is carried out in two stages to overcome the thermodynamic limitation for the reaction at higher temperatures and to achieve almost complete CO conversions (unconverted CO below 1000 ppm). The two steps involve a high temperature (350-500°C) shift (HTS) over Fe<sub>2</sub>O<sub>3</sub>/Cr<sub>2</sub>O<sub>3</sub> catalyst followed by a low temperature (200-250°C) shift (LTS) over a Cu/ZnO/Al<sub>2</sub>O<sub>3</sub> catalyst [1]. This approach, which is currently practiced at industrial scale, is not an appropriate choice for mobile applications because of its technical complexity and the multiple stages involved [2]. A single stage WGS conversion is thus desirable. Supported noble metals, e.g. Pt, based catalysts are reported as promising single stage WGS catalysts because (i) they are robust, (ii) they can operate at higher temperatures where the kinetics is more favorable in contrast to Cu catalysts, (iii) less sensitive to poisons (Cl and S) than LTS catalysts (Cu based) and (iv) are more active than the HTS (Fe/Cr oxide based) catalysts [2,3].

Recently, different catalyst compositions have been explored in WGS by varying Pt loading (from 0.1 to 5 wt. %) and the oxide supports (CeO<sub>2</sub> [4–6], ZrO<sub>2</sub> [7, 8], TiO<sub>2</sub> [9–11], Ce<sub>x</sub>Zr<sub>1-x</sub>O<sub>2</sub> [12-15], Ti<sub>x</sub>Ce<sub>1-x</sub>O<sub>2</sub> [16] *etc.*). Activity is reported to depend on a number of factors, such as, catalyst preparation [4, 5, 10, 17], nature of support [16], testing conditions and reactor design [18]. Despite the fact that noble metal based catalysts are very active, their straightforward application to provide hydrogen feed for PEM fuel cells

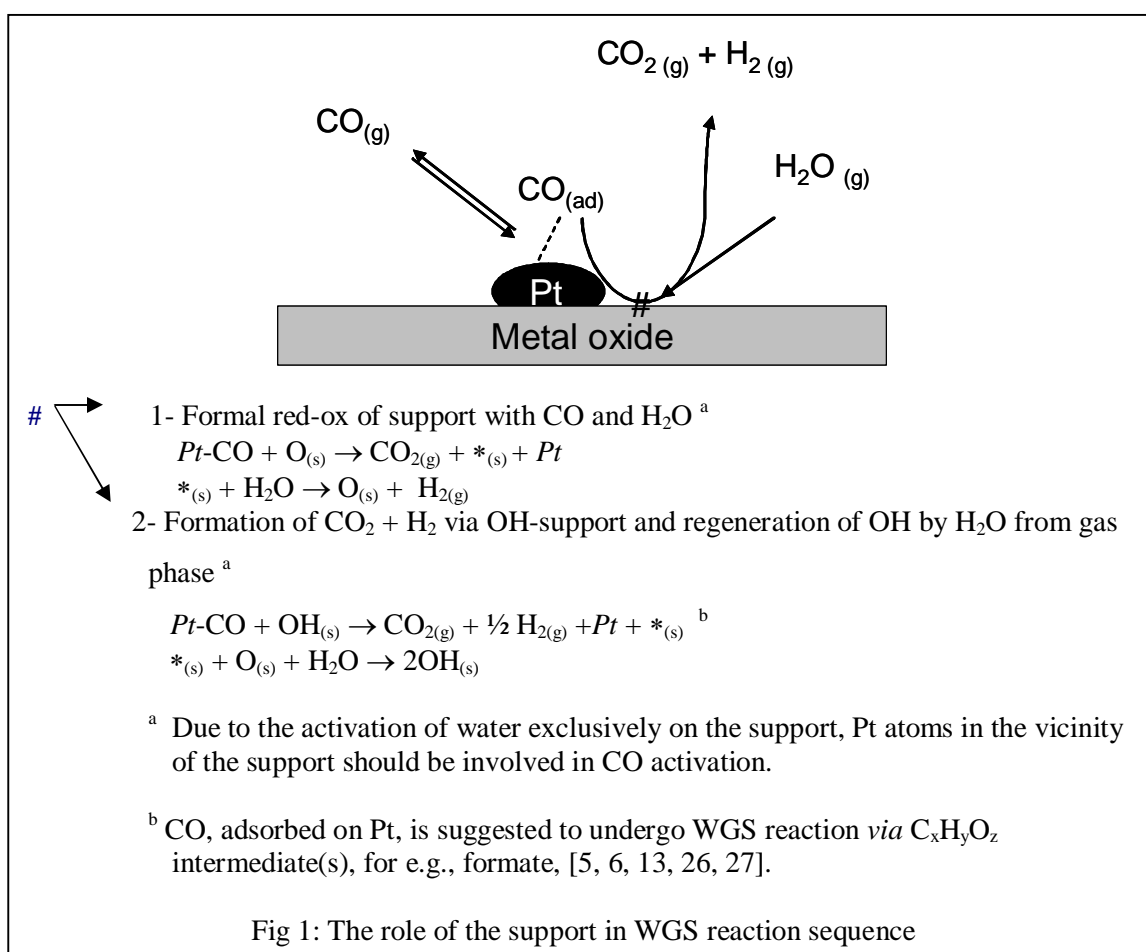
is not feasible because of limited conversion of CO due to thermodynamic constraints. This can be overcome by selective product separation to shift the equilibrium to the product side, by, for example, using a hydrogen-selective permeable membrane [19, 20], or CO<sub>2</sub> sorbents [21]. Removal of CO by preferential oxidation or methanation is an option to further lower the CO concentration [22, 23]. The experiments in this study were carried out at 300°C inspired by the option that hydrogen selective membranes are stable at those conditions.

In general, it is agreed that both the metal and the support have essential roles for the WGS reaction. Among the two reactants for WGS reaction, CO and H<sub>2</sub>O, the latter is more difficult to activate [24] due to its thermodynamic stability. Metals such as Cu and Fe are reported to undergo oxidation by water [25] thereby activating it. However, Pt does not interact chemically with water because the PtO<sub>x</sub> that would be formed is not thermodynamically stable [26] at WGS temperatures. Thus for Pt based WGS catalysts a hydrophilic oxide support is essential to adsorb and activate water [24-30]. Therefore, such catalysts are bi-functional, with platinum activating CO and support activating H<sub>2</sub>O.

Different WGS reaction pathways have been suggested in literature [4, 27]; these are schematically presented in Fig. 1. Water, either re-oxidizes the support oxide after reduction by CO, activated on Pt, or forms hydroxyl groups and completes the catalytic cycle. The exact nature of intermediates formed, that are relevant, and the mechanistic route(s) for the WGS reaction are still a matter of debate, however. In the case of Pt/CeO<sub>2</sub>, the most studied catalytic system for WGS, two reaction mechanisms have been proposed: *viz.* (i) associative (surface formate) [5, 6, 13, 31, 32] and (ii) regenerative red-ox mechanism [26, 28, 33, 34].

In the associative mechanism [5, 6, 13, 31, 32] hydroxyl groups on the support react with CO and form surface formates. The decomposition of formate species is suggested to be facilitated by presence of water in gas phase and is rate determining. During this step, hydroxyl groups are regenerated on the oxide surface. No oxygen is removed from the surface during the catalytic cycle and the oxide does not undergo any red-ox changes

during the WGS sequence. This mechanism was supported by FTIR measurements, isotopic exchange experiments, pulse type experiments and kinetic studies of CO<sub>2</sub> hydrogenation (reverse WGS) [5, 6, 13, 31, 32, 35]. The role for Pt is not clear from the studies, and even can not be elucidated from the reaction schemes proposed. However, it has been suggested without clear experimental evidence, that Pt helps in the generation of bridging OH group, which are claimed to be necessary for the formation of surface formate groups. Platinum also facilitates decomposition of formate groups in presence of H<sub>2</sub>O [5].



In the case of the red-ox mechanism, CO adsorbs on the metal and reacts at the metal-support interface with oxygen from the support surface, forming CO<sub>2</sub> and reducing support surface. The latter is then re-oxidized by H<sub>2</sub>O forming H<sub>2</sub>. This mechanism was

supported by kinetic studies, TPD, TPR and oxygen storage capacity measurements [26, 28, 33, 34].

In our efforts for the development of single stage Pt based WGS catalysts for fuel cell applications; we observed strong influence of the support on the catalyst activity [16]. Here, we explore the influence of the oxide support ( $\text{ZrO}_2$ ,  $\text{CeO}_2$ ,  $\text{TiO}_2$ ) for Pt based catalysts, on the mechanistic reaction sequence(s) for WGS reaction. We performed kinetic pulse transient studies using CO,  $\text{H}_2\text{O}$ ,  $\text{N}_2\text{O}$  and *in-situ* FTIR spectroscopic measurements to elucidate elementary reaction steps and identify reaction intermediates during WGS reaction sequence. We used  $\text{N}_2\text{O}$  to reoxidize the oxide surface without regeneration of OH groups to study the role of surface OH groups in the WGS reaction. In this way, we avoid high-temperature dehydroxylation of the catalyst surface; preventing any structural changes in the catalyst (*e.g.* decrease in Pt dispersion). In Chapter 3 [16], we report on the use of these concepts to develop an active, selective and stable single-stage WGS catalyst.

## **2.2. Experimental**

### **2.2.1. Catalyst preparation**

The following commercial supports were used,  $\text{TiO}_2$  (Degussa, P-25),  $\text{CeO}_2$  (Aldrich),  $\text{ZrO}_2$  (Daiichi Kagaku Kogyo, RC100). The catalysts were prepared by wet impregnation of the solid supports with aqueous solutions of  $\text{H}_2\text{PtCl}_6$  (Aldrich) to yield catalysts with 0.5wt% Pt. The catalysts were dried at  $75^\circ\text{C}$  for 2 h in vacuum and subsequently calcined at  $450^\circ\text{C}$  for 4 h.

### **2.2.2. Characterization**

Platinum contents of the catalysts were determined using Philips X-ray fluorescence spectrometer (PW 1480). The BET surface area of the supports and catalysts were measured using the BET method on ASAP 2400 (Micromeritics). Pt dispersions were

measured by H<sub>2</sub> chemisorptions at room temperature using Chemisorb 2750 (Micromeritics). Teschner *et al.* [36] showed in a detailed study that hydrogen spill-over does not occur significantly on Pt/CeO<sub>2</sub> at lower temperatures (*i.e.* 20°C), resulting in reliable dispersion measurements. Therefore, H<sub>2</sub> spillover from Pt particles to support surface is not influencing dispersion measurements in the case of ceria supported catalysts. The properties of the supports and the catalysts are summarized in Table 1.

Table 2.1: Supports and catalysts properties

| Sample                | Calcination<br>T, time | XRF<br>Pt (wt %) | Pt<br>dispersion<br>(%) at 25°C | Surface Pt,<br>μmol/g | BET, m <sup>2</sup> /g |
|-----------------------|------------------------|------------------|---------------------------------|-----------------------|------------------------|
| CeO <sub>2</sub>      | 500°C, 4 h             | -                | -                               | -                     | 85                     |
| TiO <sub>2</sub>      | 500°C, 4 h             | -                | -                               | -                     | 50                     |
| ZrO <sub>2</sub>      | 500°C, 4h              | -                | -                               | -                     | 25                     |
| Pt/CeO <sub>2</sub> * | 450°C, 4h              | 0.54             | 65                              | 16.6                  | 81                     |
| Pt/TiO <sub>2</sub>   | 450°C, 4h              | 0.49             | 55                              | 14.1                  | 48                     |
| Pt/ZrO <sub>2</sub>   | 450°C, 4h              | 0.47             | 60                              | 15.4                  | 22                     |

\* H<sub>2</sub> chemisorption at 0°C gave 61% Pt dispersion

### 2.2.3. Pulse experiments

Kinetic transient pulse experiments were performed at 300°C, at atmospheric pressure using a fixed-bed reactor. A 50 mg catalyst was placed between two quartz plugs in a quartz tubular reactor (d = 4 mm). For all the experiments described below, the gases (He, H<sub>2</sub>, CO, N<sub>2</sub>O) used were of > 99.9 % purity. The catalyst was first reduced at 300 °C in 10 vol% H<sub>2</sub>/He, 30 ml/min flow for 1 h. After this the catalyst was heated at 330°C in He (30 ml/min) for 30 min. Pulse experiments were then carried out by contacting fixed amounts of reactant gases with catalyst at 300°C using He as carrier gas. Each pulse contained 3.9 μmol of respective gas (CO, N<sub>2</sub>O). H<sub>2</sub>O (1.0 μl) was injected using a micro syringe directly into the reactor. Pulses were repeated until the responses for reactants and products did not change anymore. To determine the products formed, the outlet of the

reactor was directly connected to a Porapak column (5 m, 100°C) and TCD detector. Downstream to the TCD detector, gases were analysed by an online mass spectrometer (BALZERS QMS 200 F). Quantitative determination of all gaseous products, except of H<sub>2</sub> and H<sub>2</sub>O, was obtained from TCD data with accuracy not lower than  $\pm 0.1 \mu\text{mol/g}_{\text{cat}}$ . H<sub>2</sub> was detected by MS; the data for H<sub>2</sub> are semi-quantitative for each catalyst, and quantitative comparison between catalysts is not applicable.

#### 2.2.4. FTIR studies

The FTIR spectra were recorded using a Bruker Vector 22 with MCT detector under flow conditions (5% CO/He, 10 % H<sub>2</sub>O/He and (5% CO + 10 % H<sub>2</sub>O)/He) at the same temperature used in the kinetic experiments (300°C). Pulse experiments were mimicked by fast switching between He and mixture of He containing CO or H<sub>2</sub>O.

### 2.3. Results

A typical experimental result during subsequent pulsing of CO and H<sub>2</sub>O over a (*e. g.* Pt/CeO<sub>2</sub>) catalyst at 300°C is presented in Fig. 2. Cumulative consumption and formation of reactants and products, respectively, were quantified and the data are shown in Table 2. We started the pulse sequence experiments with hydroxylated catalyst surfaces.

#### 2.3.1. Pt/CeO<sub>2</sub>

The first CO pulse resulted in partial CO consumption and production of CO<sub>2</sub>. In the subsequent CO pulses, the amounts of CO<sub>2</sub> formed decreased. After four CO pulses, only traces of CO<sub>2</sub> were observed and the CO amount detected in the outlet of the reactor was close to the amount of CO in the pulse applied ( $\pm 0.1 \mu\text{mol/g}_{\text{cat}}$ ). No H<sub>2</sub> formation was observed. The cumulative amount of CO<sub>2</sub> formed (68  $\mu\text{mol/g}_{\text{cat}}$ , Table 2) was much lower than the amount of CO consumed (158  $\mu\text{mol/g}_{\text{cat}}$ ) during pulsing. FTIR spectra of Pt/CeO<sub>2</sub> after exposure to CO at the same temperature (compare Figs. 3 and 4) showed a band at 2050–2060 cm<sup>-1</sup> typical for linearly adsorbed CO on Pt [37], a band at 2856 cm<sup>-1</sup>

corresponding to the C-H stretching of formate [31], as well as bands in the spectra interval  $1600 - 1300 \text{ cm}^{-1}$  corresponding to carbonate and/or formate on ceria [13, 31, 37]. These species were relatively stable and could not be removed by flushing with He at  $300^\circ\text{C}$ .

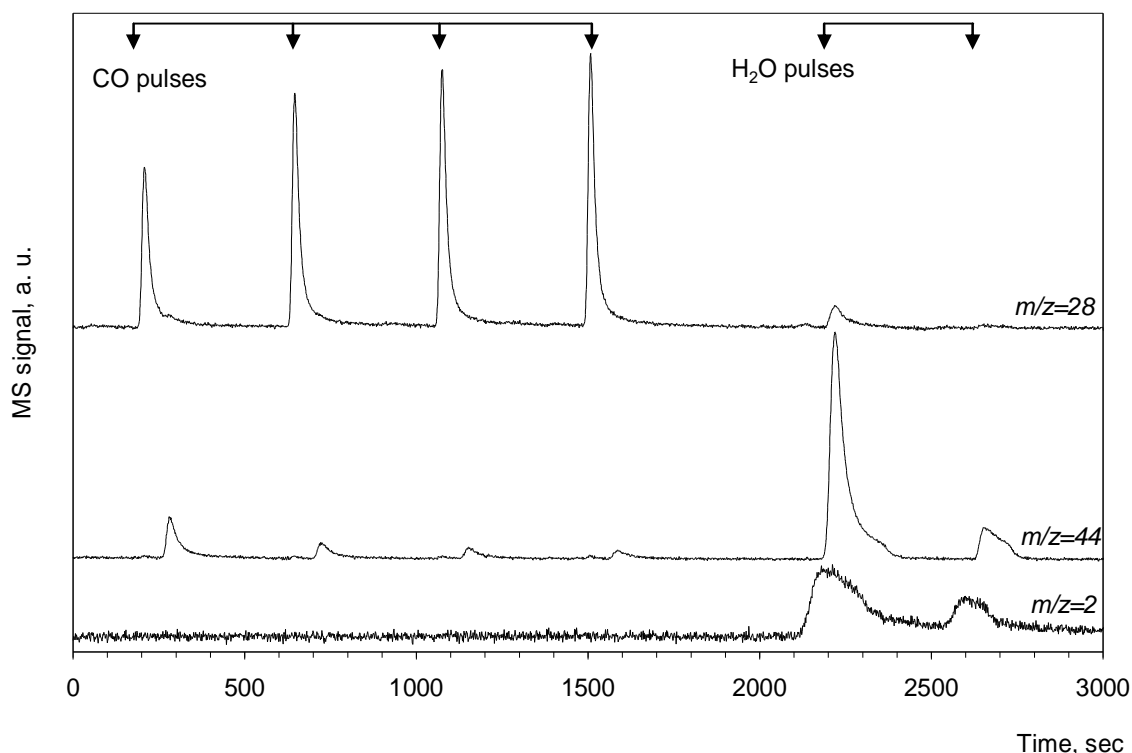


Fig. 2: Typical MS response for pulse experiment over Pt/CeO<sub>2</sub> catalyst reduced at  $300^\circ\text{C}$  in H<sub>2</sub>(10%)/He flow. Four pulses CO are followed with two pulses H<sub>2</sub>O. Difference in time between products detected is due to their separation with GC (porapak column).

After CO, the subsequent H<sub>2</sub>O pulses resulted in simultaneous production of CO<sub>2</sub> and H<sub>2</sub> (Fig. 2, Table 2). Most of the CO<sub>2</sub> and H<sub>2</sub> were formed during the first two pulses. The next H<sub>2</sub>O pulses produced only traces of CO<sub>2</sub> and H<sub>2</sub>. Only part of the formate/carbonate groups formed and retained at the surface during CO pulses, was reactive to H<sub>2</sub>O. After contacting with H<sub>2</sub>O, the FTIR band at  $2856 \text{ cm}^{-1}$ , which correspond to formate (Fig. 4), disappeared and the intensity of the bands  $1600 - 1300 \text{ cm}^{-1}$  (Fig. 3) corresponding to formate/carbonate decreased. However, an appreciable amount of oxygenate species were still present on the surface.

Table 2.2: Analysis of gaseous products during pulse experiments over Pt based catalysts.

| Catalyst                | (I) CO pulse                   |   |                             |                           | (II) H <sub>2</sub> O pulse after CO        |                           | (III) CO pulse after CO-H <sub>2</sub> O |   |                             |                           |
|-------------------------|--------------------------------|---|-----------------------------|---------------------------|---|---------------------------|--|---|-----------------------------|---------------------------|
|                         | CO consumed, $\mu\text{mol/g}$ | CO <sub>2</sub> released, $\mu\text{mol/g}$ | C uptake, $\mu\text{mol/g}$ | H <sub>2</sub> production | CO <sub>2</sub> released, $\mu\text{mol/g}$ | H <sub>2</sub> production | CO consumed, $\mu\text{mol/g}$           | CO <sub>2</sub> released, $\mu\text{mol/g}$ | C uptake, $\mu\text{mol/g}$ | H <sub>2</sub> production |
| I Pt/CeO <sub>2</sub>   | 158                            | 68  | 90                          | -                         | 60  | +                         | 118                                      | 57  | 60                          | -                         |
| II Pt/TiO <sub>2</sub>  | 52                             | 51  | 1                           | +                         | 0.6   | +                         | 49                                       | 48  | 1                           | +                         |
| III Pt/ZrO <sub>2</sub> | 40                             | 40  | 0                           | +                         | No  | -                         | 37                                       | 34  | 3                           | +                         |

| Catalyst                 | (IV) N <sub>2</sub> O pulse after CO        |                           | (V) CO pulse after CO – N <sub>2</sub> O |   |                             |                           | (VI) H <sub>2</sub> O pulse after CO – N <sub>2</sub> O-CO |                           |
|--------------------------|---|---------------------------|--|---|-----------------------------|---------------------------|--|---------------------------|
|                          | CO <sub>2</sub> released, $\mu\text{mol/g}$ | H <sub>2</sub> production | CO consumed, $\mu\text{mol/g}$           | CO <sub>2</sub> released, $\mu\text{mol/g}$ | C uptake, $\mu\text{mol/g}$ | H <sub>2</sub> production | CO <sub>2</sub> released, $\mu\text{mol/g}$                | H <sub>2</sub> production |
| Ia Pt/CeO <sub>2</sub>   | 60  | +                         | 220                                      | 135   | 85                          | -                         | 56   | -                         |
| IIa Pt/TiO <sub>2</sub>  | 0.6   | -                         | 52                                       | 50  | 2                           | -                         | 0.8  | +                         |
| IIIa Pt/ZrO <sub>2</sub> | No  | -                         | 32                                       | 31  | 1                           | -                         | 0  | -                         |

In quantitative terms, only  $60 \mu\text{mol/g}_{\text{cat}}$   $\text{CO}_2$  was released from the surface during  $\text{H}_2\text{O}$  pulses and  $30 \mu\text{mol/g}_{\text{cat}}$  “C” was retained at the surface. The next  $\text{CO} - \text{H}_2\text{O}$  sequence of pulses showed the same product distribution as in the first sequence.

When  $\text{N}_2\text{O}$  was used instead of  $\text{H}_2\text{O}$  to remove oxygenate species from  $\text{Pt/CeO}_2$ , the following gaseous products were observed; (i)  $\text{N}_2$  due to decomposition of  $\text{N}_2\text{O}$  (not shown) and (ii)  $\text{CO}_2$  and  $\text{H}_2$  due to decomposition of surface formate/carbonate formed during  $\text{CO}$  pulsing. No  $\text{O}_2$  was observed.  $\text{CO}$  pulses after  $\text{N}_2\text{O}$  treatment (Table 2) showed products ( $\text{CO}_2$ , no  $\text{H}_2$ ) similar to those during  $\text{CO}$  pulses over  $\text{Pt/CeO}_2$ , although somewhat more  $\text{CO}$  was converted to  $\text{CO}_2$ . At the same time, the amount of carbon retained on the surface was comparable ( $85 \mu\text{mol/g}_{\text{cat}}$ ). Pulsing with water after the sequence “ $\text{CO-N}_2\text{O-CO}$ ” resulted in the formation of essentially only  $\text{CO}_2$ . No  $\text{H}_2$  was detected by MS.

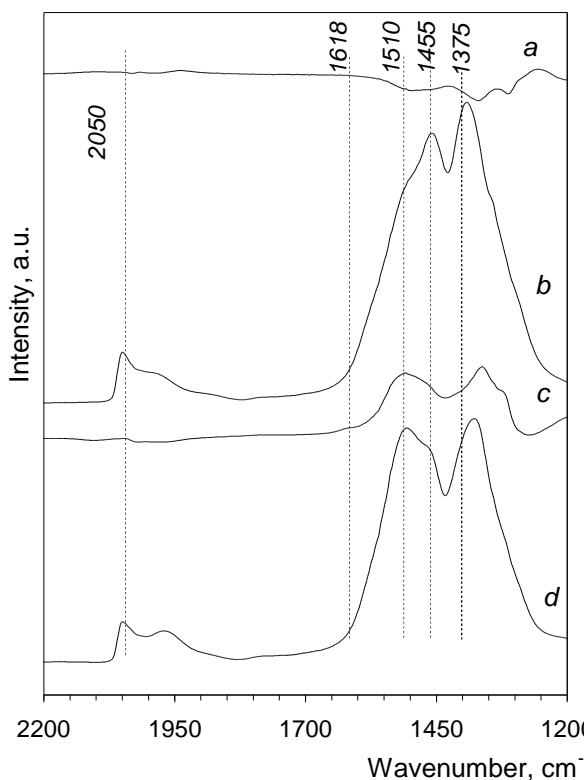


Fig.3: FTIR spectra at  $300^\circ\text{C}$  of  $\text{Pt/CeO}_2$  catalyst; reduced in 10 vol%  $\text{H}_2/\text{He}$  flow (a); after  $\text{CO}$  pulses (b); after  $\text{H}_2\text{O}$  pulses (c); *in situ* WGS conditions (d).

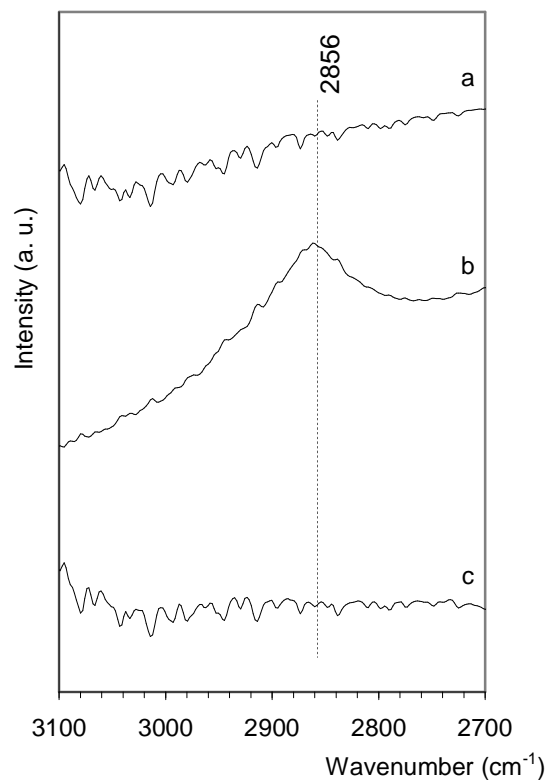


Fig.4: FTIR spectra at  $300^\circ\text{C}$  of  $\text{Pt/CeO}_2$  catalyst; reduced in 10 vol%  $\text{H}_2/\text{He}$  flow (a); after  $\text{CO}$  pulses (b); after  $\text{H}_2\text{O}$  pulses (c).

### 2.3.2 Pt/TiO<sub>2</sub>

In contrast to Pt/CeO<sub>2</sub>, contacting Pt/TiO<sub>2</sub> with CO resulted simultaneously in the formation of CO<sub>2</sub> and H<sub>2</sub> (Fig. 5, Table 2). With repetitive CO pulses, the amount of CO consumed decreased in line with decreasing H<sub>2</sub> and CO<sub>2</sub> formation. After four pulses, the amount of CO at the reactor outlet was similar to that in the feed, and only traces of CO<sub>2</sub> and H<sub>2</sub> were detected. The cumulative CO consumption over Pt/TiO<sub>2</sub> was 52 μmol/g. This value was in agreement with the amount of CO<sub>2</sub> formed (i.e. 51 μmol/g<sub>cat</sub>). Thus, unlike in the case of Pt/CeO<sub>2</sub>, no oxygenate species were retained on the Pt/TiO<sub>2</sub> surface. FTIR data (Fig. 6) also showed no formation of carbonate/ formate surface species during the CO pulsing. Only CO adsorbed on Pt (Fig. 6) was detectable in the FTIR spectra (2060-2080 cm<sup>-1</sup>) [9, 11] after flushing with He at 300°C.

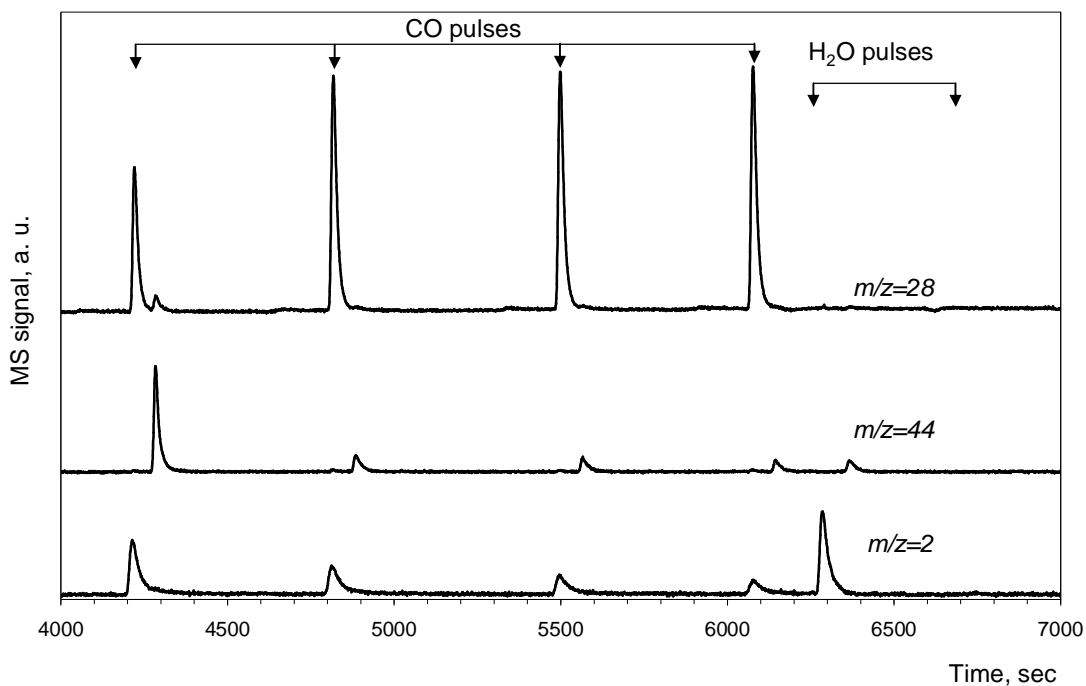


Fig. 5: Typical MS response for pulse experiment over Pt/TiO<sub>2</sub> catalyst reduced at 300°C in H<sub>2</sub>(10%)/He flow. 4 pulses CO are followed with two pulses H<sub>2</sub>O. Difference in time between products detected is due to their separation with GC (porapak column).

The H<sub>2</sub>O pulses after CO treatment resulted in H<sub>2</sub> as the main product (Fig. 5); CO<sub>2</sub> was observed only in negligible amounts (0.6 μmol/g<sub>cat</sub>). Subsequent CO pulses produced the

same gaseous products ( $\text{CO}_2$  and  $\text{H}_2$ ) as in the case of first CO pulse sequence demonstrating that the surface was regenerated by  $\text{H}_2\text{O}$  and catalytic cycle was completed. The amount of  $\text{CO}_2$  formed during CO pulses over surface treated with  $\text{H}_2\text{O}$  was  $48\mu\text{mol}/\text{g}_{\text{cat}}$  (Table 2).

When  $\text{Pt}/\text{TiO}_2$  was exposed to  $\text{N}_2\text{O}$  pulses, after subjecting it to CO pulses (Table 2) no  $\text{H}_2$  was observed.  $\text{N}_2$  was observed, but no  $\text{O}_2$  could be detected indicating oxygen uptake by the support. The amount of  $\text{N}_2$  (not shown) was close to the amount of  $\text{CO}_2$  formed during the following CO pulses ( $52\mu\text{mol}/\text{g}_{\text{cat}}$ ). Subsequent CO pulses (after  $\text{N}_2\text{O}$ ) resulted in  $\text{CO}_2$  production ( $50\mu\text{mol}/\text{g}_{\text{cat}}$ ); no  $\text{H}_2$  was detected. In case of the sequence “CO- $\text{N}_2\text{O}$ -CO- $\text{H}_2\text{O}$ ” the last  $\text{H}_2\text{O}$  pulse produced the same amount of  $\text{H}_2$  (semi-quantitatively) as compared with the amount produced during  $\text{H}_2\text{O}$  pulse after direct CO exposure.

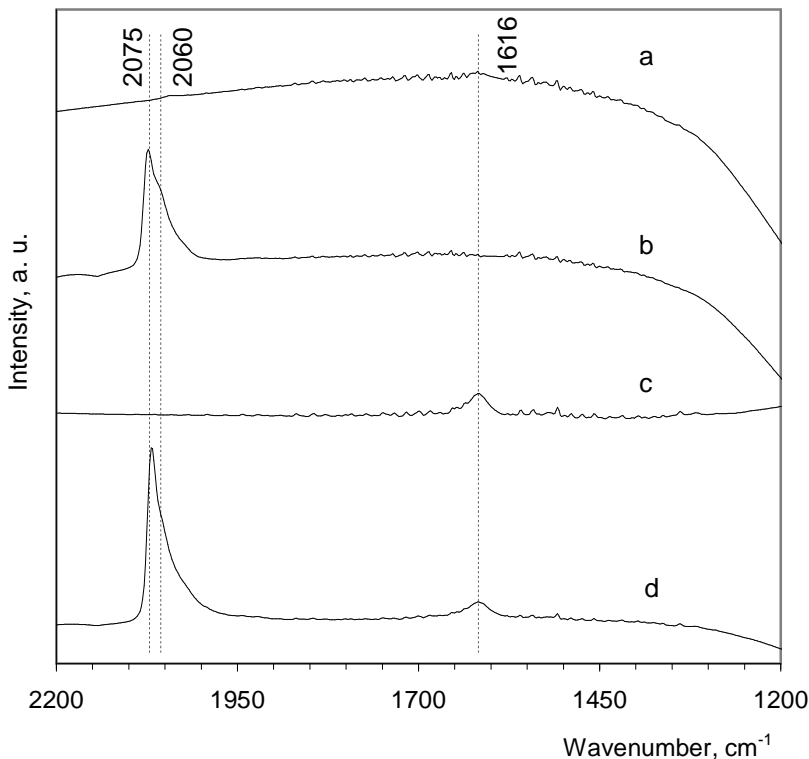


Fig. 6: FTIR spectra at  $300^\circ\text{C}$  of  $\text{Pt}/\text{TiO}_2$  catalyst; reduced in  $\text{H}_2(10\%)/\text{He}$  flow (a); after CO pulses (b); after  $\text{H}_2\text{O}$  pulses (c); *in situ* WGS conditions (d).

### 2.3.3 Pt/ZrO<sub>2</sub>

For Pt/ZrO<sub>2</sub> catalyst (Fig. 7), the trend was similar to that observed in the case of Pt/TiO<sub>2</sub>. CO pulses resulted in H<sub>2</sub> and CO<sub>2</sub> release. The amount of CO consumed was in agreement with amount of CO<sub>2</sub> released, both 40 μmol/g, closing the carbon balance. In agreement to this, no formation of stable carbonate/formate group was observed from FTIR (Fig. 8) for Pt/ZrO<sub>2</sub> after CO pulses. Only the band around 2050 – 2080 cm<sup>-1</sup> related to CO adsorbed on Pt [7] was present.

Surprisingly, in case of Pt/ZrO<sub>2</sub>, H<sub>2</sub>O pulses after CO exposure (Table 2) did not produce any gaseous products. However, pulsing H<sub>2</sub>O seemed to have regenerated the catalyst because the following CO pulses resulted in the formation of CO<sub>2</sub> and H<sub>2</sub>, similar to the initial CO pulses. In contrast, treatment with N<sub>2</sub>O reactivated Pt/ZrO<sub>2</sub> only partly. During the following CO pulses, consumption of CO and production of only CO<sub>2</sub> was observed, whereas only traces of H<sub>2</sub> were detected.

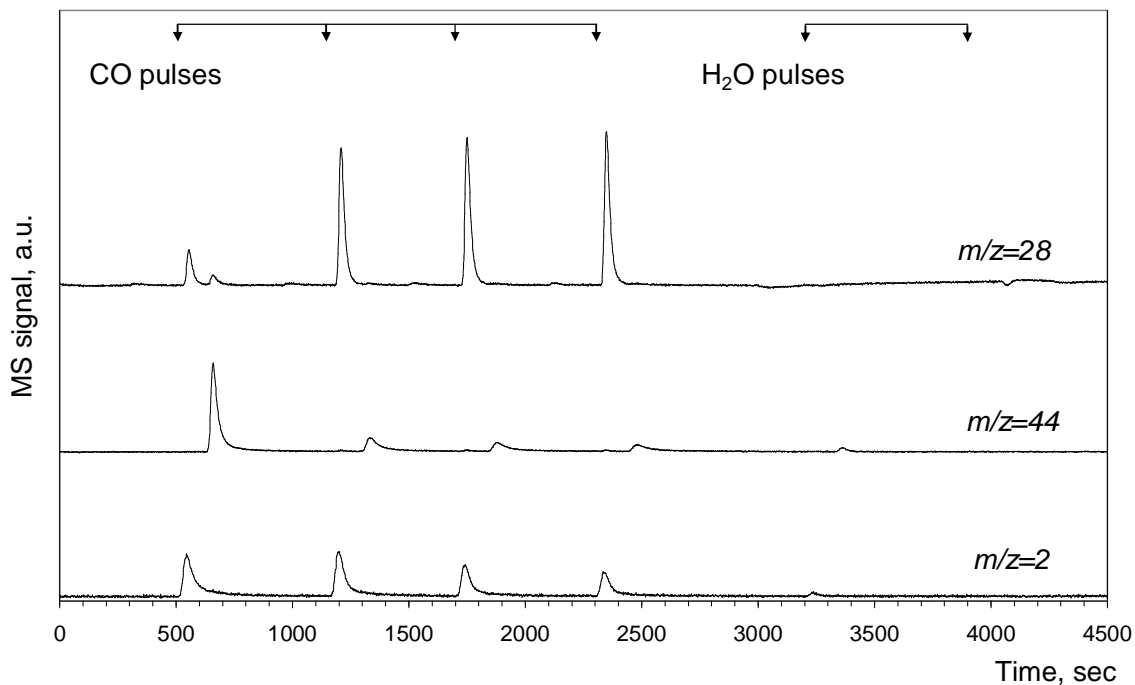


Fig. 7: Typical MS response for pulse experiment over Pt/ZrO<sub>2</sub> catalyst reduced at 300°C in H<sub>2</sub>(10%)/He flow. Four pulses CO are followed with two pulses H<sub>2</sub>O. Difference in time between products detected due to their separation with GC (porapak column).

## 2.4. Discussion

Kinetic pulse studies were used to follow the elementary steps that occur during WGS reaction. The results of pulse transient experiments are not directly equivalent to data obtained with steady state experiments; nonetheless, pulse experiments allow us to rule out those reaction pathways that cannot be induced by sequentially pulsing CO and H<sub>2</sub>O. Furthermore, the conclusion obviously only hold for the conditions chosen in this study, since it is reported elsewhere [38, 39] that the dominant reaction mechanism depends on the experimental parameters, such as reaction temperature and gas compositions.

As outlined in the introduction, two mechanistic routes have been reported in the literature for the WGS reaction sequence over Pt/CeO<sub>2</sub> catalysts, namely (i) an associative formate mechanism and (ii) regenerative red-ox mechanism. In our view, there are more possible routes to WGS reaction over oxide supported Pt catalysts. Four possible sequences are outlined in Fig. 9. These are (A) red-ox route, (B) associative formate route, (C) associative formate with a red-ox regeneration of the oxide support and (D) carbonate route. In all for sequences, we propose, in agreement with literature [24-30], that CO is adsorbed on Pt and reacts at the Pt-support periphery as in a typical bi-functional catalyst. The support oxide plays a role in the activation of water and to close the WGS catalytic cycle.

The feasible reaction route(s) for each support can be elucidated from kinetic pulse experiments based on the gaseous products formed during sequential CO and H<sub>2</sub>O pulses (Table 3). Thus, in the case of red-ox mechanism formation of only CO<sub>2</sub> or H<sub>2</sub> should be observed during CO and H<sub>2</sub>O pulses, respectively. For the associative formate route, CO pulsing should not result in any gaseous products but in stable intermediates, *i.e.* surface formate groups [5,6,31,32], which are decomposed during H<sub>2</sub>O pulse producing simultaneously CO<sub>2</sub> and H<sub>2</sub>. The associative formate route with a red-ox regeneration as proposed in Fig. 9 implies that intermediate formate specie are not stable and decompose immediately producing both CO<sub>2</sub> and H<sub>2</sub> during CO pulsing. The following H<sub>2</sub>O pulse should only regenerate hydroxyl-groups at the support surface without releasing any

gaseous products. In this case (Route C) CO<sub>2</sub> is formed taking oxygen from the oxide support surface, whereas in the classical associative formate mechanism (Route B) oxygen for CO<sub>2</sub> is supplied by H<sub>2</sub>O.

We will now discuss the results obtained with Pt catalysts over different supports in view of the various proposed routes.

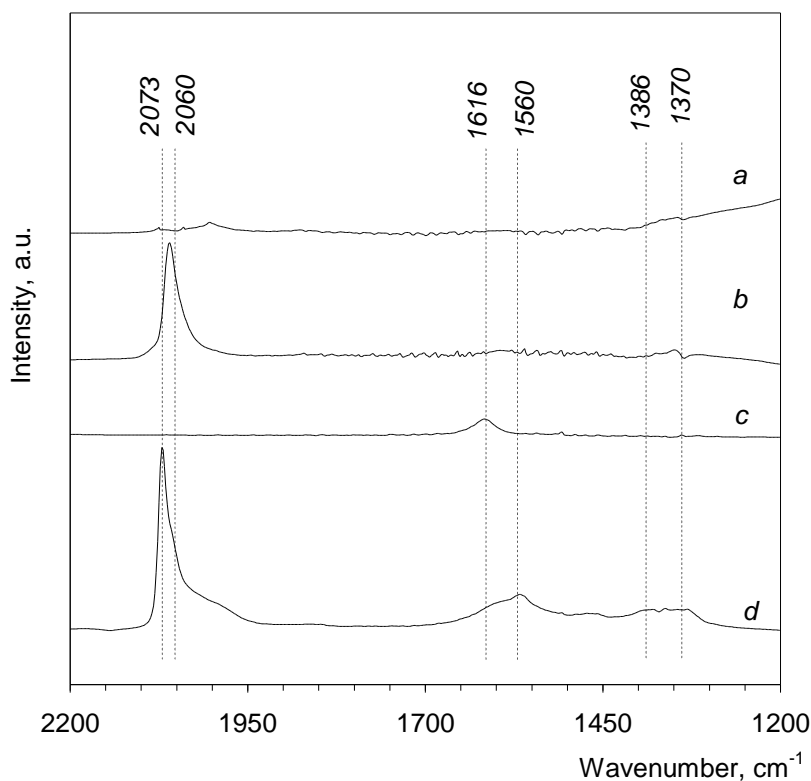


Fig. 8: FTIR spectra at 300°C of Pt/ZrO<sub>2</sub> catalyst; reduced in H<sub>2</sub>(10%)/He flow (a); after CO pulses (b); after H<sub>2</sub>O pulses (c); *in situ* WGS condition (d).

In the case of Pt/CeO<sub>2</sub>, the results presented indicate that the WGS reaction follows an associative formate mechanism, in agreement with earlier reported data [4-6,13,31,32]. Evidence for this comes from the observation in FTIR spectra (Fig. 3 and 4) of formates on Pt/CeO<sub>2</sub> after pulsing CO. This is further supported by the simultaneous formation of H<sub>2</sub> and CO<sub>2</sub> during H<sub>2</sub>O pulses (Table 2, row I). Furthermore, the carbon uptake (90 μmol/g<sub>cat</sub>) was much higher than would be expected from exclusively CO adsorption on Pt (16 μmol/g<sub>cat</sub> if CO to surface-Pt is 1:1, which is typical for CO adsorption over Pt at room temperature [40]).



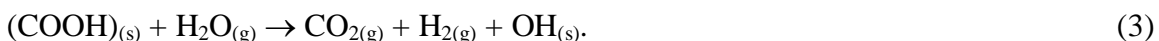
formate/carbonate surface species, in agreement with FTIR observation (Fig. 3 and 4). The amount of carbon remaining on the ceria surface ( $90 \mu\text{mol/g}_{\text{cat}}$ ) is much smaller than the calculated monolayer capacity ( $6.10^{18}$  molecule/m<sup>2</sup> [41]) for the CeO<sub>2</sub> support for carbonate and/or formate groups, i.e.  $810\mu\text{mol/g}_{\text{cat}}$ . It is very difficult to assign the bands observed in Fig. 3 to either formate or carbonate, despite of the significant efforts made in literature [5,14,31,37], the bands are very broad and too strongly overlapping to make definite assignments. However, the band at  $2856 \text{ cm}^{-1}$  (C-H stretching of formate [31]) shows presence of formate species on ceria surface during CO pulses. In this paper, we will not go into the details of differentiating between formate and carbonate bands in the IR spectra (Fig. 3), however, for the moment we can only conclude that both oxygenate species are formed during CO pulsing, they are stable and their formation can be described by following equations:



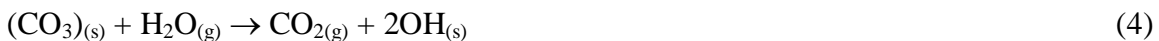
and



where (s) denotes support site. We conclude that formation of CO<sub>2</sub> and H<sub>2</sub> during the following H<sub>2</sub>O pulse is due to decomposition of formate since formate is known to be unstable on ceria in presence of H<sub>2</sub>O [5, 31, 42]. This is also substantiated by the disappearance of formate band at  $2856 \text{ cm}^{-1}$  in FTIR results (Fig. 4).



In agreement with literature [43], carbonates were retained on ceria at this temperature even in presence of water. However, we do not, at this point, exclude decomposition of part of surface carbonates during H<sub>2</sub>O pulses.



Both reactions (3) and (4) result in re-hydroxylation of the ceria surface closing the catalytic cycle for the WGS reaction.

In the absence of OH groups, the formate route is not possible. The importance of OH<sub>(s)</sub> groups in the WGS reaction is confirmed by the experiments with N<sub>2</sub>O over Pt/CeO<sub>2</sub> containing formate/carbonate groups (Table 2, row Ia). It is important to emphasize that

N<sub>2</sub>O is not involved in WGS reaction. However, the aim of using N<sub>2</sub>O here is to decompose the surface formate formed during CO pulses without regenerating the hydroxyl groups. In this way, the catalyst will be free of reactive OH groups and thus it is possible to probe if a red-ox pathway (Fig. 9, route A) is involved in the reaction mechanism. During N<sub>2</sub>O pulses, both H<sub>2</sub> and CO<sub>2</sub> were formed (Table 2, row Ia) indicating the decomposition of surface formate:



The subsequent CO pulse (Table 2, row Ia) did not produce any hydrogen, as expected. Part of the CO is oxidized and released to gas phase as CO<sub>2</sub>. The remaining CO (85 μmol/g<sub>cat</sub>) is retained on ceria. The carbon balance was quite good. The amount (85 μmol/g<sub>cat</sub>) was remarkably close to the amount of carbon retained (90 μmol/g<sub>cat</sub>, as both carbonate and formate in total) in row A after CO pulse. Because no hydroxyl groups were available (regeneration was by N<sub>2</sub>O, not H<sub>2</sub>O), creation of the formate specie on the ceria surface could be ruled out. Only carbonates are present. Thus, in the absence of formates, some sites are occupied by carbonates, implying that under WGS conditions carbonates and formates were competing for surface sites on ceria.

The fact that only carbonates were present and formates were absent is further highlighted by the absence of hydrogen formation during the subsequent H<sub>2</sub>O pulse (row Ia). If formates had been present, we would have seen hydrogen when pulsing water (Row I). Only partial decomposition of the carbonates (~65%) to CO<sub>2</sub> is observed (Table 2, row Ia). This observation unambiguously proves that an associative formate mechanism (reaction 1, route B in Fig. 9) contributes significantly to H<sub>2</sub> formation. Alternatively, formation of CO<sub>2</sub> during CO pulses can also be a result of the reduction of the ceria surface according to the sequence



where \*<sub>(s)</sub> denotes an oxygen vacancy on the support. In principle, oxidation of these sites by H<sub>2</sub>O can proceed in two ways:



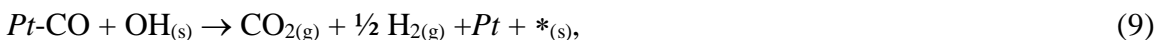
Reaction 7, which completes a typical red-ox cycle with reaction (6), can be neglected based on the results from the “N<sub>2</sub>O-CO-H<sub>2</sub>O” pulse sequence (row Ia), since no H<sub>2</sub> was observed as would be expected. Formation of hydroxyl groups *via* reaction 8 is possible.

There is only a subtle difference between reactions (3) and (8). In reaction (3), the oxygen of the OH group comes from the water molecule, and oxygen from ceria is not involved. This would be a classical associative mechanism (route B, Fig. 9). In reaction (8), oxygen from ceria is also involved in hydroxyl formation and thus consequently also in formate formation. This would then be an associative mechanism involving red-ox regeneration (route C, Fig 9).

Based on the results over Pt/CeO<sub>2</sub> catalyst under these experimental conditions, we conclude that WGS reaction proceeds *via* associative mechanism (route B, Fig. 9). We exclude route C from the reaction pathways because no H<sub>2</sub> formation occurred during CO pulses. Route A is also not involved because there was no H<sub>2</sub> formation during H<sub>2</sub>O pulses after oxidizing the reduced ceria with N<sub>2</sub>O (H<sub>2</sub>O after CO-N<sub>2</sub>O-CO pulses, Table 2, row Ia). At this moment, we do not rule out route D. However, because (i) cerium carbonate is stable up to 430°C [43] and (ii) Pt/CeO<sub>2</sub> deactivated due to the blocking of the active sites by carbonate [16]; we propose that route D does not contribute to WGS reaction. This is substantiated by the fact that no hydrogen was formed during H<sub>2</sub>O pulses after the sequence (CO-N<sub>2</sub>O-CO), when only carbonates were present.

Gorte *et al.* [28] recently reported that WGS proceeds via the red-ox mechanism at 450°C over Pt/CeO<sub>2</sub> catalyst, based on the responses to CO and H<sub>2</sub>O pulses at 450°C. Both CO<sub>2</sub> and H<sub>2</sub> were formed during CO pulses [28]. This observation was explained by interaction of CO with hydroxyl H<sub>2</sub>, reducing the ceria and forming H<sub>2</sub> and CO<sub>2</sub>. As a result of H<sub>2</sub>O pulses, both CO<sub>2</sub> and H<sub>2</sub> were also formed. It was claimed that H<sub>2</sub> formation is due to oxidation of reduced ceria and that CO<sub>2</sub> formation results from decomposition of carbonate. However, the temperature in the work of Gorte *et al.* is significantly higher (450°C) as compared to our study (300°C). Formates and carbonates are not stable at the higher temperature, inducing a change in mechanism.

In the case of Pt/TiO<sub>2</sub>, the sequence for WGS reaction is different from that for ceria discussed above. Unlike Pt/CeO<sub>2</sub>, H<sub>2</sub> is also formed simultaneously with CO<sub>2</sub> during CO pulsing (Table 2, row II,). There is only one source for hydrogen in the Pt/TiO<sub>2</sub> catalyst during CO pulsing at 300°C-surface hydroxyl groups. Thus, the net reaction can be represented as



and this would correspond to an associative mechanism with red-ox regeneration in our scheme (route C, Fig. 9). It is not clear at this moment which type of hydroxyl groups on reduced Pt/TiO<sub>2</sub> surface is relevant for WGS reaction. This requires additional studies, which are beyond the scope of this article.

The carbon balance indicates that no carbon specie was left on the surface (row II). This is also confirmed by *in-situ* FTIR measurements (Fig. 6). The fact that no formate/carbonate species were detected under reaction conditions implies that their decomposition to CO<sub>2</sub> and H<sub>2</sub> is facile. We propose, in agreement with Panagiotopoulou *et al.* [10], that formate type intermediates are the only relevant oxygenate species to WGS sequence over Pt/TiO<sub>2</sub> catalyst. Thus, an associative formate mechanism with red-ox regeneration is operative. We can also confirm that CO is quantitatively converted to gaseous products in the case of TiO<sub>2</sub>. This is unlike ceria where part of the CO is retained as carbonate, occupying sites for formate formation, which cannot yield any hydrogen.

Contacting the catalyst with water after exposure to CO (Table 2, row II) results in hydrogen (no CO<sub>2</sub> was observed as no oxygenate was left on the surface). Formation of hydrogen indicates that re-oxidation of the support occurs according to



It was reported before that the surface of TiO<sub>2</sub> is can be reduced by CO (Eq. 11) and oxidized by H<sub>2</sub>O [44],



The red-ox nature of TiO<sub>2</sub> is also indicated by the formation of hydrogen during the water pulsing after a “CO-N<sub>2</sub>O-CO” sequence. Therefore, we cannot exclude, as in the case of

CeO<sub>2</sub> and ZrO<sub>2</sub> (see below), the red-ox route (route A, Fig. 9) for the WGS in case of Pt/TiO<sub>2</sub> implying involvement of the sequence of reactions (10) and (11). Quantitative determination of the amount of H<sub>2</sub> produced during CO pulsing (Table 2, row II) would enable discrimination, but these data were unfortunately not available.

We conclude from the above results that both oxygen vacancies on the reduced TiO<sub>2</sub> and hydroxyl groups on TiO<sub>2</sub> can take part in the catalysis of WGS reaction. Thus, both the associative with red-ox regeneration pathway (route C, Fig. 9) and the classical red-ox pathway (route A, Fig. 9) may significantly contribute in the WGS mechanism. Route B can be excluded because there was no CO<sub>2</sub> formation during H<sub>2</sub>O pulses (Table 2, row II). Route D can again be ruled out because (i) there was no CO<sub>2</sub> formation during H<sub>2</sub>O pulses after oxidizing the reduced titania with N<sub>2</sub>O (H<sub>2</sub>O after CO-N<sub>2</sub>O-CO pulses, Table 2, row IIa) and (ii) carbonate is not present on TiO<sub>2</sub> after pulsing CO according to FTIR data (Fig. 6). Activity of Pt/TiO<sub>2</sub> seems to be determined by the ability of TiO<sub>2</sub> to undergo red-ox as well as allow formation of OH groups. Decomposition of the intermediate formate species seems to be facile.

For Pt/ZrO<sub>2</sub> catalyst, WGS reaction seems to follow an associative route with red-ox regeneration (route C, Fig. 9). During CO pulses, the catalyst showed behavior similar to Pt/TiO<sub>2</sub>. CO pulsing results in CO<sub>2</sub> and H<sub>2</sub> formation, which can be described by reaction (9), part of route C in Fig. 9. The carbon balance indicates that no carbon specie was left on the surface (Table 2, row III). This is also confirmed by *in-situ* FTIR measurements (Fig. 8). It is still not clear whether intermediate formate species are involved. They can be observed with *in-situ* FTIR during reaction (Fig. 8), but as soon as the flow is switched to inert gas the bands disappeared from the spectrum. During H<sub>2</sub>O pulses, no gaseous products were observed but the catalyst was able to produce CO<sub>2</sub> and H<sub>2</sub> at the next CO pulse. From this, we conclude that route B is not operative and that catalyst activation occurs mainly due to hydroxyl groups formed according to (8).

Normally ZrO<sub>2</sub> is considered as a non-reducible oxide, even though evidence exists that the surface is partly reducible at relatively higher temperatures (>600°C) [45]. However,

the fact that at 300°C, CO<sub>2</sub> and H<sub>2</sub> were formed on a hydroxylated surface (Table 2, row III), implies that the surface OH groups were converted, leaving an oxygen vacancy (route C, Fig. 9). When this surface is reoxidized by N<sub>2</sub>O, no active hydroxyls are formed. The observation that CO<sub>2</sub> is detected (Table 2, row IIIa) during CO pulsing after the CO - N<sub>2</sub>O sequence, demonstrates that some lattice oxygen can be removed even at 300°C (6). Therefore, both observations demonstrate that ZrO<sub>2</sub> is able to provide oxygen. We speculate that low coordination sites in the zirconia surface are responsible. Accordingly, regeneration occurs according (8), similar to titania. The gaseous product distribution during pulse experiments indicates that WGS reaction over Pt/ZrO<sub>2</sub> follows the associative mechanism with red-ox regeneration (route C, fig. 9). Routes A, B and D can be excluded since there were no gaseous products during H<sub>2</sub>O pulses (Table 2, row III). Recently, Trovarelli *et al.* [46], using isotopic transient kinetics (<sup>12</sup>CO and <sup>13</sup>CO) and in situ DRIFTS at 200°C, concluded that oxygenates, not excluding formate, are involved as a reaction intermediate, in agreement with our conclusion.

## 2.5. Conclusion

The reducibility of the support as well as the stability of formate and carbonate species together determine the reaction pathways contributing to the WGS reaction. Water activation is achieved over the support through formation of surface hydroxyl groups on oxides and/or oxidation of the reduced support with H<sub>2</sub>O, resulting in H<sub>2</sub> formation. Under the experimental conditions of this work (300°C), it appears that the classical associative mechanism is in operation (route B) for Pt/CeO<sub>2</sub>. In Pt/ZrO<sub>2</sub>, the dominant reaction pathway is associative formate route with red-ox regeneration (route C), implying that OH groups react with CO, leaving oxygen vacancies. This result is surprising as ZrO<sub>2</sub> is much more difficult to reduce than CeO<sub>2</sub>. Apparently, the remarkable stability of surface formates on CeO<sub>2</sub> contributes to this. Finally, for Pt/TiO<sub>2</sub>, both the associative formate route with red-ox regeneration (route C) as well as the classical red-ox route (route A) are possible reaction pathways contributing to the WGS reaction. Pt/TiO<sub>2</sub> was the only catalyst able to dissociate H<sub>2</sub>O to H<sub>2</sub> while re-oxidizing oxygen vacancies generated by reduction with CO.

## 2.6. References

- [1] D. S. Newsome, *Catal. Rev. – Sci. Eng.* 21 (1980) 275.
- [2] C.H. Bartolomew, R.J. Farrauto, in: C.H. Bartolomew, R.J. Farrauto (Eds.) *Fundamentals of industrial catalytic processes*, John Wiley & Sons, Hoboken, NJ, 2006, p. 909.
- [3] W. Ruettinger, O. Ilinich, R. J. Farrauto, *J. Power Sources* 118 (2003) 61.
- [4] G. Jacobs, S. Ricote, B. H. Davis, *Appl. Catal. A* 302 (2006) 14.
- [5] G. Jacobs, U. M. Graham, E. Chenu, P. M. Patterson, A. Dozier, B. H. Davis, *J. Catal.* 229 (2005) 499.
- [6] A. Goguet, S. O. Shekhtman, R. Burch, C. Hardcare, F. C. Meunier, G. S. Yablonsky, *J. Catal.* 237 (2006) 102.
- [7] E. Chenu, G. Jacobs, A. C. Crawford, R. A. Keogh, P. M. Patterson, D. E. Sparks, B. H. Davis, *Appl. Catal. B* 59 (2005) 45.
- [8] E. Xue, M. O'Keefe, J. R. H. Ross, *Surf. Sci. Catal.* 130 (2000) 3813.
- [9] Y. Sato, K. Terada, S. Hasegawa, T. Miyao, S. Naito, *Appl. Catal. A* 296 (2005) 80.
- [10] P. Panagiotopoulou, A. Christodoulakis, D. I. Kondarides, S. Boghosian, *J. Catal.* 240 (2006) 114.
- [11] H. Iida, A. Igarashi, *Appl. Catal. A* 298 (2006) 152.
- [12] P. S. Querino, J. R. C. Bispo, M.C. Rangel, *Catal. Today* 107-108 (2005) 920.
- [13] S. Y. Choung, M. Ferrandon, T. Krause, *Catal. Today* 99 (2005) 257.
- [14] S. Ricote, G. Jacobs, M. Milling, Y. Ji, P. M. Patterson, B. H. Davis, *Appl. Catal. A* 303 (2006) 35.
- [15] W. Ruettinger, X. Liu, R.J. Farrauto, *Appl. Catal. B* 65 (2006) 135.
- [16] K. G. Azzam, I.V. Babich, K. Seshan and L. Lefferts, *J. Catal.* 251 (2007) 163.
- [17] H. Iida, K. Kondo, A. Igarashi, *Catal. Comm.* 7 (2006) 240.
- [18] O. Goerke, P. Pfeifer, K. Schubert, *Appl. Catal. A* 263 (2004) 11.
- [19] Brunetti, G. Barbieri, E. Drioli, K.-H. Lee, B. Sea and D.-W. Lee, *Chem. Eng. Proc.* 46 (2007) 119.

- [20] M. E. Adrover, E. Lopez, D. O. Borio, M. N. Pedernera, in: F. N. Noronha, M. Schmal, E. F. Sousa-Aguiar (Eds.), *Studies in Surface Science and Catalysis* 167 (2007) Elsevier, Amsterdam, p.183
- [21] Ch. Han, D. P. Harrison, *Chem. Eng. Sci.* 49 (1994) 5875.
- [22] D. Tibiletti, E. A. Bart de Graaf, S. Ph. Teh, G. Rothenberg, D. Farrusseng, C. Mirodatos. *J. Catal.* 225 (2004) 489.
- [23] O. Pozdnyakova, D. Teschner, A. Wootsch, J. Kröhnert, B. Steinhauer, H. Sauer, L. Toth, F.C. Jentoft, A. Knop -Gericke, Z. Paál, R. Schlögl, *J. Catal.* 237 (2006) 17.
- [24] M. A. Henderson, *Surf. Sci. Rep.* 46 (2002) 1.
- [25] J. R. Rostrup-Nielsen, in: J.R. Anderson and M. Boudart (Eds), *Catalysis, Science and Technology*, Springer-Verlag, Berlin, 1984, Vol 5, p. 1.
- [26] K. Takanabe, K. Aika, K. Seshan and L. Lefferts, *J. Catal.* 227 (2004) 101.
- [27] T. Bunluesin, R. J. Gorte, G.W. Graham, *Appl. Catal. B* 15 (1998) 107.
- [28] R. J. Gorte, S. Zhao, *Catal. Today* 104 (2005) 18.
- [29] P. Panagiotopoulou, D. I. Kondarides, *Catal. Today* 112 (2006) 49.
- [30] D. C. Grenoble, M. M. Estadt, D. F. Ollis, *J. Catal.* 67 (1981) 90.
- [31] G. Jacobs, E. Chenu, P. M. Patterson, L. Williams, D. Sparks, G. Thomas, B. H. Davis, *Appl. Catal. A* 258 (2004) 203.
- [32] G. Jacobs, S. Ricote, U.M. Graham, P.M. Patterson, B. H. Davis, *Catal. Today.* 106 (2005) 259.
- [33] S. Hilaire, X. Wang, T. Luo, R.J. Gorte, J. Wagner, *Appl. Catal. A* 215 (2001) 271.
- [34] X. Wang, R.J. Gorte, *Appl. Catal. A* 247 (2003) 157.
- [35] H. Sakurai, T. Akita, S.Tsubota, M. Kiuchi, M. Haruta, *Appl. Catal. A* 291 (2005) 179
- [36] D. Teschner, A. Wootsch, T. Roder, K. Matusek, Z. Paal, *Solid State Ionic* 141-142 (2001) 709.
- [37] A. Holmgren, B. Andersson, D. Duprez, *Appl. Catal. B* 22 (1999) 215.
- [38] D. Tibiletti, A. Goguet, F. C. Meunier, J. P. Breen, R. Burch, *Chem. Comm.* 14 (2004) 1636.
- [39] A. Goguet, F. C. Meunier, D. Tibiletti, J. P. Breen, R. Burch, *J. Phys. Chem. B* 108 (2004) 20240.

- [40] P. B. Wells, *Appl. Catal.* 18 (1985) 259.
- [41] S. Sharma, S. Hilaire, J. M. Vohs, R. J. Gorte, H. W. Jen, *J. Catal.* 190 (2000) 199.
- [42] G. Jacobs, P.M. Patterson, L. Williams, D. Sparks, B.H. Davis, *Catal. Lett.* 96 (2004) 97.
- [43] X. Liu, W. Ruettinger, X. Xu, R. Farrauto, *Appl. Catal. B* 56 (2005) 69.
- [44] M. Calatayud, A. Markovits, M. Menetrey, B. Mguig, C. Minot, *Catal. Today* 85 (2003) 125.
- [45] J. Zhu, S. Albertsma, J. G. van Ommen, L. Lefferts, *J. Phys. Chem. B* 109 (2005) 9550.
- [46] D. Tibiletti, F. C. Meunier, A. Goguet, D. Reid, R. Burch, M. Boaro, M. Vicario, A. Trovatelli, *J. Catal.* 244 (2006) 183.

# Chapter 3

## Role of support and promoter on catalyst activity and stability

---

### *Abstract*

*The nature of oxide supports has a crucial effect on the performance of Pt based catalyst in water gas shift reaction. Supports not only determine the activity of the catalyst, but also influence their stability (deactivation mechanism). Among the catalysts studied, Pt/TiO<sub>2</sub> was the most active catalyst. Pt/CeO<sub>2</sub> deactivated with time due to formation of stable carbonate on ceria surface. Sintering of Pt was found to be the cause of Pt/TiO<sub>2</sub> deactivation. Using-mixed-oxides as catalyst supports did not improved the activity despite the better red-ox properties of mixed-oxides compared with the single-oxide supports. Pt/TiO<sub>2</sub> could be stabilized by adding a second metal (Re), which prevents Pt sintering. In addition, Pt-Re/TiO<sub>2</sub> catalyst was more active than Pt/TiO<sub>2</sub>. Under WGS conditions, part of Re was present in oxidizing form (ReO<sub>x</sub>); we speculate that this helped improve the catalyst activity.*

**Keywords:** *WGS reaction; Platinum; Rhenium; Tin; Oxide supports; Activity; Stability; Deactivation*

### 3.1. Introduction

The Water Gas Shift (WGS) reaction,  $\text{CO} + \text{H}_2\text{O} \rightleftharpoons \text{CO}_2 + \text{H}_2$ , is applied in the conversion of syngas produced by steam reforming or partial oxidation of hydrocarbons to increase  $\text{H}_2$  yield [1]. In recent years, there has been renewed interest in this reaction because of its potential for use in  $\text{H}_2$  based fuel cells in mobile applications.

In chapter 2 [2], we reported based on spectroscopic and kinetic transient studies, that the support plays a crucial role in determining the WGS reaction sequence over Pt-based catalysts. These catalysts are thus bi-functional, with CO activated over metal platinum and  $\text{H}_2\text{O}$  activated over the support oxide surface [3-5]. Platinum has been reported to also facilitate the decomposition of intermediate surface formate in the presence of  $\text{H}_2\text{O}$  [6]. We showed earlier [2] that the nature of the support not only determined the mode of activation of  $\text{H}_2\text{O}$  (either by formation of surface hydroxyls or *via* oxidation of reduced support with  $\text{H}_2\text{O}$  forming  $\text{H}_2$ ), but also affected the formation and stability of the intermediates (*e.g.* formates, carbonates) on the catalyst surface.

Various oxide supports that differ in term of reducibility or oxygen mobility (*e.g.*  $\text{CeO}_2$  [6-10],  $\text{TiO}_2$  [11],  $\text{ZrO}_2$  [12]) supporting noble metals have been reported as promising WGS catalysts. Catalyst activity reportedly depends on catalyst preparation [6,11,13,14], catalyst testing conditions and reactor designs [15].

Ceria has been reported as an oxide support with high red-ox capacity and mobility of surface oxygen/hydroxyl groups [16]. Reduction of  $\text{Ce}^{4+}$  to  $\text{Ce}^{3+}$  aids in the formation of bridging hydroxyls, which are claimed to be active for WGS reaction [6-10]. Our results of *in situ* IR and kinetic studies [2] confirmed that over Pt/ $\text{CeO}_2$ , the WGS reaction proceeds *via* the classical associative formate mechanism, in agreement with others [5-7].

Although titania is more resistant to reduction in comparison to ceria, it can be partially reduced under the WGS reaction conditions studied. Calatayud *et al.* [17] reported that reduction of  $\text{TiO}_2$  is facile, resulting in creation of oxygen vacancies (defects) *via* the

reduction of the cation charge ( $\text{Ti}^{x+}$ ,  $x < 4$ ). We showed [2] that the oxygen vacancies over Pt/TiO<sub>2</sub> catalyst, formed by the reduction with CO, could dissociate H<sub>2</sub>O to H<sub>2</sub> and regenerate surface oxygen sites and also form hydroxyls groups. For Pt/TiO<sub>2</sub>, both the classical red-ox route and the associative formate route with red-ox regeneration [2] are possible reaction pathways for the WGS reaction.

Although ZrO<sub>2</sub> is a difficult-to-reduce oxide [18], it can form hydroxyl groups in the presence of water [19]. Nevertheless, we demonstrated that surface oxygen on ZrO<sub>2</sub> catalyst is reactive at WGS reaction temperature (300°C) [2]. The dominant reaction pathway is the associative formate route with a red-ox regeneration.

Thus, WGS reaction in the case of Pt/TiO<sub>2</sub> and Pt/ZrO<sub>2</sub> catalysts follows a pathway which includes a red-ox step. Red-ox properties of bulk oxides can be effectively modified by incorporation of dopant atoms. It has been shown [20,21] that incorporation of Zr into CeO<sub>2</sub> lattice promotes the red-ox properties of the support. Recently, Ruettinger *et al.* [22] reported that addition of Zr to CeO<sub>2</sub> improved the catalyst performance in the WGS reaction by suppressing the carbonate build up on CeO<sub>2</sub> surface. Dong *et al.* [23] found that palladium supported over ceria-titania mixed oxides (Pd/CeO<sub>2</sub>-TiO<sub>2</sub>) have superior activity for CO oxidation compared with Pd/CeO<sub>2</sub> or Pd/TiO<sub>2</sub> catalyst under the same condition. These findings suggest that manipulating the red-ox properties of the supports and surface oxygen mobility could be a way to improve catalyst performance.

Investigation of mechanistic pathways over supported Pt catalysts in chapter 2 [2] indicate that water activation can follow different sequences (hydroxyl formation vs red-ox water splitting) and thus influence catalytic activity. Further, we showed that the support influences the reaction pathway (formate vs. red-ox routes) which also may result in different catalytic activities. In addition, the formation of carbonate-type species on the support blocks sites for water activation and are detrimental to catalyst stability. Thus studies on WGS catalysts based on supports with varying red-ox properties, hydroxyl formation, and carbonate stability would be useful in designing efficient WGS catalysts.

In this work, we report on the activity, selectivity, and stability of Pt based catalysts studied in chapter 2, along with catalysts with enhanced red-ox properties based on mixed oxides. We investigate deactivation scenarios for different supports and describe possible ways to regenerate and stabilize catalyst activity.

## 3.2. Experimental

### 3.2.1. Catalyst preparation

This study used commercial supports: TiO<sub>2</sub> (Degussa, P-25), CeO<sub>2</sub> (Aldrich), and ZrO<sub>2</sub> (Daiichi Kagaku Kogyo, RC100). A series of mixed oxides supports were prepared in our laboratory. Ce<sub>x</sub>Zr<sub>1-x</sub>O<sub>2</sub> (x=0.2, 0.5) solid solutions were prepared by the co-precipitation using appropriate ratios of Ce(NO<sub>3</sub>)<sub>3</sub>.6H<sub>2</sub>O (99.99% Aldrich) and ZrOCl<sub>2</sub> (99.9% ABCR) [20]. Mixed Ti<sub>x</sub>Ce<sub>1-x</sub>O<sub>2</sub> and Ti<sub>x</sub>Zr<sub>1-x</sub>O<sub>2</sub> (x=0.2; 0.5) were prepared by the sol-gel method using an ethanol solution of Titanium (IV) iso-propoxide (98%) and an aqueous solution of Ce(NO<sub>3</sub>)<sub>3</sub>.6H<sub>2</sub>O (0.4M) or ZrOCl<sub>2</sub> (0.4M). The precursor solutions were mixed in appropriate amounts at room temperature and left for 24 h to form a gel. After gelation, the samples were dried under vacuum in a rotary evaporator at 75°C for 3 h. All of the supports were calcined at 500°C for 4 h before Pt incorporation.

The monometallic catalysts were prepared by wet impregnation of supports with aqueous solutions of H<sub>2</sub>PtCl<sub>6</sub>. Required amounts of H<sub>2</sub>PtCl<sub>6</sub> solution were used to yield catalysts with 0.5wt% Pt. The bimetallic (Pt/Re and Pt/Sn) on TiO<sub>2</sub> catalysts were prepared with 0.5wt% of Pt and Pt/Re or Pt/Sn molar ratio close to unity. TiO<sub>2</sub> was impregnated first with the required concentration of NH<sub>4</sub>ReO<sub>4</sub> or SnCl<sub>2</sub>.2H<sub>2</sub>O for 1 h at room temperature and then contacted with H<sub>2</sub>PtCl<sub>6</sub> before drying to yield 0.5wt%Pt-0.48wt%Re/TiO<sub>2</sub> and 0.5wt%Pt-0.3wt%Sn/TiO<sub>2</sub> catalysts, respectively.

All catalysts prepared in this study were dried at 75°C for 2 h under vacuum in a rotary evaporator and subsequently calcined at 450°C for 4 h (heating rate 10°C min<sup>-1</sup>).

### 3.2.2. Characterization

The surface areas of the catalysts were measured with the BET method using a Micromeritics ASAP 2400 device. Platinum loading was determined using a Philips PW 1480 X-ray Fluorescence Spectrometer. Pt dispersions for all of the catalysts except Pt-Re/TiO<sub>2</sub> were measured with H<sub>2</sub> chemisorption at room temperature using a Micromeritics Chemisorb 2750. Teschner *et al.* [24] showed in a detailed study that significant hydrogen spill-over did not occur on Pt/CeO<sub>2</sub> at lower temperatures (*e.g.* 20°C), resulting in reliable dispersion measurements. This demonstrates that H<sub>2</sub> spillover from Pt particles to support surface does not influence dispersion measurements in the ceria supported catalysts. CO chemisorption at room temperature was used to measure the dispersion of Pt in Pt-Re/TiO<sub>2</sub> catalyst based on the finding of Pieck *et al.* [25] and Carvalho *et al.* [26]. Based on the comparison of Pt particle size measured by H<sub>2</sub> or CO chemisorption with TEM results, these authors reported that addition of Re to Pt decreases the chemisorption capacity for H<sub>2</sub>. They found that Pt particle size was comparable with CO chemisorption and TEM; but was much larger with H<sub>2</sub> chemisorption; this result did not match with TEM data. Moreover, Re did not chemisorb CO at 30-50°C [25]. This is also in agreement with our IR results (not shown) on Pt-Re/TiO<sub>2</sub>, showing that, at room temperature, CO was only adsorbed on Pt.

The Platinum particle size for Pt/TiO<sub>2</sub> and Pt-Re/TiO<sub>2</sub> catalysts was also measured with a TEM using Philips CM30 microscope, with sizes of about 30 particles.

The oxidation state of rhenium in Pt-Re/TiO<sub>2</sub> catalyst was characterized with X-ray Photoelectron spectroscopy (XPS) using  $\Phi$  Quantera Scanning ESCA Microprobe spectrometer using Al K <sub>$\alpha$</sub>  (1486.7 eV, 25.64 W).

Temperature programmed reduction (H<sub>2</sub>-TPR) studies were conducted in a Micromeritics Autochem II 2920 device. Here 1 g of catalyst was placed in a U-quartz tube and preheated to 300°C and then cool down to -75°C under Ar flow (20 ml/min). Once the TCD signal was stabilized, the feed was switched to 15% H<sub>2</sub>/Ar flow (20 ml/min). The temperature of the sample was raised from -75 to 850°C at a constant rate of 10°C/min.

### 3.2.3. Catalytic tests

Catalytic tests for WGS reaction were carried out in a fixed bed quartz tubular reactor (3 mm i.d.) under differential conditions. Typically, the catalysts were pressed into pellets, crushed, and sieved to yield grains having diameter between 0.25 and 0.3 mm. A 10 mg of catalyst diluted with 90 mg quartz grains (0.25-0.30 mm) was packed between two layers of quartz wool. Using the quartz grains ensured plug flow criterion and minimized the effect of heat generated by the exothermic reaction. The temperature of the catalyst bed was monitored by thermocouples (Fe-Cr) and maintained by a temperature controller (Eurotherm, 2416). All catalysts were first reduced in 10% H<sub>2</sub> in N<sub>2</sub> (total flow was 100ml/min) for 30 min and subsequently purged with N<sub>2</sub> for another 30 min at 300°C. All gases used (He, H<sub>2</sub>, N<sub>2</sub>, CO<sub>2</sub>, and CO) were of > 99.9 % purity. A gas mixture containing 3 vol. % CO, 7.5% H<sub>2</sub>O and N<sub>2</sub> balance was used for catalytic tests. Steam was provided to the system *via* a steam generator consisting of a hollow cylinder (i.d. 50 mm, L 150 mm) packed with quartz wool. Water was fed by a pulse-free syringe pump (ISCO series D) into the steam generator *via* a long capillary tube (5m) in order to obtain a stable water concentration. The whole system was heated to 125°C to avoid condensation of H<sub>2</sub>O. The feed was adjusted in bypass mode to obtain constant CO/H<sub>2</sub>O/N<sub>2</sub> (=3/7.5/89.5 mol/mol%, N<sub>2</sub> as an internal standard) before the experiment. The total flow rate of the feed gas into the reactor was kept at 350 ml/min using Brooks mass flow controllers. The inlet and outlet gases (CO, CO<sub>2</sub>, H<sub>2</sub>, H<sub>2</sub>O, and N<sub>2</sub>) were analyzed using Varian Micro GC (CP4900) using MS5 and PPQ columns.

### 3.2.4. Pulse experiments

Kinetic transient pulse experiments were performed at 300°C, using a fixed-bed reactor. The details were described in chapter 2 [2].

### 3.3. Results and discussion

Physical and chemical characteristics of the catalysts such as BET surface area, composition (XRF) and Pt dispersion are summarized in Table 1. The surface area of the catalysts varied from 22m<sup>2</sup>/g for Pt/ZrO<sub>2</sub> to 147m<sup>2</sup>/g for Pt/Ti<sub>0.8</sub>Ce<sub>0.2</sub>O<sub>2</sub>. All catalysts had comparable Pt dispersions of around 60 ± 5%, except for Pt/Ti<sub>0.5</sub>Zr<sub>0.5</sub>O<sub>2</sub> (45%), demonstrating that this set of catalysts with comparable Pt loading and dispersion is thus suitable for determining the effect of the support on the catalytic performance.

Table 1: BET surface area, metal loading and Pt dispersion of the mono metallic catalysts used in this work

| Catalyst (0.5wt% Pt)                               | S <sub>BET</sub> (m <sup>2</sup> /g) support | XRF Pt (wt%) | H/Pt (%) |
|--|--|--------------|----------|
| ZrO <sub>2</sub>                                   | 22   | 0.47         | 60       |
| Ti <sub>0.5</sub> Zr <sub>0.5</sub> O <sub>2</sub> | 145  | 0.53         | 45       |
| Ce <sub>0.8</sub> Zr <sub>0.2</sub> O <sub>2</sub> | 100  | 0.52         | 63       |
| Ti <sub>0.8</sub> Ce <sub>0.2</sub> O <sub>2</sub> | 147  | 0.49         | 65       |
| CeO <sub>2</sub>                                   | 81   | 0.54         | 65       |
| Ce <sub>0.5</sub> Zr <sub>0.5</sub> O <sub>2</sub> | 107  | 0.58         | 62       |
| Ti <sub>0.5</sub> Ce <sub>0.5</sub> O <sub>2</sub> | 88   | 0.50         | 60       |
| TiO <sub>2</sub>                                   | 48   | 0.49         | 55       |

#### 3.3.1. Catalytic performance

To account for the small differences in Pt dispersions and loadings, catalyst activities are expressed in TOF (s<sup>-1</sup>), the number of molecules converted (CO) or produced (H<sub>2</sub>, CO<sub>2</sub>) per surface Pt atom and per second. CO conversion was kept below 15%, working close to differential conditions. All catalysts tested were selective to H<sub>2</sub>. Methane formation was below detection limits (<10ppm), and the rate of hydrogen formation was equal to the rate of CO<sub>2</sub> formation (±2%).

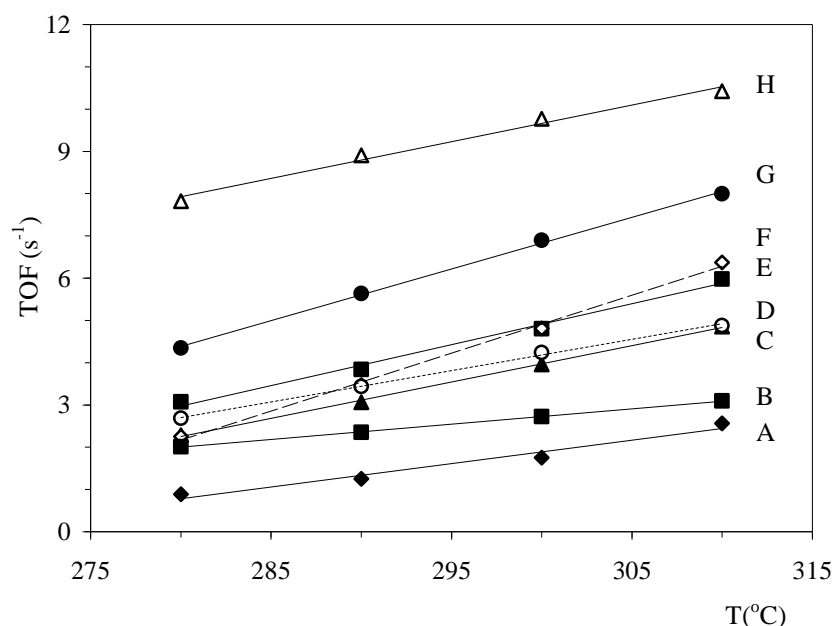


Fig. 1: Turn over frequency (TOF) for the WGS reaction on various catalysts using partial pressure of 60 and 150 mbar for CO and H<sub>2</sub>O respectively, P =2bar, and HSGV =2,100,000h<sup>-1</sup>. Data are shown for 0.5wt% of Pt on different supports: (A, ♦) ZrO<sub>2</sub>; (B, ■) Ti<sub>0.5</sub>Zr<sub>0.5</sub>O<sub>2</sub>; (C, ▲) Ce<sub>0.8</sub>Zr<sub>0.2</sub>O<sub>2</sub>; (D, ○) Ti<sub>0.8</sub>Ce<sub>0.2</sub>O<sub>2</sub>; (E, ■) CeO<sub>2</sub>; (F, ◇) Ce<sub>0.5</sub>Zr<sub>0.5</sub>O<sub>2</sub>; (G, ●) Ti<sub>0.5</sub>Ce<sub>0.5</sub>O<sub>2</sub>; (H, △) TiO<sub>2</sub>

Figure 1 presents the intrinsic activities by TOF for hydrogen formation during WGS reaction over the catalysts studied. The figure shows, in agreement with other studies [5,27,28], that the oxide support had a strong influence on the rate of formation of hydrogen. Among the catalysts studied Pt/TiO<sub>2</sub> was the most active. Activity followed the order Pt on TiO<sub>2</sub> > Ti<sub>0.5</sub>Ce<sub>0.5</sub>O<sub>2</sub>, > Ce<sub>0.5</sub>Zr<sub>0.5</sub>O<sub>2</sub>, ~ CeO<sub>2</sub>, > Ti<sub>0.8</sub>Ce<sub>0.2</sub>O<sub>2</sub>, > Ce<sub>0.8</sub>Zr<sub>0.2</sub>O<sub>2</sub>, > Ti<sub>0.5</sub>Zr<sub>0.5</sub>O<sub>2</sub>, > ZrO<sub>2</sub>. Recalling that the order of activity for single oxide supports was Pt/TiO<sub>2</sub> > Pt/CeO<sub>2</sub>, > Pt/ZrO<sub>2</sub>, it can be seen that mixed oxide support did not result in any enhanced catalytic performance. In the order of activity they are between that of single oxides, indicating performance of oxide mixtures. However, the red-ox capacity of Pt/Ti<sub>0.5</sub>Ce<sub>0.5</sub>O<sub>2</sub> was much higher than that of the individual Pt/TiO<sub>2</sub> or Pt/CeO<sub>2</sub>, based on experiments with subsequent pulsing of CO and H<sub>2</sub>O over Pt/Ti<sub>0.5</sub>Ce<sub>0.5</sub>O<sub>2</sub> catalyst (Fig. 2). This was substantiated by the amount of CO<sub>2</sub> formed during CO pulses (553, 68 and 51 μmoles g<sup>-1</sup> CO<sub>2</sub> for Pt/Ti<sub>0.5</sub>Ce<sub>0.5</sub>O<sub>2</sub>, Pt/CeO<sub>2</sub>, and Pt/TiO<sub>2</sub>, respectively [2]). Therefore Pt/Ti<sub>0.5</sub>Ce<sub>0.5</sub>O<sub>2</sub> is not a physical mixture of Pt/TiO<sub>2</sub> and Pt/CeO<sub>2</sub>. The mixed oxide support must be, at least partially, a solid solution, influencing the catalytic properties as well as

red-ox properties; unfortunately, XRD did not reveal any details. Based on these data, we can conclude that increasing oxygen mobility and redox capacity of the support did not significantly improve catalyst performance under WGS conditions that we studied.

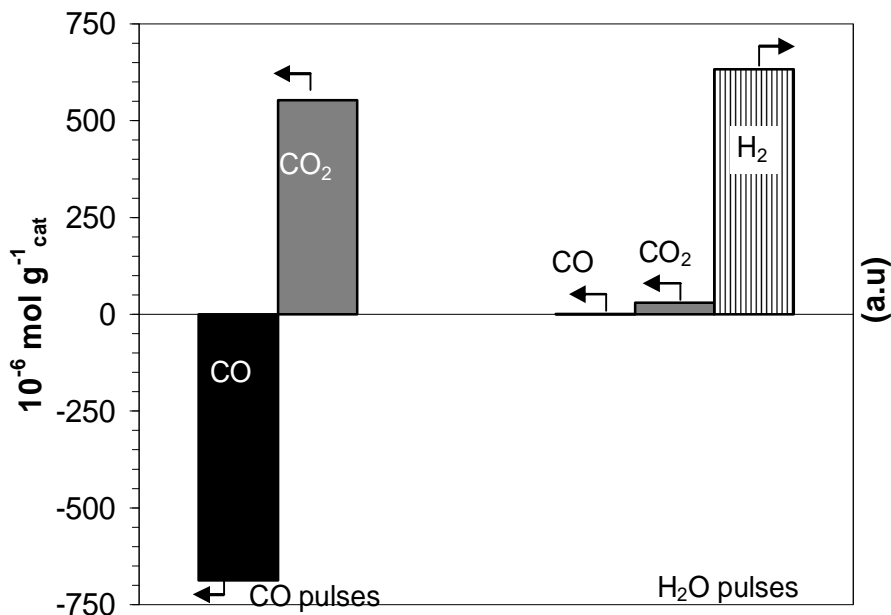


Fig. 2: CO and H<sub>2</sub>O pulse results over 0.5%Pt/Ti<sub>0.5</sub>Ce<sub>0.5</sub>O<sub>2</sub> catalyst at 300°C.

Two Pt/TiO<sub>2</sub> catalysts with different Pt metal dispersions (55% and 35 %) showed the same TOF for hydrogen formation (10 s<sup>-1</sup> at 300°C) indicating an absence of particle size effects on catalytic activity. We showed earlier [2] that the oxide support influences the mechanistic reaction sequence for WGS reaction; thus, it is not surprising to see that the support oxide influences the catalyst activity.

### 3.3.2. Catalysts Deactivation

Catalyst stability with time on stream is one of key factor that must be taken into account when considering commercial application of the catalyst. For example, Pt/CeO<sub>2</sub> is often cited as the most promising single stage WGS catalyst [7-9]. However, earlier studies have made little mention of catalyst stability. Figure 3a shows changes in relative activity, (normalized to its initial activity), for Pt/CeO<sub>2</sub>, Pt/TiO<sub>2</sub>, Pt/ZrO<sub>2</sub> and

Pt/Ti<sub>0.5</sub>Ce<sub>0.5</sub>O<sub>2</sub>, comparing initial catalyst activity, activity after 20 h on a WGS reaction stream, and activity after regeneration of the used catalyst with O<sub>2</sub> at 450°C. Figure 3b shows Pt dispersions for these catalysts before and after the 20 h activity tests. All of the catalysts, except Pt/ZrO<sub>2</sub>, lost about 40% of their initial activity after 20 h of testing. Pt/ZrO<sub>2</sub> showed stable activity; recall, however, that it had the lowest activity (Fig. 1). Therefore it was not considered for further study.

Because the oxide supported Pt catalysts are bi-functional in the WGS shift reaction [2,4,5,27,28], loss of activity may be caused by deactivation of Pt or oxide surface sites, or both. In Pt/CeO<sub>2</sub>, no Pt sintering was observed during time on stream. The Pt dispersion was 65% on fresh catalyst and 67% on used catalyst (Fig. 3b), even though the catalyst showed strong deactivation. Oxidative treatment at 450°C for 1 h allowed almost complete recovery (95%) of initial catalyst activity (Fig. 3a). As shown earlier [2], stable oxygenates (formate and/or carbonate) on ceria are formed while contacting the catalyst with CO. Moreover, on Pt/CeO<sub>2</sub>, part of the “C” containing specie was retained on the surface even in the presence of H<sub>2</sub>O at 300°C. Because formate is reactive in the presence of H<sub>2</sub>O, we concluded [2] that the majority of “C” specie must consist mainly of carbonates:



This is in agreement with stability of cerium carbonate up to 430°C under WGS conditions [29].

Our conclusion is also in agreement with the finding of Liu *et al.* [29] who reported instability of Pt/CeO<sub>2</sub> catalyst during start up and shut down cycles due to carbonate formation. Zalc *et al.* [30] attributed the deactivation of Pt/CeO<sub>2</sub> during WGS reaction to “irreversible” over-reduction of CeO<sub>2</sub> by H<sub>2</sub>. Our results (Figs. 3a and b) disagree with that, because an oxidative treatment of the used catalyst results in complete recovery of catalyst activity.

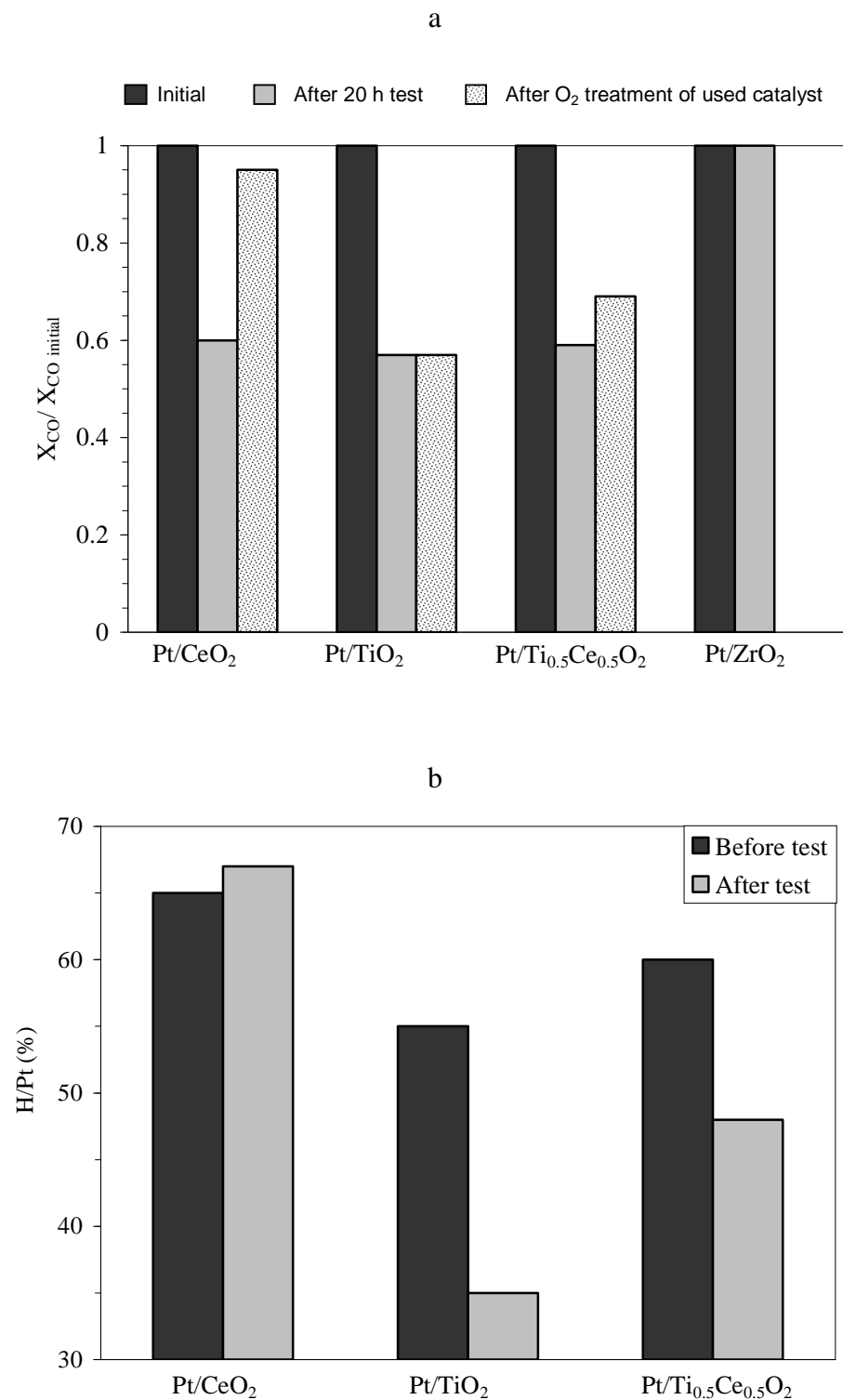


Fig.3: (a) WGS CO conversion (normalized) at 300°C as for Pt/CeO<sub>2</sub>, Pt/TiO<sub>2</sub> and Pt/Ti<sub>0.5</sub>Ce<sub>0.5</sub>O<sub>2</sub>; Conditions: partial pressure of 60 and 150 mbar for CO and H<sub>2</sub>O respectively, P =2bar, and GHSV =1,025,000h<sup>-1</sup>. (b) Pt dispersion; before test and after 20 h test on the stream

Because formates are reactive intermediates [2], we propose that the deactivation of Pt/CeO<sub>2</sub> catalyst is caused by reactive self-poisoning, CO<sub>2</sub> poisons sites for water sorption/activation *via* carbonate build up on ceria. We further propose that this carbonates build up progressively, block ceria sites for the formation of reactive surface formate and thereby cause catalyst deactivation. The poisoning of the active sites is not reversible below 430°C, the temperature needed to decompose ceria carbonate under WGS conditions [29]. This will be a problem for single stage WGS catalysts operated at lower temperatures, especially since the reactor feed from the hydrocarbon conversion step contains large amounts of CO<sub>2</sub> (2-15% depending on the route to syngas production, *i.e.*, catalytic partial oxidation or steam reforming). The fact that Pt/ZrO<sub>2</sub> is stable (Fig. 3a), agrees with the observation that no stable carbonates are formed during the CO pulses [2] and no Pt sintering occurs (Fig. 3b).

In the case of Pt/TiO<sub>2</sub>, carbonate is known to be unstable [31], thus TiO<sub>2</sub> as a support might have an advantage over ceria in regard to the catalyst stability as well as activity. This catalyst deactivated with time (Fig. 3a), however. Its activity can not be restored by heating in oxygen as was the case for Pt/CeO<sub>2</sub>. Pt dispersion decreased during exposure to WGS conditions from 55% to 34% after 20 h testing (Fig. 3b).

Sintering of Pt was also visible in TEM micrographs for fresh and used Pt/TiO<sub>2</sub> catalysts (Fig. 4). Pt particles had an average size of  $1.2 \pm 0.2$  nm before 20 h activity test, increasing to  $2.7 \pm 0.4$  nm after test. Therefore we consider that Pt sintering and loss of metal surface area to be the main cause of deactivation.

In the case of Pt/TiO<sub>2</sub>, carbon mass balance during kinetic transient experiments [2] indicated that neither coke nor oxygenate species (formates, carbonates) remained on the surface. Pt sintering is the cause of deactivation exclusively. We will discuss the deactivation mechanism of Pt/TiO<sub>2</sub> catalyst, in details, in chapter 4.

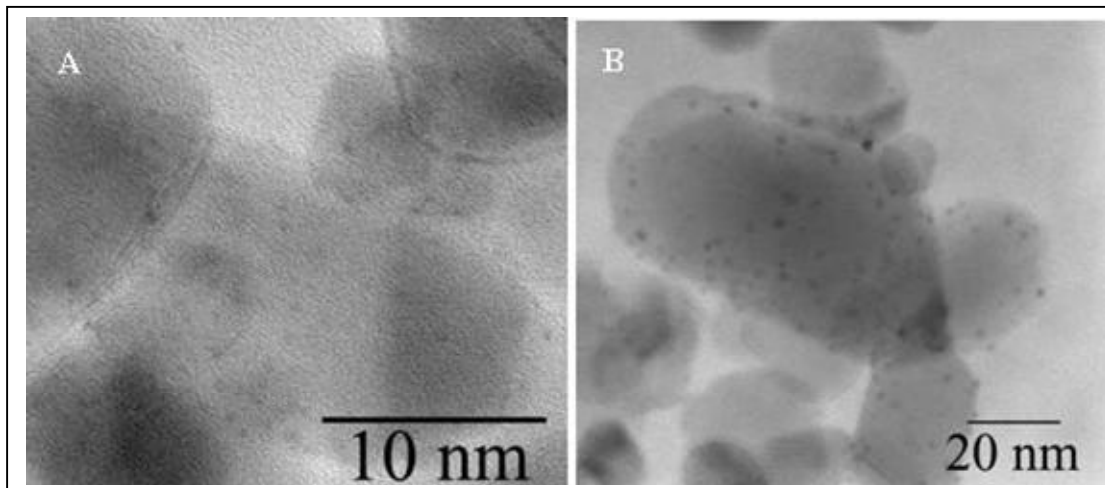


Fig. 4: TEM images of 0.5Pt/TiO<sub>2</sub>, (A) before test and (B) after 20 h test

Among the mixed oxide supports, Ce<sub>0.5</sub>Ti<sub>0.5</sub>O<sub>2</sub> was studied in a more detail. For the Pt/Ti<sub>0.5</sub>Ce<sub>0.5</sub>O<sub>2</sub>, the activity and deactivation profile were between those for ceria- and titania- based catalysts. Figures 3a and b show that both Pt sintering and formation of carbonaceous species on the surface caused catalyst deactivation. Oxidative treatment with O<sub>2</sub> at 450°C for 1 h (Fig. 3a) allowed partial recovery (up to 70%) of initial catalyst activity. Moreover, Pt dispersion for fresh catalyst was 60% and dropped to 47% after 20 h testing. The role of carbonaceous species on catalyst deactivation is also confirmed by the result of subsequent pulsing of CO and H<sub>2</sub>O over Pt/Ti<sub>0.5</sub>Ce<sub>0.5</sub>O<sub>2</sub> catalyst (Fig. 2). During the CO pulses, 687 μmoles/g CO was consumed and 553 μmoles/g CO<sub>2</sub> was formed. As in the case of Pt/CeO<sub>2</sub> [2], no hydrogen was observed. When H<sub>2</sub>O was pulsed consecutively, both H<sub>2</sub> and CO<sub>2</sub> (30 μmoles g<sup>-1</sup><sub>cat</sub>) were observed. Carbon mass balance indicated that 15% of the CO introduced (104 μmoles g<sup>-1</sup><sub>cat</sub>) was retained on the catalyst surface as carbonaceous species, causing loss of active sites and inducing deactivation. These observations confirm that, similar to catalyst activity discussed above, the stability of mixed-oxide based catalyst were again between that of the single-oxide based catalysts. The mixed oxide was at least partly truly mixed, as discussed above as well. Nevertheless, it is obvious that no synergy whatsoever was obtained for both activity and stability.

### 3.3.3 Development of a stable and efficient catalyst

The Pt/TiO<sub>2</sub> catalyst can be considered a promising catalyst for industrial application in single-stage WGS, provided Pt dispersion on titania could be maintained under WGS conditions. For Pt/Al<sub>2</sub>O<sub>3</sub>-reforming catalysts, deactivation has been attributed to Pt sintering and coke formation. It has been recognized [32-38] that adding a second metal (rhenium (Re) or tin (Sn)) improved the lifetime of Pt/Al<sub>2</sub>O<sub>3</sub> catalyst by (i) preventing sintering by occupying Pt grain boundaries and (ii) suppressing coke formation by helping hydrogenation of coke precursors. Rezgui *et al.* [33] and Reitmair *et al.* [34] reported that the Pt-O-Al bond is strengthened by the addition of Re, which helps to anchor the Pt and maintain its dispersion. Further conversion of carbonaceous specie on the support surface to the more inert graphitic carbon is suppressed. Coq *et al.* [37] and Dautzenberg *et al.* [38] proposed that adding Sn on Pt/Al<sub>2</sub>O<sub>3</sub> changes the intrinsic catalytic properties of Pt, weakening the Pt-C bond during reforming reactions and leading to changes in selectivity and reduced coke formation on platinum. Recent studies [39, 40] reported that the activity of Pt/TiO<sub>2</sub> catalyst for WGS can be enhanced by the addition of Re; however the reason of improving the catalyst activity remains unclear. Moreover, catalyst stability was not discussed at all.

Figure 5 shows the WGS activity for 0.5%Pt/TiO<sub>2</sub>, 0.5%Pt-0.48%Re/TiO<sub>2</sub>, 0.5%Re/TiO<sub>2</sub> and 0.5%Pt-0.3%Sn/TiO<sub>2</sub> catalysts as function of time on stream at 300°C. This figure clearly that addition of Re to Pt/TiO<sub>2</sub> improves the stability of the catalyst. The catalyst showed almost no deactivation during 20 h time on stream. The Pt-Sn/TiO<sub>2</sub> catalyst was also stable but because it showed very low activity, this is not of further interest. To check the influence of Re on Pt/TiO<sub>2</sub> catalyst, Pt dispersion was measured for both Pt/TiO<sub>2</sub> and Pt-Re/TiO<sub>2</sub> catalysts before and after 20h activity test (Fig. 6). Both catalysts demonstrated almost identical Pt dispersion before testing: 49% for Pt/TiO<sub>2</sub> and 50% for Pt-Re/TiO<sub>2</sub>. After the activity tests, Pt/TiO<sub>2</sub> lost 36% (relative loss) of the initial Pt dispersion; however, Pt-Re/TiO<sub>2</sub> was affected much less significantly (8% loss).

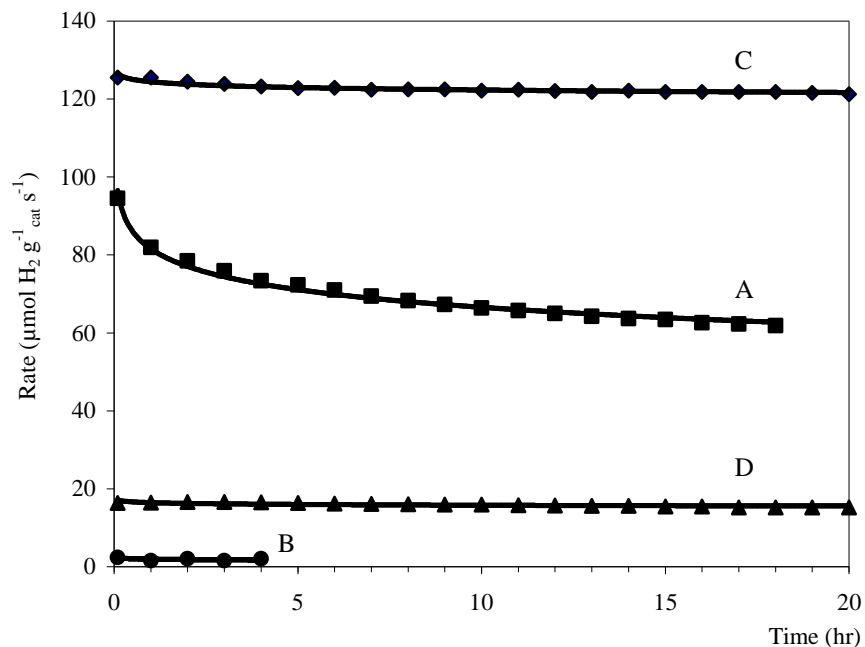


Fig. 5: WGS rates at 300°C as a function of time on stream for (A) 0.5Pt/TiO<sub>2</sub>; (B) 0.5Re/TiO<sub>2</sub> (C) 0.5Pt-0.48Re/TiO<sub>2</sub>; (D) 0.5Pt-0.3Sn/TiO<sub>2</sub> catalysts. Conditions: partial pressure of 60 and 150 mbar for CO and H<sub>2</sub>O respectively, P =2bar, and HSGV =410,000 h<sup>-1</sup>

TEM measurements on fresh and deactivated Pt-Re/TiO<sub>2</sub> catalysts confirmed this finding (Fig. 7). Pt particles on Pt-Re/TiO<sub>2</sub>, before and after 20-h test had an average size of 2.1 ± 0.3 nm. These findings demonstrate that the addition of Re indeed improved the stability of Pt particles by preventing sintering.

It is remarkable that Re not only stabilized the Pt/TiO<sub>2</sub> catalyst but also enhances activity, that is, the rate of H<sub>2</sub> production. By itself, Re/TiO<sub>2</sub> demonstrated no activity in the WGS reaction (Fig. 5). In our case, the activity increase for Pt-Re/TiO<sub>2</sub>, was not due to improved Pt dispersion in the presence of Re, as claimed by Iida *et al.* [39]. The two catalysts tested, Pt/TiO<sub>2</sub> and Pt-Re/TiO<sub>2</sub>, had very similar Pt dispersions, but differing activities (95 and 125 μmol H<sub>2</sub> g<sup>-1</sup> cat s<sup>-1</sup>, respectively).

To elucidate the role of Re in the WGS reaction sequence, it is essential to determine the form in which it is present in the Pt-Re/TiO<sub>2</sub> catalyst under *in-situ* WGS conditions. Based on XPS and XAS techniques, Onuferko *et al.* [41] found that Re in Pt-Re/Al<sub>2</sub>O<sub>3</sub> exists in oxidized state (IV) even after *in situ* reduction at 485°C. An ESR study by

Nacheff *et al.* [42] also confirmed the existence of Re(IV) along with Re(0) in Pt-Re/ $\text{Al}_2\text{O}_3$  reduced at  $500^\circ\text{C}$ . Huang *et al.* [43] showed using TEM/EDX analysis, that the most of Re in Pt-Re/ $\text{Al}_2\text{O}_3$  reduced at  $400^\circ\text{C}$  is present as  $\text{ReO}_2$ .

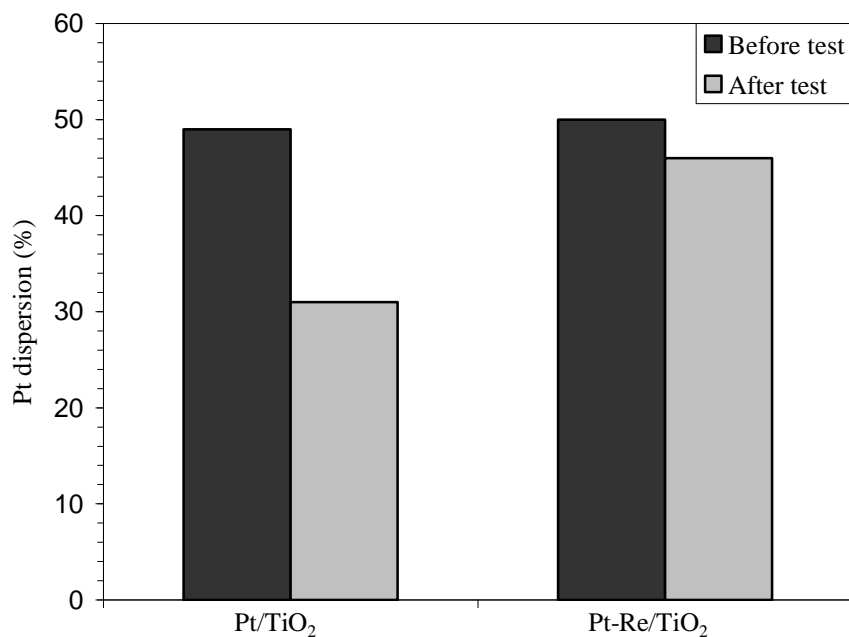


Fig. 6: Pt dispersion of 0.5%Pt/TiO<sub>2</sub> and 0.5%Pt-0.48%Re/TiO<sub>2</sub> using CO chemisorption; before test and after 20 h test on the stream

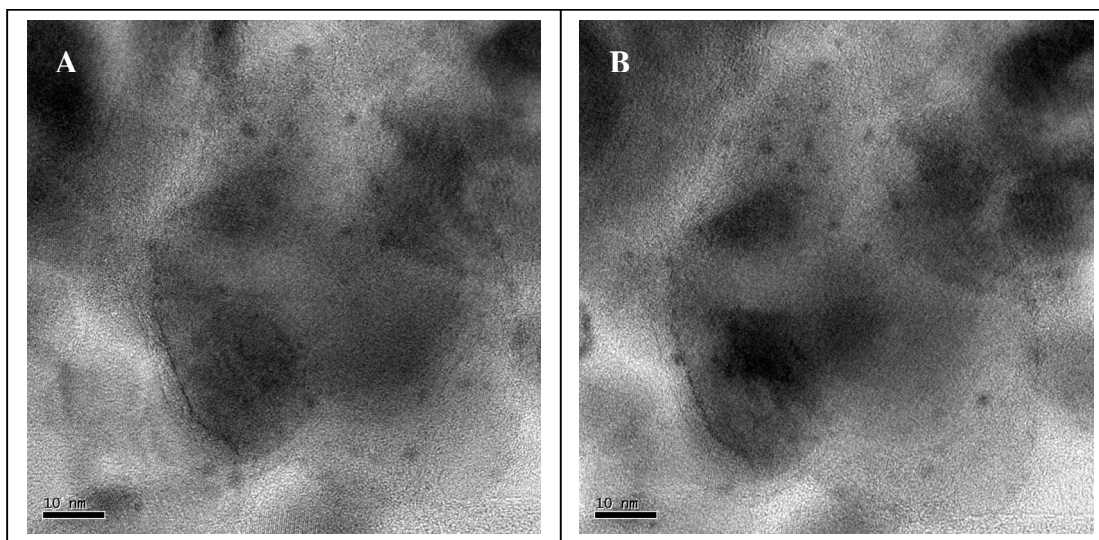


Fig. 7: TEM images of 0.5Pt-0.48Re/TiO<sub>2</sub>; (A) before test and (B) after 20 h test

Our own XPS measurements of the 0.5%Re/TiO<sub>2</sub>, 0.5%Pt/TiO<sub>2</sub> and 0.5%Pt-0.48%Re/TiO<sub>2</sub> after *ex situ* reduction with H<sub>2</sub> at 300°C also suggest that at least part of Re is present as ReO<sub>x</sub> (Fig. 8).

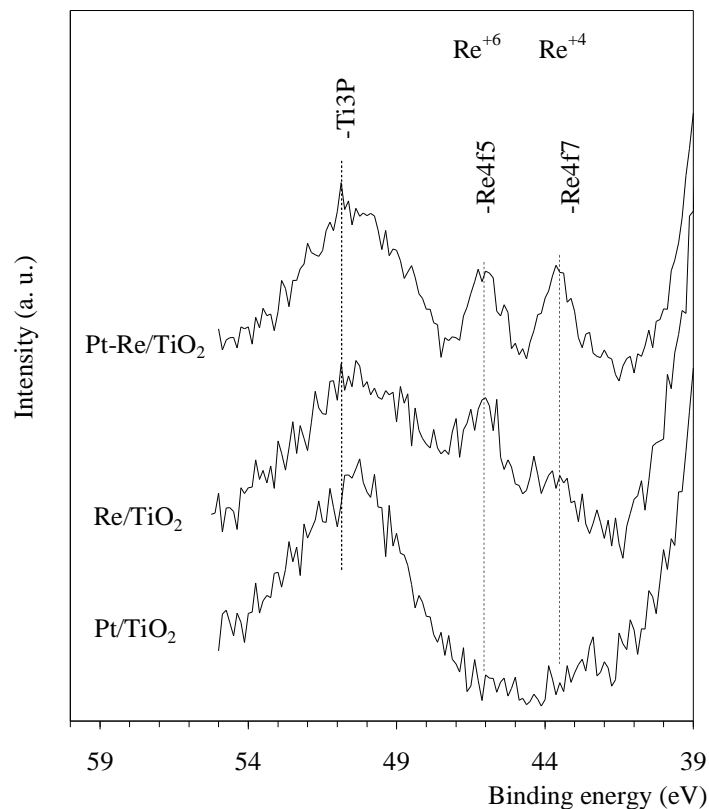


Fig. 8: XPS spectra for Re4f in 0.5%Pt/TiO<sub>2</sub>, 0.5%Re/TiO<sub>2</sub> and 0.5%Pt-0.48%Re/TiO<sub>2</sub> catalysts after reduction at 300°C

Figure 9 shows the TPR profile of Pt-Re/TiO<sub>2</sub> catalyst. The reduction profile is complex, with four different reduction stages. In accordance with data reported previously [26, 44, 45] the first peak corresponds to reduction of Pt and the three subsequent peaks to reduction of ReO<sub>x</sub>. Two observations are important for our current discussion: (i) complete reduction of ReO<sub>x</sub> to Re<sup>0</sup> occurs only above 500°C, and (ii) part of the ReO<sub>x</sub> can be reduced at WGS conditions (300°C/H<sub>2</sub>). We speculate that ReO<sub>x</sub> provides an additional reaction pathway for H<sub>2</sub>O sorption/activation and thereby improve the catalyst activity. This is a subject of ongoing detailed investigation.

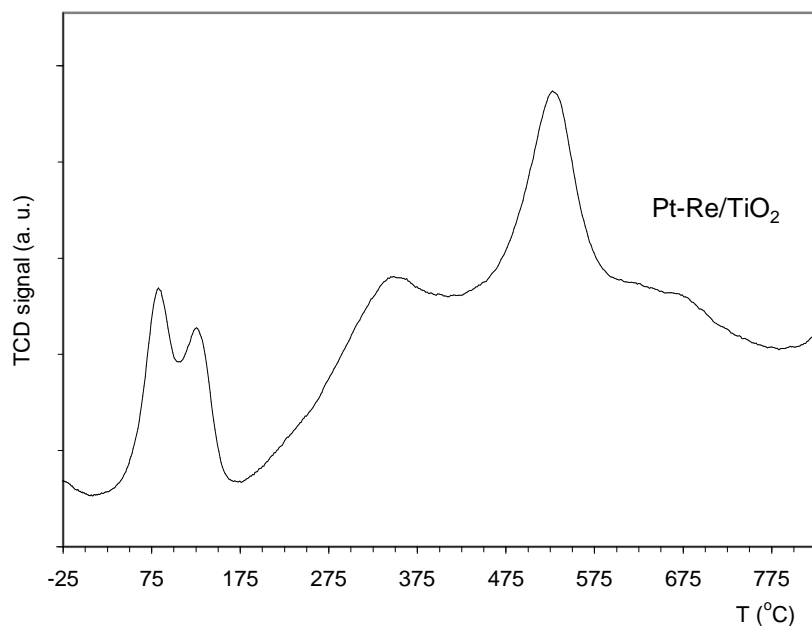


Fig. 9: H<sub>2</sub>-TPR profile of Pt-Re/TiO<sub>2</sub>. Heating rate was 10/min; gas contains 15% H<sub>2</sub> in Ar. The gas flow was 20 ml/min

### 3.4. Conclusion

Our findings indicate that the nature of the oxide support has a strong influence on the activity and stability of the catalysts in the WGS reaction. The Pt/TiO<sub>2</sub> catalyst showed the best activity for WGS reaction among the catalysts studied, even better than Pt/CeO<sub>2</sub>, which is often claimed as a promising catalyst for fuel cell application. Using mixed-oxides as catalyst supports did not improve the activity despite the enhanced red-ox properties of mixed-oxides compared with the single-oxide supports.

Pt/CeO<sub>2</sub> catalyst suffered from deactivation caused by self poisoning, that is, formation of stable carbonate on the ceria surface. The surface carbonates blocked the WGS reaction sequence by preventing creation of seemingly crucial formate intermediates that seem crucial. Carbonates caused no deactivation on the Pt/TiO<sub>2</sub> catalyst, because carbonates were not stable on titania under WGS temperatures. Pt/TiO<sub>2</sub> deactivation was caused by Pt sintering exclusively. Accordingly, the stability of Pt/TiO<sub>2</sub> can be improved by adding Re, which prevents Pt sintering. In addition, the presence of Re increased the catalytic

activity of Pt/TiO<sub>2</sub>. We proposed that part of the Re was present under reaction conditions in oxidized form (ReO<sub>x</sub>).

### 3.5 References

- [1] C.H. Bartolomew, R.J. Farrauto, in: C.H. Bartolomew, R.J. Farrauto (Eds.) Fundamentals of industrial catalytic processes, John Wiley & Sons, Hoboken, NJ, 2006, p. 909.
- [2] K. G. Azzam, I.V. Babich, K. Seshan and L. Lefferts, *J. Catal.* 251 (2007) 153.
- [3] M. A. Henderson, *Surf. Sci. Rep.* 46 (2002) 1.
- [4] T. Bunluesin, R. J. Gorte, G.W. Graham, *Appl. Catal. B* 15 (1998) 107.
- [5] P. Panagiotopoulou, D. I. Kondarides, *Catal. Today* 112 (2006) 49.
- [6] G. Jacobs, U. M. Graham, E. Chenu, P. M. Patterson, A. Dozier, B. H. Davis, *J. Catal.* 229 (2005) 499.
- [7] G. Jacobs, L. Williams, U. Grham, G. A. Thomas, D. E. Sparks, B. H. Davis, *Appl. Catal. A: General* 252 (2003) 107.
- [8] T. Shido, Y. Iwasawa, *J. Catal.* 141 (1993) 71.
- [9] D. Tibiletti, A. Goguet, D. Reid, F. Meunier, R. Burch, *Catal. Today* 113 (2006) 94.
- [10] G. Jacobs, A. Crawford, L. Williams, P. M. Patterson, B. H. Davis, *Appl. Catal. A: General* 267 (2004) 27.
- [11] P. Panagiotopoulou, A. Christodoulakis, D. I. Kondarides, S. Boghosian, *J. Catal.* 240 (2006) 114.
- [12] E. Xue, M. O'Keeffe, J. R. H. Ross, *Surf. Sci. Catal.* 130 (2000) 3813.
- [13] G. Jacobs, S. Ricote, B. H. Davis, *Appl. Catal. A* 302 (2006) 14.
- [14] H. Iida, K. Kondo, A. Igarashi, *Catal. Comm.* 7 (2006) 240.
- [15] O. Goerke, P. Pfeifer, K. Schubert, *Appl. Catal. A* 263 (2004) 11.
- [16] D. Martin, D. Duprez, *J. Phys. Chem.* 1996 (100) 9429.
- [17] M. Calatayud, A. Markovits, M. Menetrey, B. Mguig, C. Minot, *Catal. Today* 85 (2003) 125.
- [18] L. Mattos, E. R. Oliveira, P. D. Resende, F. B. Noronha, F. B. Passos, *Catal. Today* 77 (2002) 245.
- [19] K. Takanebe, K. Aika, K. Inazu, T. Baba, K. Seshan, L. Lefferts, *J. Catal.* 227 (2004) 101.

- [20] S. Pengpanich, V. Meeyoo, T. Riraksomboon, K. Bunyakiat, *Appl. Catal. A: General* 234 (2002) 221.
- [21] A. Wootsch, C. Descorme, D. Duprez, *J. Catal.* 225 (2004) 259.
- [22] W. Ruettinger, X. Liu, R. Robert, J. Farrauto, *Appl. Catal B: Environmental* 65 (2006) 135.
- [23] G. Dong, J. Wang, Y. Cao, S. Chen, *Catal. Lett.* 58 (1999) 37.
- [24] D. Teschner, A. Wootsch, T. Roder, K. Matusek, Z. Paal, *Solid State Ionic* 141-142 (2001) 709.
- [25] C. L. Piek, C. R. Vera, J. M. Perera, G. N. Gimenez, L. R. Serra, L. S. Carvalho, M. C. Rangel, *Catal. Today* 107-108 (2005) 637.
- [26] L. S. Carvalho, C. L. Pieck, M. C. rangel, N. S. Figoli, J. M. Grau, P. Reyes, J. M. Parera, *Appl. Catal. A: General* 269 (2004) 91.
- [27] R. J. Gorte, S. Zhao, *Catal. Today* 104 (2005) 18.
- [28] D. C. Grenoble, M. M. Estadt, D. F. Ollis, *J. Catal.* 67 (1981) 90.
- [29] X. Liu, W. Ruettinger, X. Xu, R. Farrauto, *Appl. Catal. B: Environmental* 56 (2005) 69.
- [30] J. M. Zalc, V. Sokolovskii, D. G. Loffler, *J. Catal.* 206 (2002) 169.
- [31] J. A. Wang, A. Cuan, J. Salamones, N. Nava, S. Castillo, M. Moran-Pineda, F. Rojas, *Appl. Surf. Sci.* 230 (2004) 94.
- [32] C. Audo, J. F. Lambert, M. Che, B. Didillon, *Catal. Today* 65 (2001) 157.
- [33] S. Rezgui, R. Jentoft, B. C. Gates, *J. Catal.* 136 (1996) 496.
- [34] S. F. Reitmaier, A. Subramaniam, P. A. Sermon, *Catal. Today* 19 (1993) 345.
- [35] H. Dexpert, P. Lagarade, *J. Mol. Catal.* 25 (1984) 347.
- [36] C. L. Pieck, P. Marecot, C. A. Querini, J. M. Peraera, *Appl. Catal. A: General* 133 (1995) 281.
- [37] B. Coq, F. Figueras, *J. Catal.* 85 (1984) 197.
- [38] F. M. Dautzenberg, J. N. Helloen, W. M. H. Sachtler, *J. Catal.* 63 (1980) 119.
- [39] H. Iida, A. Igarashi, . *Appl. Catal. A: General* 303 (2006) 192.
- [40] Y. Sato, K. Terada, S. Hasegawa, T. Miyao, S. Naito, *Catal. Comm.* 7 (2006) 91.
- [41] J. H. Onuferko, *Appl. Surf. Sci.* 19 (1984) 227.

- [42] M. S. Nacheff, L. S. Kraus, M. Ichikawa, B. M. Hoffman, J. B. Butt, W. M. H. Sachtler, *J. Catal.* 106 (1987) 263.
- [43] Z. Huang, J. R. Fryer, C. Park, D. Stirling, G. Webb, *J. Catal.* 148 (1994) 478.
- [44] P. Reyes, G. Pecchi, M. Morales, J. L. G. Fierro, *Appl. Catal. A: General* 163 (1997) 145.
- [45] C. L. Pieck, C. R. Vera, J. M. Parera, G. N. Gimenez, L. R. Serra, L. S. Carvalho, M. C. Rangel, *Catal. Today* 107-108 (2005) 637.

# Chapter 4

## Deactivation mechanism of Pt/TiO<sub>2</sub> catalyst in Water Gas Shift reaction

---

### *Abstract*

*Pt/TiO<sub>2</sub> is an active and selective catalyst for single stage water gas shift reaction. However, the catalyst deactivated with time on stream. Detailed studies of fresh, used, and reactivated Pt/TiO<sub>2</sub> catalysts were carried out using kinetic (steady state and transient) and in situ IR spectroscopic methods in order to understand the mechanism of deactivation. The loss of Pt surface area was the cause of Pt/TiO<sub>2</sub> deactivation, exclusively. Pt sintering occurred mainly due to the presence of traces of formaldehyde formed under WGS reaction conditions by reaction of H<sub>2</sub> and CO. Details concerning the deactivation behavior are discussed.*

**Keywords:** *WGS; Bifunctional; Catalysts; Platinum; Titania; Stability; Deactivation; SMSI; Sintering.*

## 4.1. Introduction

Water Gas Shift (WGS) conversion,  $\text{CO} + \text{H}_2\text{O} \leftrightarrow \text{CO}_2 + \text{H}_2$ ,  $\Delta H = -41.1 \text{ kJ/mol}$ , is a key reaction in the production of hydrogen for fuel cell applications. This reaction increases the hydrogen content from synthesis gas produced during steam reforming or partial oxidation of hydrocarbons. There has been much interest in the use of noble metal (*e.g.* Pt) based WGS catalysts for *in situ* hydrogen generation in the auto-mobile fuel cell applications because of the limitations and complexity of the current two stage commercial WGS technology. We reported earlier [1] that Pt/TiO<sub>2</sub> promoted with Re, which contains very low contents of Pt and Re (<0.5wt% each), showed an excellent activity, stability, and selectivity to WGS at moderate temperature (300°C). These characteristics of the catalyst make it very promising single stage WGS catalyst that can be used in a hydrogen selective catalytic membrane reactor for hydrogen generation for auto-mobile applications.

Pt/CeO<sub>2</sub> is one of the most studied catalysts [1-11]. In general, Pt based catalysts are reported to be bifunctional [1,3,11,12], in which the noble metal and the oxide support sorbs/activates CO and H<sub>2</sub>O, respectively. We have shown recently [1] that the oxide support not only determines activity of Pt based catalysts but also influence their stability.

Pt/CeO<sub>2</sub> is usually cited as a promising WGS catalyst to make hydrogen, *in situ*, for fuel cell applications [2-4, 6, 9], but this catalyst deactivates with time on stream. Since Pt-based catalysts are bifunctional [1, 3, 11, 12], the deactivation of Pt/CeO<sub>2</sub> during WGS can involve Pt and/or CeO<sub>2</sub> [5-7, 11]. Wang *et al.* [5] reported the reason for the deactivation of Pt/CeO<sub>2</sub> and Pd/CeO<sub>2</sub> due to the loss of active metal surface area. Zalc *et al.* [11], on the other hand, attributed deactivation of Pt/CeO<sub>2</sub> catalyst (WGS, 250°C) to the irreversible “over”-reduction of Ceria by H<sub>2</sub>. Still differently, Kim *et al.* [7] claimed that the formation of carbonate and/or formate on ceria surface was the reason for the deactivation of Au/CeO<sub>2</sub> catalyst. The most plausible explanation in our view is given by Farrauto and co-workers [6] who found that, during startup and shutdown cycles in WGS reaction, stable carbonate build up on ceria surface led to catalyst deactivation. They [6]

indicated that the catalyst could be regenerated by heating it in air to 430°C. We have shown [1, 13], using H<sub>2</sub> chemisorptions, *in situ* FTIR and transient kinetic studies that carbonate buildup on CeO<sub>2</sub> surface indeed caused the deactivation of Pt/CeO<sub>2</sub> catalyst, in agreement with Farrauto and co-workers [6]. We found that these carbonates were stable at the reaction temperature (300°C) and decomposed only above 430 °C. Accordingly, the catalyst could be completely regenerated by heating it in air to 450°C. However, this will be a problem for single stage WGS catalysts operated at lower temperatures (300°C) because the reactor feed from the hydrocarbon conversion step contains significant amounts of CO<sub>2</sub> (2-15% depending on the route to syngas production, *i.e.*, catalytic partial oxidation or steam reforming) as well as the fact that CO<sub>2</sub> is produced during WGS conversion. In order to overcome this, it is essential that carbonates are not stable at the reaction conditions. TiO<sub>2</sub> or ZrO<sub>2</sub> have the advantage over CeO<sub>2</sub> as support because surface carbonates are unstable on TiO<sub>2</sub> and ZrO<sub>2</sub> at 300°C [1, 13, 14]. Accordingly, Pt/ZrO<sub>2</sub> catalyst [1] showed excellent stability during WGS; however, it showed very low activity. Interestingly, Pt/TiO<sub>2</sub> was even more active than Pt/CeO<sub>2</sub>, but deactivated with time on stream.

To our knowledge, there is no detailed study on the causes of deactivation of Pt/TiO<sub>2</sub> catalyst during WGS reaction. Obviously, a better understanding of the deactivation mechanism of Pt/TiO<sub>2</sub> may allow design of efficient and stable catalyst. In this manuscript, we report on a detailed study on fresh, deactivated, and regenerated oxide supported Pt catalysts and analyse the reasons for deactivation.

## **4.2. Experimental**

### **4.2.1. Catalyst preparation**

Pt/TiO<sub>2</sub> catalyst was prepared by wet impregnation of TiO<sub>2</sub> (P25, Degussa) with aqueous solution of H<sub>2</sub>PtCl<sub>6</sub> (Aldrich). TiO<sub>2</sub> was brought in contact with a solution containing the required concentration of H<sub>2</sub>PtCl<sub>6</sub> for 1 h at room temperature to yield catalysts with

0.5wt%. The catalyst was then dried at 75°C for 2 h under vacuum in a rotary evaporator and subsequently calcined at 450°C for 4 h (heating rate 10°C min<sup>-1</sup>).

#### 4.2.2. Characterization

Surface areas of the catalysts were measured by the BET method using ASAP 2400 (Micromeritics). Pt dispersions were measured by H<sub>2</sub> chemisorption [13] at room temperature using Chemisorb 2750 (Micromeritics). About 50mg sample was used for each measurement. Prior to measuring H<sub>2</sub> uptake, the samples were oxidized in air at 450°C, reduced in pure H<sub>2</sub> (99.9%) after cooling down to 300°C, flushed with Ar at 425°C for 1 h and then cooled to room temperature (25°C) in Ar. The H<sub>2</sub> uptake measurements were conducted at room temperature by injecting a series of pulses containing 1 mL of H<sub>2</sub> into Ar stream flowing over the sample at a rate of 25 mL/min and measuring the amount of H<sub>2</sub> adsorbed per pulse.

FTIR spectra were recorded using a Bruker Vector 22 with MCT detector under flow conditions (50% CO and 50% H<sub>2</sub>) at the same temperature used in the catalytic activity measurements (300°C).

#### 4.2.3. Catalytic tests

Catalytic tests for WGS reaction were carried out in a fixed bed quartz tubular reactor (i.d. 3 mm). Details of the kinetic setup are described elsewhere [1, 13]. The total flow rate of the feed gas into the reactor was 350 ml/min. The feed gas mixture was 3 vol. % CO, 7.5% H<sub>2</sub>O and N<sub>2</sub> balance (N<sub>2</sub> is used as internal standard).

Pulse transient experiments were performed at 300°C, at atmospheric pressure using also a fixed-bed reactor. A 14 mg catalyst was placed between two quartz plugs in a quartz tubular reactor (d = 2 mm). The reactor was then filled with quartz particles (d = 0.25 - 0.3 mm in size) to reduce the volume of reactor system. The gases (He, H<sub>2</sub>, CO) used were of > 99.9 % purity. The catalyst was first reduced at 300°C in 10 vol% H<sub>2</sub>/He, 20

ml/min flow for 1 h. After this, the catalyst was flushed with He at 300°C (20 ml/min) for 30 min. The catalyst was then contacted with pulses of CO/H<sub>2</sub> mixture at 300°C using He as carrier gas (13.4 μmol each pulse, CO/H<sub>2</sub> ratio of 1:1) in order to investigate the catalysts deactivation.

In order to simulate deactivation, Pt/TiO<sub>2</sub> catalyst was first reduced in H<sub>2</sub> at 300°C for 1 h then pre-treated for 20 h in pure gas or 50% each in case of binary mixtures of reactants, intermediates and products. Details are discussed in the manuscript, wherever relevant.

### 4.3. Results and discussions

We have shown earlier [1] that Pt/TiO<sub>2</sub> catalyst has excellent activity in WGS (TOF of 10s<sup>-1</sup> at 300°C) and was even more active than Pt/CeO<sub>2</sub> (TOF of 5s<sup>-1</sup>). The stability of the catalyst is a critical issue for catalyst application in WGS, especially for the auto-mobile use because of the severe conditions that exist during start up and shutdown cycles [6].

Figure 1 shows CO conversion for Pt/TiO<sub>2</sub> catalyst, during WGS, plotted as a function of time on stream. It can be seen that activity decreased by more than 35% of the initial value during 22 h on stream. Since both Pt and TiO<sub>2</sub> have catalytic functions during WGS (bi-functional catalyst), deactivation may be occurring through Pt, TiO<sub>2</sub>, or both. In an attempt to regenerate the catalyst after this 22 h testing, it was heated to 450°C in oxygen for 1 h (Fig. 1, stage a). This was done to burn off any coke formed or remove any stable carbonates/formates species present. The catalyst was then reduced in H<sub>2</sub> at 300°C (stage b) for 1 h. Subsequently, the catalyst was flushed with N<sub>2</sub> at 300°C for 1 h (stage c) prior to the second cycle of activity test (Fig. 1). It can be seen from the figure that this regeneration/oxidation treatment did not help to regain catalyst activity.

Figure 2(a) shows the IR spectra of the catalyst in He, *in situ*, after reduction in H<sub>2</sub> at 300°C. After exposure to CO at 300°C (Fig. 2(b)), the bands appearing at 2071 and 2060 cm<sup>-1</sup> represent linearly adsorbed CO on Pt [13, 15, 16]. In the case of *in situ* IR during WGS reaction (Fig. 2(c)), an extra band appeared at 1612 cm<sup>-1</sup> corresponding to (weakly)

adsorbed H<sub>2</sub>O on titania [17]. It can be seen from Fig. 2 that oxygenate species (carbonate/ formate, region of 1200 – 1600 cm<sup>-1</sup>), are not stable on Pt/TiO<sub>2</sub> at 300°C. Such species could clearly be seen for Pt/CeO<sub>2</sub> with *in situ* IR at WGS conditions (inset in Fig.2). Therefore, in contrast to Pt/CeO<sub>2</sub> [1], we exclude the role of any stable oxygenate intermediates on catalyst deactivation, in agreement with the regeneration experiments discussed earlier in Fig. 1.

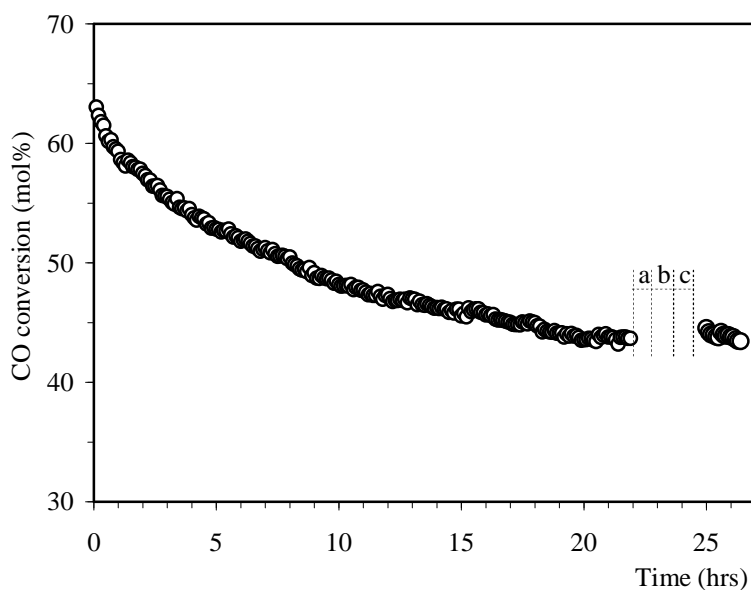


Fig. 1: WGS CO conversion for Pt/TiO<sub>2</sub> with time on stream at 300°C. After 22hrs tests, the catalyst subjected to the following treatment for 1 hr each: (a) O<sub>2</sub> at 450°C, (b) H<sub>2</sub> at 300°C, (c) N<sub>2</sub> at 300°C, then tested in WGS. Testing conditions:  $p_{\text{CO}}=60\text{mbar}$ ,  $p_{\text{H}_2\text{O}}=150\text{mbar}$ ,  $P=2\text{bar}$ , and  $\text{GHSV}=410,000\text{hr}^{-1}$ ,  $m_{\text{cat}}=51\text{mg}$ .

In addition, to check if traces of carbon deposition played any significant role in the catalyst deactivation, we performed O<sub>2</sub> pulse titration experiments over Pt/TiO<sub>2</sub> catalyst after running the catalytic test for 20 h (Fig. 3). To determine the O<sub>2</sub> consumption and product formation, the outlet of the reactor was directly connected to a Porapak column (5m, 100°C, to separate O<sub>2</sub> and CO<sub>2</sub>) and TCD detector. Downstream to the TCD detector, gases were analyzed by an online mass spectrometer.

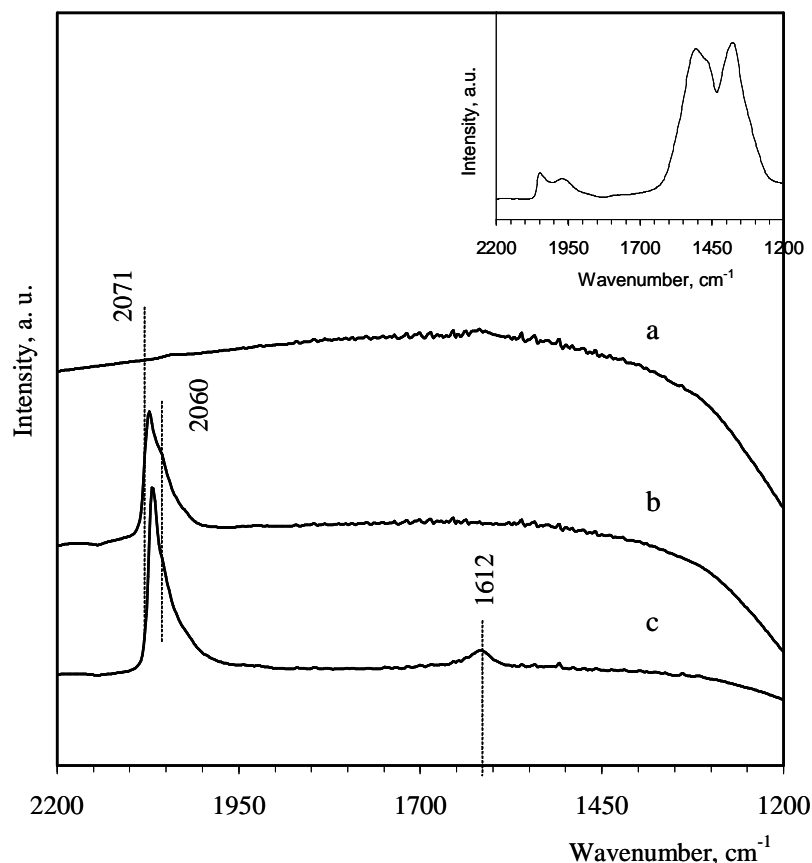


Fig. 2: *In situ* FTIR spectra at 300°C of Pt/TiO<sub>2</sub> catalyst. (a) reduced in H<sub>2</sub>(10%)/He flow; (b) during CO flow; (c) *in situ* WGS conditions. Inset fig. is the *in situ* IR spectra of Pt/CeO<sub>2</sub> under WGS shift conditions showing presence of carbonate.

For the used Pt/TiO<sub>2</sub> sample (Fig. 3) three O<sub>2</sub> pulses were introduced consequently at 300°C. After that, the temperature was increased to 450°C and three additional O<sub>2</sub> pulses were introduced. The total amount of CO<sub>2</sub> released from the catalyst during O<sub>2</sub> pulses at 300 and 450°C was  $2.8 \pm 0.1 \mu\text{moles/g}_{\text{cat}}$ . To recall, the catalyst contained  $14 \mu\text{moles/g}_{\text{cat}}$  accessible Pt. Thus, the CO<sub>2</sub> formed can originate from the oxidation of CO adsorbed on Pt, and/or carbonaceous specie present on catalyst. The amount of CO<sub>2</sub> observed corresponded to about 20% of all the accessible Pt sites covered with CO (IR shows that CO is present on Pt at these temperatures, see Fig. 2). Thus very little or no coke type species are present on the catalyst. Accordingly, we exclude blockage by coke species to be the reason for catalyst deactivation since an oxidative regeneration also did not result in regaining catalyst activity (Fig. 1).

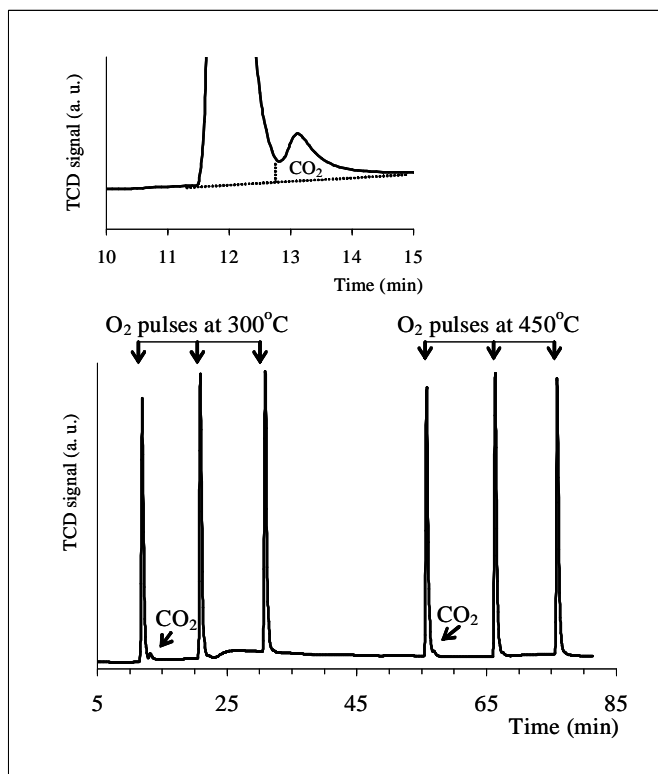


Fig. 3: CO<sub>2</sub> response using TCD observed from the successive pulses of O<sub>2</sub> at 300 and 450°C on Pt/TiO<sub>2</sub> catalyst after 20 h testing on the stream.

In the case of Pt/TiO<sub>2</sub> catalyst, the phenomenon of Strong Metal Support Interaction (SMSI) can also be of critical importance [18-20]. This phenomenon occurs when the catalyst is reduced (*e.g.* in H<sub>2</sub> or CO) at higher temperatures (>300°C) resulting in covering (blockage) of metal Pt by partially reduced titania (TiO<sub>2-x</sub>) species [18-20]. SMSI, if present, can thus affect the catalytic activity. For Pt/TiO<sub>2</sub>, SMSI is usually observed when the reduction temperature is above 300°C [18-20]. The criterion for the presence of SMSI state is the loss of hydrogen or CO adsorption capacity without significant enlargement of Pt particle size. An oxidation treatment usually reverses the SMSI state [18].

In order to check the relevance of SMSI, the influence of reduction temperature on Pt metal dispersion was studied. Table 1 shows the effect of reduction temperature ( $T_R$ ) on hydrogen chemisorption capacity for Pt/TiO<sub>2</sub> catalyst. Indeed, reduction at temperatures higher than 300°C seemingly induced SMSI. The chemisorption capacity (H/Pt) dropped

from 55% to 15% when the reduction temperature increased from 300 to 450°C. When the last catalyst (*i.e.*, reduced at 450°C) was re-oxidized in O<sub>2</sub> at 450°C (followed by standard pre-reduction in H<sub>2</sub> at 300°C), the hydrogen chemisorption capacity was completely recovered. It increased from 15% to 56% indicating return to pre-SMSI state as well as absence of any Pt particles sintering.

Table 1: Effect of reduction temperature ( $T_R$ ) on H<sub>2</sub> chemisorption (H/Pt) of Pt/TiO<sub>2</sub> catalyst (SMSI effect).

| $T_R$ (°C) | H/Pt (%)        |
|------------|-----------------|
| 200        | 55              |
| 250        | 54              |
| 300        | 54              |
| 350        | 42              |
| 400        | 34              |
| 450        | 15 <sup>a</sup> |

<sup>a</sup> The H/Pt increased to 56% when this sample re-oxidized in O<sub>2</sub> at 450°C and reduced in H<sub>2</sub> at 300°C.

To check if SMSI influenced Pt/TiO<sub>2</sub> deactivation, samples were reduced in pure hydrogen stream at three different temperatures (*i.e.* 300, 350 and 400°C) prior to catalytic testing. Figure 4 shows the influence of reduction temperature on WGS CO conversion. For the samples reduced at 350 and 400°C (where SMSI can occur) initial CO conversions were 32 and 30%, respectively. However, CO conversions increased to 38% after 4 minutes time on stream indicating that the catalyst activity was completely recovered. After this all catalysts followed the same trend in deactivation. This means that the SMSI effect, if present, was almost immediately reversed under WGS reaction conditions. Our observations are in agreement with those of Haller *et al.* [18] who proposed that presence of H<sub>2</sub>O is able to reverse the SMSI state. We can conclude therefore that any influence of SMSI on catalyst deactivation can be excluded during WGS conditions used in our study.

Further, it is possible that, TiO<sub>2</sub> support is susceptible to reduction due to the presence of CO and H<sub>2</sub> during WGS. This might lead to loss of support surface area and probably affect catalyst activity, as was observed for ceria [11]. BET surface area measurements before and after 20 h catalytic testing showed no change in the catalyst surface area (48 ±

1 m<sup>2</sup>/g). Moreover, results shown in Fig. 4 also indicate no irreversible deactivation when the catalyst was reduced in pure H<sub>2</sub> at higher temperature (e.g. 400°C).

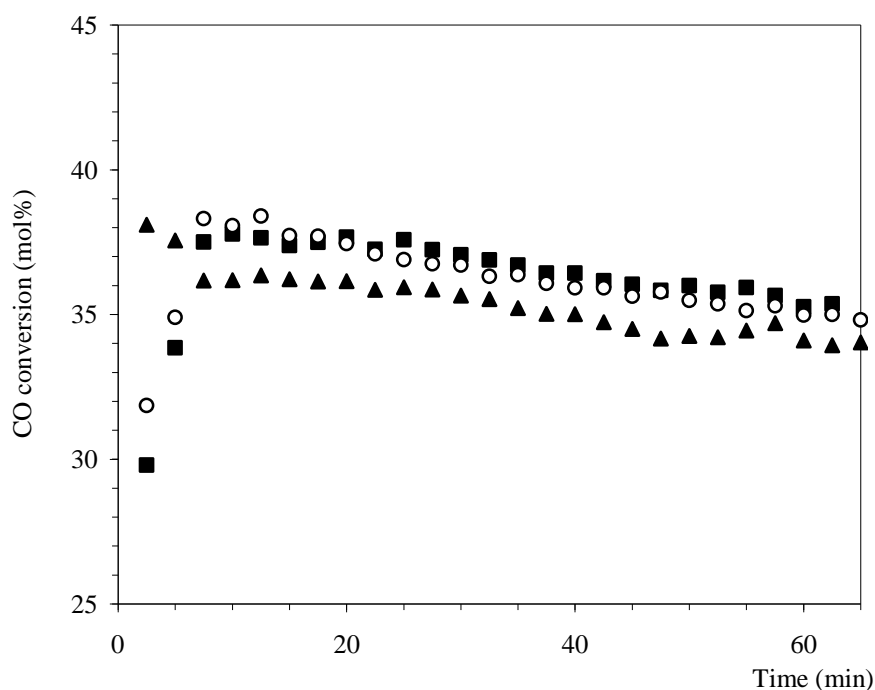


Fig. 4: Effect of reduction temperature in WGS CO conversion over Pt/TiO<sub>2</sub>. Conditions:  $p_{\text{CO}}=60\text{mbar}$ ,  $p_{\text{H}_2\text{O}}=150\text{ mbar}$ ,  $T_{\text{rxn}}=300^\circ\text{C}$ ,  $P=2\text{bar}$ ,  $\text{HSGV}=1,050,000\text{ hr}^{-1}$ . Reduced in H<sub>2</sub> at (▲) 300°C; (○) 350°C; (■) 400°C.

Figure 5 shows the Pt dispersions for Pt/TiO<sub>2</sub> catalysts measured after various stages of catalyst testing. Pt dispersion was 55% (1.9 nm Pt particle size) for fresh catalyst (Fig. 5(a)); however, it dropped to 34% (Fig. 5(b)) after 20 h time on stream. Catalyst deactivation during this period can thus be related to the loss of Pt metal surface. TEM results [1] confirmed the growth of Pt particles after WGS tests, in which average Pt particle size increased from  $1.2 \pm 0.2\text{ nm}$  to  $2.7 \pm 0.4\text{ nm}$  after 20 h testing. Therefore, based on the above results, we conclude that Pt sintering is exclusively the cause of Pt/TiO<sub>2</sub> deactivation during WGS reaction.

In order to understand what causes Pt sintering and the related deactivation, we performed a set of experiments where the catalyst was pre-treated with reactants, intermediates or products prior to catalytic testing. The WGS CO conversions following the pre-treatments are illustrated in Fig. 6. The choice of HCOOH is based on the fact

that surface formate is a possible intermediate over Pt/TiO<sub>2</sub> during WGS [1]. Figure 6 shows that there is no evidence for the deactivation due to the presence of H<sub>2</sub>, CO, CO<sub>2</sub>, HCOOH or a mixture of H<sub>2</sub>/CO<sub>2</sub>. H<sub>2</sub>O had a smaller effect on the catalyst, the CO conversion dropped from 60% (no pre-treatment) to 55% after 20 h pre-treatment in H<sub>2</sub>O at 300°C. Pre-treating the catalyst with H<sub>2</sub>/CO mixture caused the most significant deactivation, CO conversion dropped to 47%, following the pre-treatment, *i.e.*, the catalyst lost about 22% (relatively) of its initial activity.

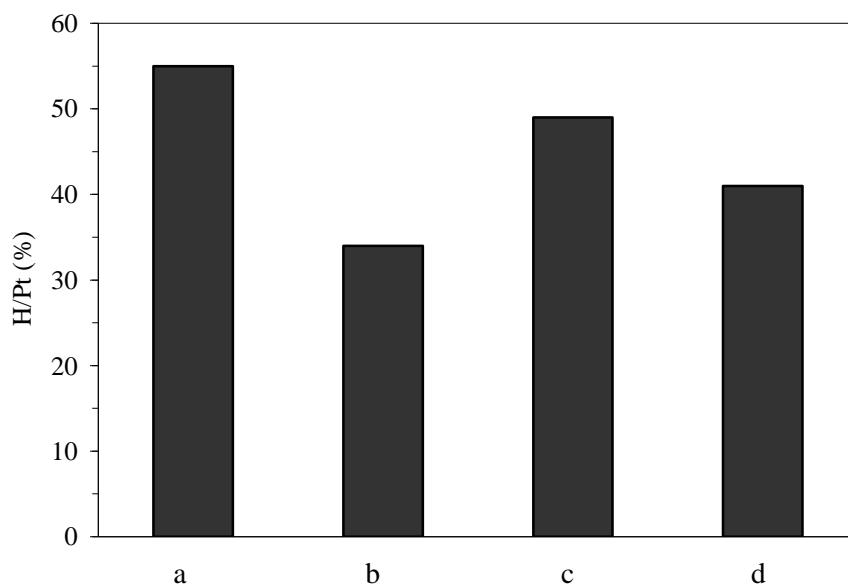


Fig. 5: Pt dispersion of Pt/TiO<sub>2</sub> using H<sub>2</sub> chemisorption. (a) before test, (b) after 20 hrs WGS catalytic test after (c) 20 hrs pretreatment in H<sub>2</sub>O, (d) after 20 hrs pretreatment in a mixture of CO/H<sub>2</sub>.

The measurements of Pt dispersions (Fig. 5) confirmed the effect of pre-treatments in H<sub>2</sub>O or mixture of CO/H<sub>2</sub> on catalyst deactivation. To recall, during WGS test Pt dispersion of the catalyst was 55% to start with and it dropped to 34% after 20 h time on stream. In the case of pre-treatment of the catalyst in H<sub>2</sub>O for 20 h, Pt dispersion dropped from 55% to 49%. However, it dropped to 41% when pre-treated in a mixture CO/H<sub>2</sub>. These results imply that both H<sub>2</sub>O (to a smaller extent) and a CO/H<sub>2</sub> mixture contributed to the loss of platinum surface area (Pt sintering).

As shown above, the decrease in activity when pre-treated with H<sub>2</sub>O does not completely mimic the deactivation behavior after 20 h catalytic testing (35% relative loss in CO conversion). A significant influence on catalyst deactivation was observed when the catalyst pre-treated with CO/H<sub>2</sub> mixture. Therefore, the major cause of deactivation may be related more to the presence of the mixture of CO/H<sub>2</sub> or surface species formed from it. Kim *et al.* [7] also reported deactivation of Au/CeO<sub>2</sub> catalyst in WGS due to the presence of CO/H<sub>2</sub>. They [7] attributed this to the formation of carbonate on CeO<sub>2</sub> surface. It is important to emphasize here that carbonates are unstable on Pt/TiO<sub>2</sub> catalyst at 300°C (Figs. 2 and 3). Moreover, we showed in Fig. 1 that treating the spent catalyst in oxygen at 450°C (conditions under which carbonate can be completely removed) did not help in regenerating the catalyst. Therefore, carbonates are ruled out as significant in our case.

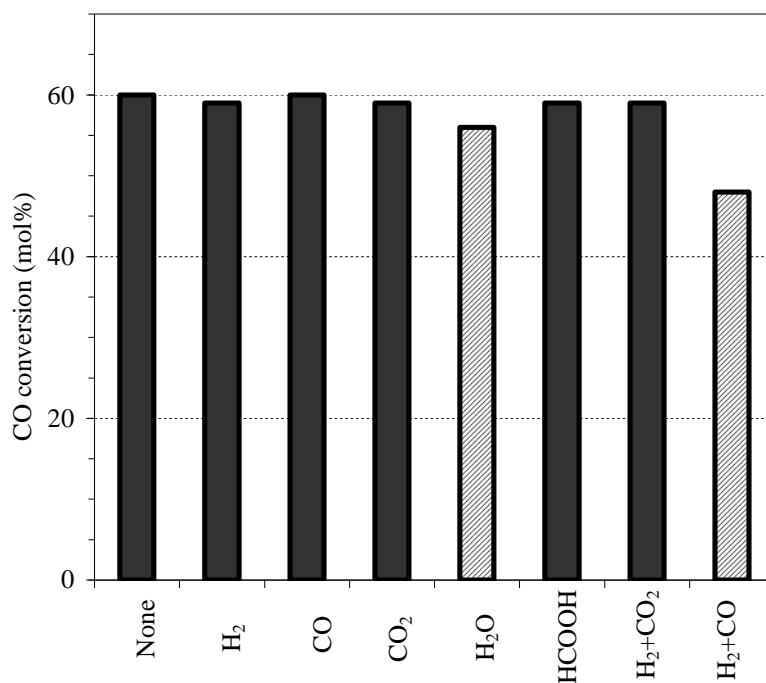


Fig. 6: Initial WGS CO conversions for Pt/TiO<sub>2</sub> catalyst following pre-treatment in gas(es) at 300°C for 20 hrs. Conditions:  $p_{\text{CO}}=60\text{mbar}$ ,  $p_{\text{H}_2\text{O}}=150\text{mbar}$ ,  $T_{\text{rxn}}=300^\circ\text{C}$ ,  $P=2\text{bar}$ , and  $\text{GHSV}=410,000\text{hr}^{-1}$ .

In our attempts to understand the role of CO/H<sub>2</sub> on catalyst deactivation (Pt sintering), we led CO/H<sub>2</sub> (50% each) at 300°C over Pt/TiO<sub>2</sub> and followed all possible mass

fragmentations by Mass Spectroscopy. Only traces of CH<sub>4</sub> were detected implying CO hydrogenation reaction to methane. Figure 7 shows *in situ* FTIR spectra obtained during the pre-treatments of Pt/TiO<sub>2</sub> catalyst with CO/H<sub>2</sub> mixture (50% each) at 300°C. In addition to gaseous CO (2143 cm<sup>-1</sup>), we observed three bands at 2071, 2830, 3015, and a broad band from 2915 – 2960 cm<sup>-1</sup>.

The band at 2071 cm<sup>-1</sup> corresponds to adsorbed CO on platinum (CO-Pt) [13, 15, 16]. It is clearly seen that the intensity of this CO-Pt band decreased with time on stream. This decrease in its intensity (2071 cm<sup>-1</sup>) implies that Pt surface area was lost with time and bigger particles (Pt sintering) were formed. This is in agreement with our observations from catalytic testing and Pt dispersion measurements.

The bands at 2830, 2915 – 2960, 3015 cm<sup>-1</sup> correspond to the C-H stretching of aldehyde [21, 22], surface formate species [23, 24], and gaseous CH<sub>4</sub> [25], respectively. The pre-treatment of Pt/TiO<sub>2</sub> catalyst with formic acid (this will generate formate species on TiO<sub>2</sub> surface) did not influence the catalyst stability (Fig. 6), therefore, we rule out the role of surface formate on Pt sintering. The other two possibilities, CH<sub>4</sub> or aldehyde (*e.g.* formaldehyde), imply a reaction of CO with H<sub>2</sub> (CO hydrogenation reaction). However, we did not observe any formation of gaseous methane during WGS reaction conditions, (the detection limit of the Micro-GC used was 10 ppm), [1, 13]. Therefore, we rule out any role of CH<sub>4</sub> in causing Pt sintering.

To check if there is any role of formaldehyde on Pt sintering, we pre-treated a fresh Pt/TiO<sub>2</sub> catalyst (Pt dispersion of 55%) with gaseous formaldehyde for 20 h. The catalyst was first reduced in 10% H<sub>2</sub>/N<sub>2</sub> at 300°C for 1 h then flushed with N<sub>2</sub> for another 1 h. Gaseous formaldehyde was provided to the catalyst by heating a vessel containing paraformaldehyde and flushed with N<sub>2</sub> stream (50ml/min) at 60°C. After 20 h pre-treatments, the catalyst was heated in oxygen at 450°C to burn off any carbon deposited on the catalyst prior to Pt dispersion measurements. Indeed a decrease in Pt dispersion from 55% to 30% was observed. This indicates a strong influence of formaldehyde, either in gaseous phase or as adsorbed species, on the sintering of small Pt particles on TiO<sub>2</sub>

surface. It is known that formaldehyde type species can be formed during WGS reaction, from the contact of CO and H<sub>2</sub> on Pt [26].

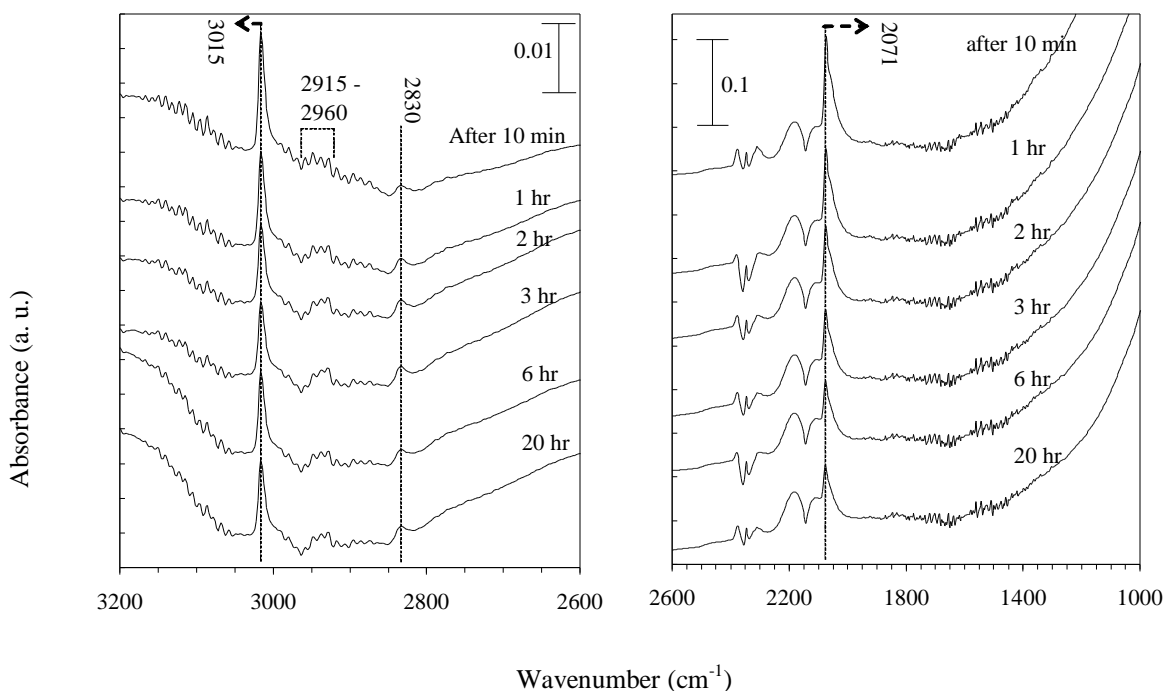


Fig. 7: *In situ* FTIR spectra for the Pt/TiO<sub>2</sub> catalyst following treatment in CO/H<sub>2</sub> with time.

No information relevant to our studies could be traced in published literature regarding sintering of Pt particles assisted by oxygenate species. Trimm [27] reported, while converting methane to formaldehyde, that further oxidation of formaldehyde to carbon oxides can result in Pt sintering due to the exothermicity of the reaction. This is highly unlikely in our case as the ambient is more reducing than oxidising during water gas shift reaction. We speculate, from our consistent observations that the presence of formaldehyde probably in combination with the presence of defect titania, enhances Pt mobility on TiO<sub>2</sub> and cause Pt sintering. More studies are necessary to pinpoint the exact steps involved.

The results discussed above and our earlier work in chapter 3 [1] showed that Pt/TiO<sub>2</sub> deactivates with time on stream during WGS reaction. The deactivation is caused from the loss of Pt surface area exclusively. We have shown in chapter 3 [1] that addition of

Re to Pt/TiO<sub>2</sub> catalyst can prevent Pt sintering and allows significant improvement on catalyst stability. The details of the influence of Re on Pt/TiO<sub>2</sub> stability (characterization) is described in chapter 5.

#### **4.4. Conclusions**

Growth of Pt metal particles during WGS reaction is the cause of Pt/TiO<sub>2</sub> deactivation, exclusively. We exclude any influence of SMSI state, carbon deposition or “over”-reduction of TiO<sub>2</sub> as reasons for catalyst deactivation. At the experimental conditions of this work, Pt particles grow because of their contacts with a mixture of CO/H<sub>2</sub> during WGS; in addition, H<sub>2</sub>O has small effect on Pt sintering. We speculate that the formation of traces of CH<sub>2</sub>O on Pt surface enhances Pt mobility on TiO<sub>2</sub> and causes Pt sintering.

## 4.5. References

- [1] K. G. Azzam, I.V. Babich, K. Seshan and L. Lefferts, *J. Catal.* 251(2007) 163.
- [2] S. Hilaire, X. Wang, T. Luo, R.J. Gorte, J. Wagner, *Appl. Catal. A* 215 (2001) 271.
- [3] T. Bunluesin, R. J. Gorte, G. W. Graham, *Appl. Catal. B* 15 (1998) 107.
- [4] Q. Fu, H. Saltsburg, M. Flytzani-Stephanopoulos, *Sci.* 301 (2003) 935.
- [5] X. Wang, R. J. Gorte, J. P. Wagner, *J. Catal.* 212 (2002) 225.
- [6] X. Liu, W. Ruettinger, X. Xu, R. Farrauto, *Appl. Catal. B* 56 (2005) 69.
- [7] C. H. Kim, L. T. Thompson, *J. Catal.* 230 (2005) 66.
- [8] F. C. Meunier, D. Tibiletti, A. Goguet, D. Reid, R. Burch, *Appl. Catal. A* 289 (2006) 104.
- [9] G. Jacobs, L. Williams, U. Graham, D. Sparks, B. Davis, *J. Phys. Chem. B* 107 (2003) 10398.
- [10] R. J. Gorte, S. Zhao, *Catal. Today* 104 (2005) 18.
- [11] J. M. Zalc, V. Sokolovskii, D. G. Löffler, *J. Catal.* 206 (2002) 169.
- [12] D. C. Grenoble, M. M. Estadt, D. F. Ollis, *J. Catal.* 67 (1981) 90.
- [13] K. G. Azzam, I.V. Babich, K. Seshan and L. Lefferts, *J. Catal.* 251 (2007) 153.
- [14] J. A. Wang, A. Cuan, J. Salamones, N. Nava, S. Castillo, M. Moran-Pineda, F. Rojas, *Appl. Surf. Sci.* 230 (2004) 94.
- [15] Y. Sato, K. Terada, S. Hasegawa, T. Miyao, S. Naito, *Appl. Catal. A* 296 (2005) 80.
- [16] H. Iida, A. Igarashi, *Appl. Catal. A* 298 (2006) 152.
- [17] J. Steyn , G. Patrick, M. S. Scurrall, D. Hildebrandt, M. C. Raphulu, E. van der Lingen, *Catal. Today* 122 (2007) 254 and references therein.
- [18] G. L. Haller, D. E. Resasco, *Adv. Catal.* 36 (1989) 173.
- [19] Y. Li, Y. Fan, H. Yang, B. Xu, L. Feng, M. Yang, Y. Chen, *Chem. Phys. Lett.* 372 (2003) 160.
- [20] H. Iddir, M. M. Disko, S. Ogut, N. D. Browning, *Micron* 36 (2005) 233.
- [21] R. Grabowski, J. haber, *React. Kinet. Catal. Lett.* 21 (1982) 455.
- [22] J. A. Atride, P. H. Dallin, U. A. Jayasooriya, *J. Chem. Phys.* 119 (2003) 2747.
- [23] A. Holmgren, B. Andersson, D. Duprez, *Appl. Catal. B* 22 (1999) 215.

- [24] G. Jacobs, E. Chenu, P. M. Patterson, L. Williams, D. Sparks, G. Thomas, B. H. Davis, *Appl. Catal. A* 258 (2004) 203.
- [25] N. M. Gupta, V. S. Kample, R. M. Iyer, *Catal. Lett.* 21 (1993) 245.
- [26] N. V. Pavlenko, N. I. O'chenko, Yu. I. Pyatnitskii, *Theoretical and Experimental Chemistry*, 33 no.5 (1997) 254.
- [27] D.L. Trimm, *Pure & Appl. Chem.*, 50 (1978) 1147.

# Chapter 5

## Optimization and characterization of Pt-Re/TiO<sub>2</sub> for WGS

---

### *Abstract*

*The catalytic performance of Pt-Re/TiO<sub>2</sub> catalyst (activity and stability) was optimized by studying the influence of preparation strategies, Pt/Re molar ratios, and metals content. Results indicated that sequential impregnation of Re precursor prior to Pt precursor without intermediate pretreatment is the optimum preparation strategy. The Pt/Re ratio of unity with 0.5wt% Pt content showed excellent activity and stability in the Water Gas Shift reaction at moderate temperature (300°C). Characterizing the monometallic and bimetallic Pt-Re catalysts with CO chemisorption, H<sub>2</sub>-TPR, CO-TPD, and in situ FTIR CO adsorption at 300°C provided no evidence for strong interaction between Pt and Re (no alloy formation). During WGS reaction at 300°C, the interaction is more pronounced. In situ XPS characterization is highly recommended to investigate this in further detail.*

**Keywords:** *Water Gas Shift (WGS); Platinum; Rhenium; Titania; Activity; Stability; Optimizations; Characterization.*

## 5.1 Introduction

Recently, there is growing interest in developing efficient, single stage water gas shift (WGS) catalysts because of the importance of this reaction in maximizing the H<sub>2</sub> yield in the reformat mixture resulting from steam-reforming and/or partial oxidation of hydrocarbons. The current commercial WGS technology, which involves multiple stages/catalysts: HTS (Fe<sub>2</sub>O<sub>3</sub>/Cr<sub>2</sub>O<sub>3</sub>) and LTS (Cu/ZnO/Al<sub>2</sub>O<sub>3</sub>) is not suitable for mobile fuel cell applications because of its technical complexity [1,2]. There is thus tremendous interest in the development of new catalysts for single stage WGS conversion. Supported noble metal, *e.g.* Pt, based catalysts are promising single stage WGS catalysts because they are robust and they can operate at higher temperatures where the kinetics is more favorable in contrast to the LTS Cu catalysts. Such catalysts should contain very low loading of precious metals (preferably <0.5 wt%) because of the high cost of Pt.

We have shown in chapter 3 [3] that Pt/TiO<sub>2</sub> catalysts exhibit excellent activity for WGS and are even more active than Pt/CeO<sub>2</sub> and Pt/Ce<sub>x</sub>Zr<sub>1-x</sub>O<sub>2</sub> which are claimed as promising catalysts for WGS reaction [4-6]. However, Pt/TiO<sub>2</sub> deactivated with time on stream. Loss of Pt active surface area, during WGS reaction, was the exclusive cause of deactivation (see Chapter 4). Deactivation can be avoided by adding Re to the Pt/TiO<sub>2</sub> catalyst [3]. Interestingly, addition of Re not only prevents catalyst deactivation, but it also enhances the catalyst activity; turn over frequency (TOF, s<sup>-1</sup>) increased from 10 s<sup>-1</sup> (Pt/TiO<sub>2</sub>) to 15 s<sup>-1</sup> (Pt-Re/TiO<sub>2</sub>) [3].

In naphtha reforming industry, bimetallic catalyst, based on Pt-Re/Al<sub>2</sub>O<sub>3</sub>, was introduced in the late sixties and offered improved activity and stability compared to monometallic Pt/Al<sub>2</sub>O<sub>3</sub> catalyst [7]. Although the Pt-Re/Al<sub>2</sub>O<sub>3</sub> catalysts have been in use for many years, there is still considerable debate about the location and the oxidation state of rhenium. However, it has been reported without clear explanation that the state of added Re and its interaction with Pt is a function of a variety of factors such as, the metal precursors employed [8,9], the preparation procedure [10,11], pretreatment conditions

(oxidation and reduction) [9,12,13], Re loading and Pt/Re ratio [8,10] and the oxide support used [8,14].

Recently, explorative optimization and characterization studies were carried out for Pt-Re/TiO<sub>2</sub> [15,16] and Pt-Re/Ce<sub>x</sub>Zr<sub>1-x</sub>O<sub>2</sub> [17] catalysts in WGS reaction. Improved activity of Re based catalysts has been reported, however, there is no agreement on the cause why WGS activity is increased by Re addition. Sato *et al.* [16] explain the higher activity due to formation of bimetallic clusters containing Pt and Re (alloy formation) in the Pt-Re/TiO<sub>2</sub> catalyst and showed that Pt/Re ratio strongly influences the WGS activity. On the other hand, Iida and Igrashi [15] attributed the influence of Re, in Pt-Re/TiO<sub>2</sub>, to increased Pt dispersion by anchoring the Pt particles, without forming any alloy. Choung *et al.* [17] concluded, from their study on Pt-Re/Ce<sub>x</sub>Zr<sub>1-x</sub>O<sub>2</sub> catalyst for WGS, that the role of Re in enhancing the WGS activity of Pt is more complex than to just increase the Pt dispersion, without providing an alternative explanation.

The objective of this chapter is (i) to optimize the performance of Pt-Re/TiO<sub>2</sub> catalyst in WGS (activity and stability) by studying the influences of the preparation strategy, Pt/Re molar ratio and metals loading and (ii) to investigate the role of Re in enhancing the activity and stability of Pt-Re/TiO<sub>2</sub> catalyst by characterizing the catalyst using a variety of experimental techniques such as CO chemisorption, H<sub>2</sub>-TPR, CO-TPD, and *in situ* FTIR during CO adsorption and during WGS reaction.

## **5.2. Experimental**

### **5.2.1. Catalysts preparation**

#### **5.2.1.1. Effect of preparation strategy**

Six bimetallic catalysts having composition 0.5wt%Pt-0.5wt%Re/TiO<sub>2</sub> (A – F) were prepared by either sequential impregnation or co-impregnation using the conventional wet impregnation technique; details of the preparation methods are summarized in

Table 1. A monometallic catalyst (A) was used as a basis for comparison. Commercial TiO<sub>2</sub> (P25, Degussa) was used as the support material. Before impregnation, the support was treated in synthetic air at 500°C for 1 h prior to impregnation of the noble metal precursor. Titania was then impregnated using appropriate quantities of aqueous H<sub>2</sub>PtCl<sub>6</sub> (Aldrich) and NH<sub>4</sub>ReO<sub>4</sub> (Aldrich) solutions, with continuous stirring for 1 h, as required by the impregnation strategy used (see Table 1). All prepared samples were then dried at 75°C for 2 h in rotary vacuum evaporator and subsequently calcined in synthetic air at 450°C for 4 h.

Table 1: Preparation strategy for Pt-Re/TiO<sub>2</sub> catalysts

| Catalyst | Amount of metals impregnated (wt%) |      | Details of impregnation sequence and other treatments                     |
|----------|------------------------------------|------|---|
|          | Pt                                 | Re   |   |
| A        | 0.5                                | -    | Pt precursor – Drying <sup>1</sup> – Calcination <sup>2</sup>             |
| B        | 0.5                                | 0.5  | Pt precursor – Re precursor – Drying – Calcination                        |
| C*       | 0.5                                | 0.5  | Pt precursor – Drying – Calcination – Re precursor – Drying – Calcination |
| D        | 0.5                                | 0.5  | Re precursor – Drying – Calcination – Pt precursor – Drying – Calcination |
| E        | 0.5                                | 0.5  | Re and Pt precursor (co-impregnation) – Drying – Calcination              |
| F        | 0.5                                | 0.5  | Re precursor – Pt precursor – Drying – Calcination                        |
| G        | 0.5                                | 1    | Re precursor – Pt precursor – Drying – Calcination                        |
| H        | 0.5                                | 0.25 | ≈   |
| I        | 0.5                                | 0.1  | ≈   |
| J        | 0.5                                | 0.05 | ≈   |
| K        | 0.3                                | 0.3  | Re precursor – Pt precursor – Drying – Calcination                        |
| L        | 0.1                                | 0.1  | ≈   |
| M        | 0.05                               | 0.05 | ≈   |

<sup>1</sup>: Drying in vacuum at 75°C

<sup>2</sup>: Calcination in air at 450°C

\* prepared from same batch of catalyst A.

### 5.2.1.2. Effect of Pt/Re molar ratios

Several catalysts with different Pt and Re molar ratios (Table 1, catalysts F – J) were prepared using the wet impregnation technique and the best preparation strategy, as will be discussed later (similar to Catalysts F, sequential impregnation without any

intermediate treatment). The molar ratio of Pt and Re was varied between (0.5/1) to (10/1) by changing the Re contents and using a fixed amount of Pt (0.5wt%).

### **5.2.1.3. Effect of Pt and Re loadings**

Catalysts F, K, L, and M were prepared with different amounts of Pt and Re, keeping the same Pt/Re molar ratio, to study the influence of metal loadings on catalyst performance. These catalysts were prepared using wet impregnation technique and using the optimum preparation strategy (Catalyst F) and optimum molar ratio of Pt and Re (Table 1), based on the results shown later. Samples F, K, L, and M contained 0.5, 0.3, 0.1, and 0.05wt. % of Pt and Re, respectively.

### **5.2.2. Catalysts characterization**

The surface areas of the catalysts were measured with N<sub>2</sub> fysisorption, applying the BET method, using a Micromeritics ASAP 2400 device. Platinum loadings were determined using a Philips PW 1480 X-ray fluorescence spectrometer.

Platinum dispersions were determined with CO chemisorption at room temperature using Micromeritics Chemisorb 2750. The amount of sample used for each measurement was ~ 250mg. Prior to measuring the CO uptake, the samples were reduced in pure H<sub>2</sub> (99.9%) from room temperature to 300°C at a heating rate of 10°C/min, flushed with He at 425°C for 1 h and then cooled to room temperature (25°C) in He. The CO uptake measurements were conducted at room temperature by injecting a series of pulses containing 1 mL of CO into a He stream flowing over the sample at a rate of 25 mL/min and measuring the amount of CO adsorbed per pulse. The experimental procedure was adopted based on our IR results on Pt-Re/TiO<sub>2</sub> which showed, in agreement with finding of Peick *et al.* [18], that at room temperature, CO adsorbed on Pt exclusively.

Temperature Programmed Reduction ( $\text{H}_2$ -TPR) measurements were conducted using Micromeritics Autochem II 2920. In the  $\text{H}_2$ -TPR measurements, about one gram of catalyst was placed in a U-shaped quartz tube and preheated in a 20 ml/min Ar atmosphere to 300°C prior to the TPR experiment, and then cooled down to (-75°C) in Ar. A feed of 15%  $\text{H}_2$ /Ar was used as the reducing gas. The temperature of the sample was raised at a constant rate of 10°C/min from -75 to 850°C.

Temperature Programmed Desorption of CO (CO-TPD) measurements were carried out using Micromeritics Chemisorb 2750 device. About 250 mg sample was used for each measurement. Prior to performing the CO-TPD, the sample was reduced in pure  $\text{H}_2$  (99.9%), heated from room temperature to 300°C at a rate of 10°C/min; next, the sample was flushed with He at 425°C for one hour and then cooled in He to room temperature (25°C). Then CO was adsorbed at room temperature by injecting a series of pulses containing 1 mL of CO into the He stream flowing over the sample at a rate of 25 mL/min. After having a stable TCD signal by flushing with He for 1 h, the sample was heated in He (25 ml/min) stream from room temperature to 400°C.

FTIR spectra were recorded on self-supported catalyst pellets (about 10 mg of the catalyst) under flow conditions (5% CO/He, or (5% CO + 10%  $\text{H}_2\text{O}$ )/He) at 300°C using a Bruker Vector 22 with MCT detector. Prior to conducting the measurements, the samples were reduced in 25%  $\text{H}_2$ /He at 300°C for 30 min, flushed with He to 425°C for one hour, and then cooled down in He to 300°C.

### **5.2.3. Catalytic test**

WGS activity and stability tests were carried out using a conventional fixed bed flow reactor (3mm i. d.). Details are described in Chapter 3 [3]. The total flow rate of the feed gas was kept at 350 ml/min. Space velocity is varied by the weight of the catalyst. The feed gas mixture contained 3 vol. % CO, 7.5%  $\text{H}_2\text{O}$  and  $\text{N}_2$  balance. For the intrinsic activity measurements (TOF,  $\text{s}^{-1}$ ), the conversion of CO was kept below 15% to work close to differential conditions by working at high space velocity (2,050,000  $\text{h}^{-1}$ ). The

stability tests were measured at higher CO conversion (integral conditions) by using a lower space velocity ( $410,000 \text{ h}^{-1}$ ).

## 5.3. Results and discussion

### 5.3.1. Catalyst optimization

#### 5.3.1.1. Effect of preparation strategy

The effects of (i) catalyst preparation strategy and (ii) impregnation sequence on catalytic performance were investigated on the bimetallic  $0.5\text{wt}\%\text{Pt}-0.5\text{wt}\%\text{Re}/\text{TiO}_2$  catalysts prepared by either sequential impregnation or co-impregnation. These effects were investigated by testing samples for their physical and chemical characteristics and their performance in WGS reaction.

The BET surface area, metal loadings and Pt metal surface area (measured by CO chemisorption) for all catalysts studied in this chapter are given in Table 2. The BET surface area measurements for selected samples (Catalysts A, F, and K) were similar ( $48 \pm 1 \text{ m}^2/\text{g}$ ) indicating no effect of Pt or Re impregnation on the surface area of  $\text{TiO}_2$ . The metal contents (XRF) of the catalysts were close to the values expected based on the preparation procedures, *e.g.*,  $0.5 \pm 0.05 \text{ wt}\%$  for the catalysts (A – F).

The results of CO chemisorption (Table 2, catalysts A – F) show that the changes in the impregnation sequence led to significant changes in the CO chemisorption capacity (Pt metal surface area) of the samples. Depositing Re prior to Pt (samples D and F) or co-impregnation of Re and Pt (sample E) resulted in better chemisorption capacity as compared to depositing Pt prior to Re (samples B and C). For instance, catalyst C is prepared by impregnation of Re precursor onto the  $0.5\text{wt}\%\text{Pt}/\text{TiO}_2$  (catalyst A, Table 1). The CO chemisorption capacity dropped from 49% (catalyst A) to 33% (catalyst C). Similarly, Catalyst B has also lower CO adsorption capacity (32%), although there was no intermediate treatment (drying and calcination) prior to Re precursor impregnation.

We have previously found, in agreement with Pieck *et al.* [18], that Re does not adsorb CO below 50°C. Therefore, this significant drop in CO chemisorption capacity in catalysts B and C is most probably caused by covering part of Pt surface by Re or ReO<sub>x</sub>. Dexpert *et al.* [19] reported using EXAFS that Re has higher affinity to react with chlorine than oxygen. Thus, it is also possible that Re reacts with the chlorine from the deposited PtCl<sub>6</sub><sup>-2</sup> on TiO<sub>2</sub>, resulting in covering part of Pt surface with Re chloride or oxy-chloride.

Table 2: Physical and chemical characteristics of the catalysts.

| Catalyst | BET surface area (±1m <sup>2</sup> /g) | Pt and Re contents (±0.05wt%) <sup>1</sup> |       | CO/Pt (±3%) <sup>2</sup> | TOF <sup>3</sup> ± 1 at 300°C |
|----------|--|--|-------|--------------------------|-------------------------------|
|          |  | Pt   | Re    |                          |                               |
| A        | 48                                     | 0.49                                       | -     | 49                       | 10                            |
| B        | n.m. <sup>4</sup>                      | 0.50                                       | 0.54  | 32                       | 15                            |
| C        | n.m                                    | 0.51                                       | 0.49  | 33                       | 14                            |
| D        | n.m                                    | 0.50                                       | 0.47  | 47                       | 16                            |
| E        | n.m                                    | 0.51                                       | 0.47  | 53                       | 14                            |
| F        | 49                                     | 0.49                                       | 0.48  | 50                       | 15                            |
| G        | n.m                                    | 0.49                                       | 0.98  | 32                       | n.m                           |
| H        | n.m                                    | 0.52                                       | 0.23  | 59                       | n.m                           |
| I        | n.m                                    | 0.50                                       | 0.12  | 60                       | n.m                           |
| J        | n.m                                    | 0.51                                       | 0.06  | 60                       | n.m                           |
| K        | 47                                     | 0.34                                       | 0.26  | 58                       | 14                            |
| L        | n.m                                    | 0.14                                       | 0.13  | 70                       | 16                            |
| M        | n.m                                    | n. m.                                      | n. m. | 40 <sup>5</sup>          | 14                            |

<sup>1</sup> Measured by XRF

<sup>2</sup> Measured by CO chemisorption

<sup>3</sup> TOF (s<sup>-1</sup>) is the activity per surface Pt, which is measured at differential conditions (X<sub>CO</sub><20%)

<sup>4</sup> n.m: not measured

<sup>5</sup> Calculated assuming a 0.05 wt% of each Pt and Re.

Figure 1 shows the influence of changes in the preparation strategy on WGS activity and stability in terms of CO conversion *versus* time at 300°C. It is obvious that impregnation of Re before Pt (catalysts D and F) gives better catalyst activity. A direct relation between the active metal surface area (CO chemisorption capacity) and the total activities of the catalyst samples is observed. For instance, the initial CO conversion on catalyst F (CO/Pt is 50%) is 90% as compared to only 70% conversion for catalyst B (CO/Pt is 32%). When the intrinsic activities, *i.e.* TOF (s<sup>-1</sup>) are considered (see Table 2), on the other

hand, the performances of all Pt-Re/TiO<sub>2</sub> samples are similar. This indicates that the nature of the synergetic interaction between the active Pt and the surrounding Re or ReO<sub>x</sub> species is not affected by the changes in the impregnation strategy. Figure 1 also shows that the various preparation strategies affect the stability (time on stream behavior) differently. For example, catalyst F, without intermediate drying and calcination, is more stable than the other samples.

Comparing the monometallic catalyst A (0.5wt%Pt/TiO<sub>2</sub>) with the bimetallic catalyst F (0.5wt%Re, 0.5wt%Pt/TiO<sub>2</sub>), a significant improvement of both the intrinsic activity (Table 2) and total CO conversion (Fig. 1) are observed, despite similar Pt dispersions. The reason of enhancement of the catalytic activity will be discussed in detail in Chapter 6 [20].

Similar to our observations, Piek *et al.* [11] reported a strong influence of the preparation procedure and activation treatment (calcination and reduction) on the performance of Pt-Re/Al<sub>2</sub>O<sub>3</sub> catalyst in petroleum reforming reactions. Similarly, Carvalho *et al.* [12] showed a strong influence of the order of metal deposition on the efficiency of Pt-Re-Sn/Al<sub>2</sub>O<sub>3</sub> reforming catalyst. In contrast, Iida *et al.* [15] suggested no effect of impregnation sequences on 3%Pt-2%Re/TiO<sub>2</sub> catalyst performance in WGS, despite their experimental observation that the CO conversion varied between 15% to 25% at 175°C. However, it should be noted that the Pt and Re loadings as well as Pt/Re molar ratios were different in the study by Iida *et al.* [15] and our study, possibly influencing Pt dispersion and catalytic performance.

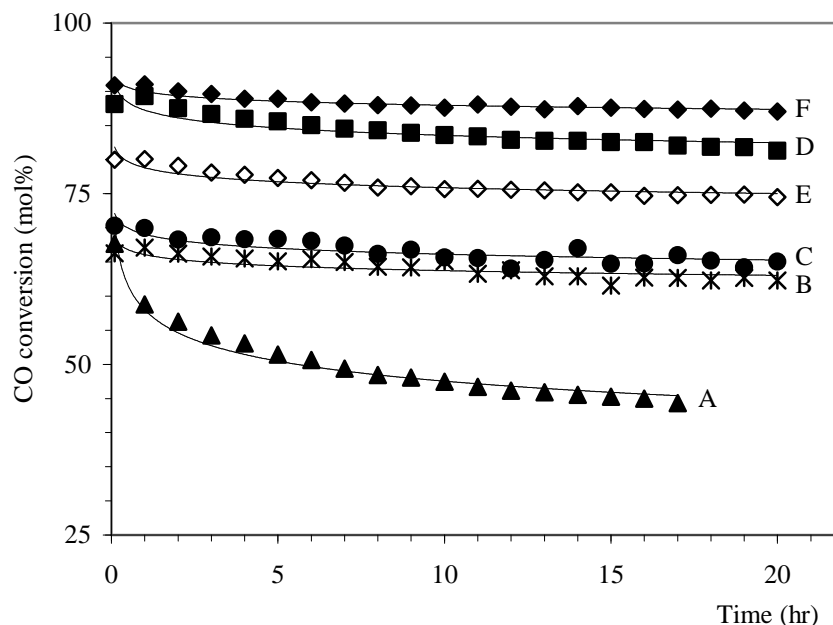


Fig. 1: WGS CO conversion at 300°C as a function of time on stream for (A) 0.5Pt/TiO<sub>2</sub>; (B, C, D, E, F) 0.5Pt-0.5Re/TiO<sub>2</sub> prepared by different strategies (see Table 1). Conditions: partial pressure of 60 and 150 mbar for CO and H<sub>2</sub>O respectively, P = 2bar, and HSGV = 410,000 hr<sup>-1</sup>

### 5.3.1.2. Effect of Pt/Re molar ratios

Figure 2 shows the WGS activity at 300°C in terms of CO conversion versus time, indicating the effect of Pt/Re molar ratio on the catalyst performance. The WGS activity increased gradually with increasing Re contents and showed a maximum at the Pt/Re molar ratio of 1/1 (catalyst F). Further increasing the Pt/Re ratio causes the activity to decrease (catalyst G). The data in Table 2 (catalysts F-J) show that also the Pt dispersion remain constant between 50 and 60% when increasing the Pt/Re ratio to 1/1. However, the Pt dispersion collapses to 32% (catalyst G) when the Re content is further increased, explaining the decrease in activity. On the other hand, the activity enhancement by Re addition for lower Pt/Re ratios is not due to increasing the Pt surface area, which is in agreement with our findings in Chapter 3 and 6 (ReO<sub>x</sub> adds extra red-ox route for WGS). The reasons for the increase in the catalyst activity for WGS will be discussed in detail in Chapter 6 [20].

Pt/Re ratio has also a significant influence on the stability of the catalysts. Increasing the Re content improves the stability, resulting in almost no deactivation within 20 h for Pt/Re ratio  $\geq 1$ . The optimum performance (higher activity and best stability) of the catalyst was clearly achieved at Pt/Re molar ratio of unity, as at higher Pt/Re ratio activity is strongly decreased.

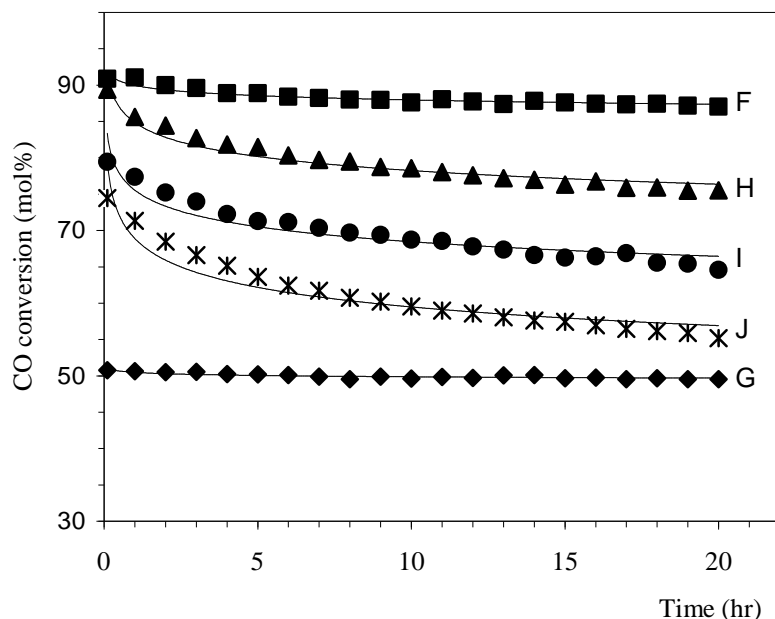


Fig. 2: WGS CO conversion at 300°C as a function of time on stream for 0.5Pt-xRe/TiO<sub>2</sub> (x=0.05–1 wt%). (F) 0.5Pt-0.5Re/TiO<sub>2</sub>, (H) 0.5Pt-0.25Re/TiO<sub>2</sub>, (I) 0.5Pt-0.1Re/TiO<sub>2</sub>, (J) 0.5Pt-0.05Re/TiO<sub>2</sub>, (G) 0.5Pt-1Re/TiO<sub>2</sub>. Conditions: partial pressure of 60 and 150 mbar for CO and H<sub>2</sub>O respectively, P =2bar, and HSGV =410,000 hr<sup>-1</sup>

### 5.3.1.3. Effect of Pt and Re loading.

Four Pt-Re/TiO<sub>2</sub> catalysts with different weight loadings (0.5, 0.3, 0.1 and 0.05wt% Pt) were prepared using the optimum preparation strategy (similar to catalyst F) and the optimum Pt/Re molar ratio (Pt/Re =1/1). Table 2 (Catalysts F, K, L) indicates that Pt dispersion increases with decreasing loading. The WGS reaction rates for these catalysts are shown in Figure 3, expressed in moles H<sub>2</sub> formed per gram of catalyst measured at differential conditions ( $X_{CO} < 15\%$ ).

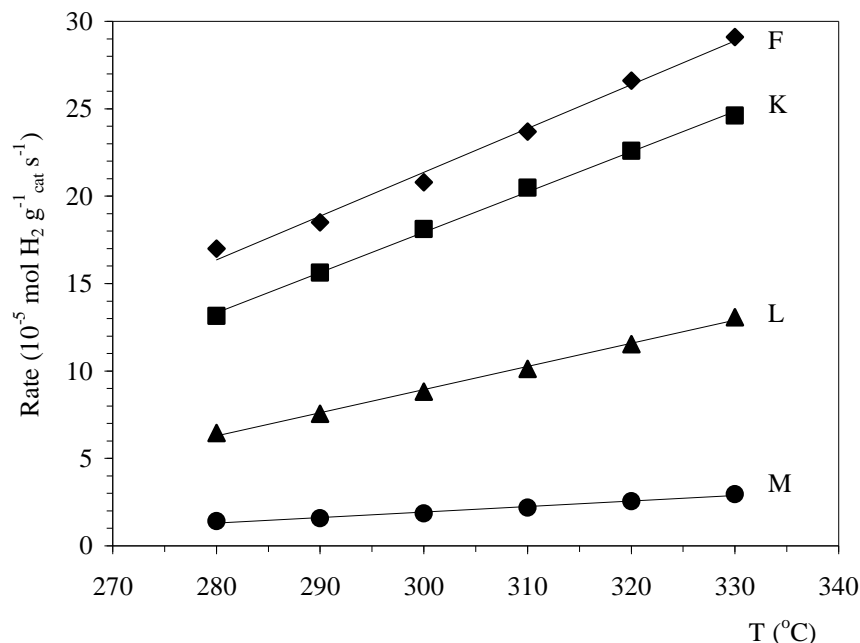


Fig. 3: WGS rate per gram catalyst of Pt-Re/TiO<sub>2</sub> at different Pt and Re weight loadings (see Table 2). Conditions: partial pressure of 60 and 150 mbar for CO and H<sub>2</sub>O respectively, P =2bar, and HSGV =2,100,000hr<sup>-1</sup>.

It is obvious from Fig. 3 that increasing Pt content results in a significant increase in WGS activity. The turnover frequencies (TOF, s<sup>-1</sup>) are compared in Fig. 4, demonstrating identical TOF's in the temperature window between 280 and 330°C, within experimental error. Apparently, the specific activity of Pt is not significantly influenced by the Pt loading or crystallite size. Similarly, it is also reported in literature that the WGS rate depends only on exposed metal surface area for Pt/TiO<sub>2</sub> [21], Pd/CeO<sub>2</sub> [22], and Pt-Re/Ce<sub>0.46</sub>Zr<sub>0.54</sub>O<sub>2</sub> [17].

The stability of catalysts with different metal loadings (F, K, L) were compared by measuring the integral WGS reaction rate at 300°C during 25 h, as shown in Figure 5. All catalysts showed good stability with time on stream, implying that catalyst stability is not significantly influenced by the metal loading. These results also confirm stability of Pt-Re/TiO<sub>2</sub> catalysts with 1/1 Pt/Re molar ratios.

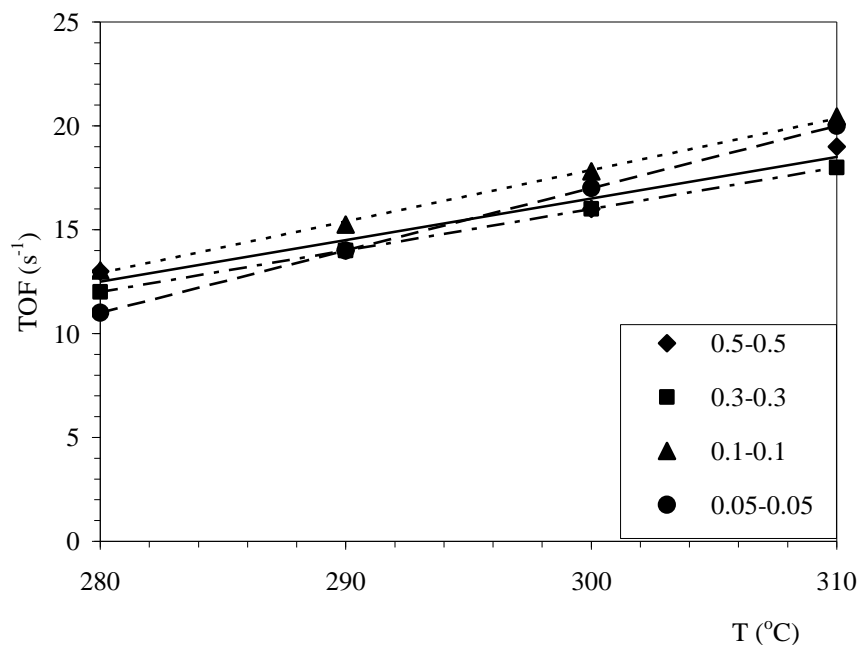


Fig. 4: TOF for the WGS reaction over Pt-Re/TiO<sub>2</sub> catalyst of variable metal loadings. Conditions: partial pressure of 60 and 150 mbar for CO and H<sub>2</sub>O respectively, P =2bar, and HSGV =2,100,000hr<sup>-1</sup>.

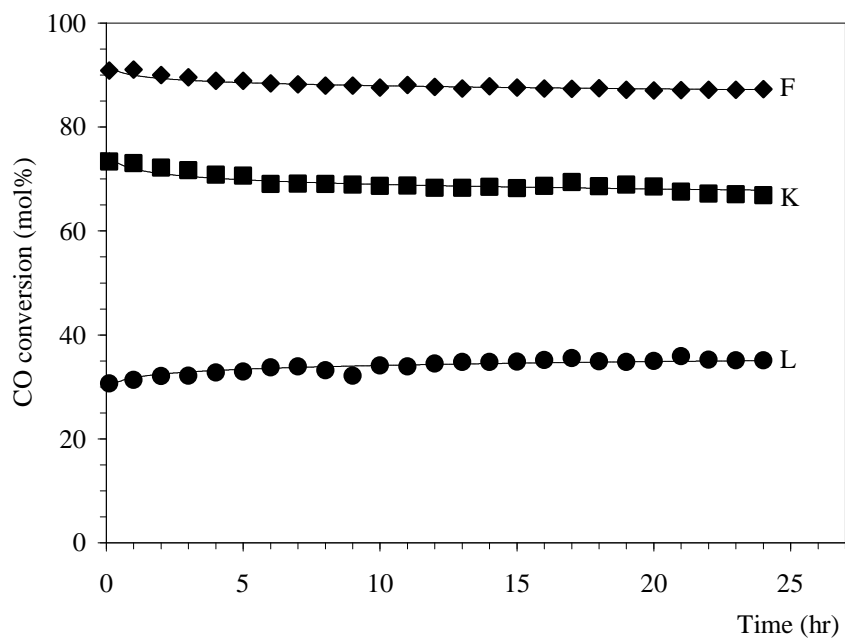


Fig. 5: WGS CO conversion at 300°C as a function of time on stream over Pt-Re/TiO<sub>2</sub> catalyst of variable metal loadings. (F) 0.5Pt-0.5Re/TiO<sub>2</sub>, (K) 0.3Pt-0.3Re/TiO<sub>2</sub>, (L) 0.1Pt-0.1Re/TiO<sub>2</sub> (see Table 2). Conditions: partial pressure of 60 and 150 mbar for CO and H<sub>2</sub>O respectively, P =2bar, and HSGV =410,000 hr<sup>-1</sup>.

### 5.3.2. Catalyst Characterization

The Pt-Re/TiO<sub>2</sub> reported in this section is the best catalyst obtained in the optimization study described above, *i.e.*, catalyst containing 0.5wt% of both Pt and Re, Pt/Re molar ratio of unity, and prepared by Re precursor to Pt, without intermediate drying or calcination (catalyst F).

#### 5.3.2.1. H<sub>2</sub> Temperature Programmed Reduction (H<sub>2</sub>-TPR)

Figure 6 shows the TPR plots for Pt/TiO<sub>2</sub>, Re/TiO<sub>2</sub>, and Pt-Re/TiO<sub>2</sub> catalysts., as well as a blank experiment. The Pt/TiO<sub>2</sub> sample showed two H<sub>2</sub> consumption peaks, a sharp peak with a maximum at 100°C and a very small peak at 375°C. The hydrogen consumption at 100°C is 37.5 μmol/g<sub>cat</sub>, in good agreement with the reduction of total PtO to Pt<sup>0</sup> [23] and hydrogen adsorption on the surface Pt at this temperature (Pt dispersion of 49%, see Table 2). The peak at around 375°C could be attributed to the reduction of the surface oxygen of TiO<sub>2</sub> [24].

The TPR plot of Re/TiO<sub>2</sub> catalyst is more complex showing three broad peaks centered at about 125, 360 and 525°C. These broad peaks indicate the heterogeneous nature of Re on titania support. Arnoldy *et al.* [25] reported the reduction of bulk ReO<sub>3</sub> at temperature ~ 150°C; thus, we speculate that the peak at the lower temperature (125°C) is corresponding to the reduction of larger particles of ReO<sub>3</sub>, having insignificant interaction with the support. The other two broad peaks centered at 360 and 525°C would correspond to the reduction of highly dispersed ReO<sub>x</sub> (x = 2 and 3), strongly interacting with the titania support [26])

In the case of the bimetallic (Pt-Re/TiO<sub>2</sub>) catalyst, the TPR plot shows 4 peaks. By comparing the reduction profile of the bimetallic with those of the monometallic catalysts, the first peak at 80°C would correspond to the reduction of PtO<sub>x</sub>. The other three peaks are at temperatures comparable to the peaks observed with the monometallic Re catalyst (125, 360 and 525°C). It can be seen that the temperature of the Pt reduction

peak in the platinum-rhenium catalyst is shifted to slightly lower temperature (20°C difference), due to the presence of rhenium, while the reduction peaks of rhenium oxides remained unchanged. These similarities in the reduction peaks of  $\text{ReO}_x$  for both  $\text{Re/TiO}_2$  and  $\text{Pt-Re/TiO}_2$  imply that Pt does not catalyze the reduction of  $\text{ReO}_x$  in the  $\text{Pt-Re/TiO}_2$  catalyst. Hongzhang *et al.* [27] reported that increasing alloy formation between platinum and rhenium in  $\text{Pt-Re/Al}_2\text{O}_3$  (reforming catalyst) results in increasingly shifting the peak temperatures in the  $\text{H}_2$ -TPR measurements. Therefore, based on our results, formation of Pt-Re alloys is not probable.

Bimetallic Pt-Re reforming catalysts (0.3%Pt-0.3%Re/ $\text{Al}_2\text{O}_3$ ) prepared by Guryev *et al.* [28] and Fung *et al.* [9] have comparable metal contents, Pt/Re ratio, precursor materials, preparation procedure and pre-treatment conditions, similar to our Pt-Re catalyst; however, different supports were used. They [9, 28] concluded existence of significant interactions between Pt and Re based on their observation of lower reduction temperature peaks for  $\text{ReO}_x$  and higher reduction temperature for  $\text{PtO}_x$ . In our case, surprisingly we observe a lower reduction temperature for  $\text{PtO}_x$  in the  $\text{Pt-Re/TiO}_2$  compared with  $\text{Pt/TiO}_2$ , in contrast to what was observed for  $\text{Pt-Re/Al}_2\text{O}_3$  reforming catalyst. This is suggesting that the support material is significant influencing in the interaction between Pt and Re which must be due to differences in the interaction of Pt and/or Re/ $\text{ReO}_x$  with the different support materials,  $\text{TiO}_2$  versus  $\text{Al}_2\text{O}_3$ .

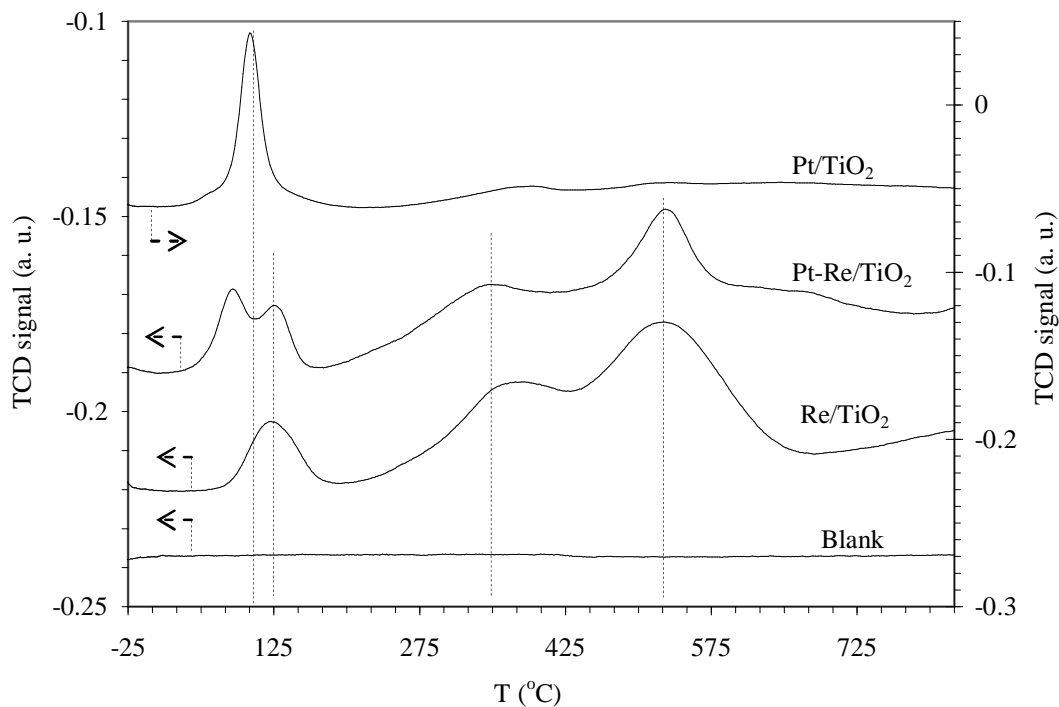


Fig. 6: H<sub>2</sub>-TPR profile of Pt/TiO<sub>2</sub>, Re/TiO<sub>2</sub>, and Pt-Re/TiO<sub>2</sub>. Heating rate was 10/min; gas contains 15% H<sub>2</sub> in Ar. The gas flow was 20 ml/min.

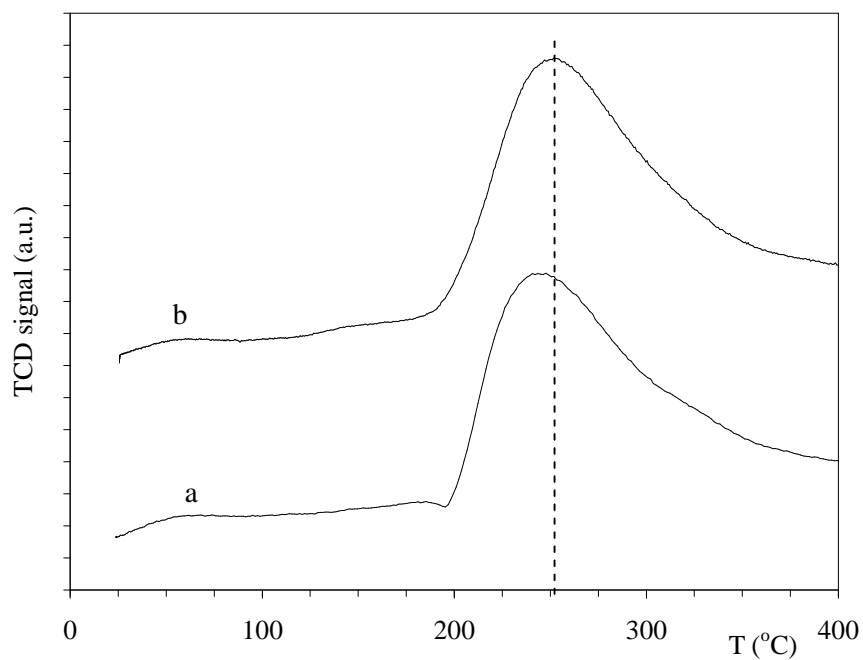


Fig.7: TPD spectra for CO desorbed from the surface of (a) 0.5%Pt-0.5%Re/TiO<sub>2</sub> and (b) 0.5%Pt/TiO<sub>2</sub>. CO adsorption at 25°C on each sample, a 1 h purge with He was allowed prior to being heated up to 400°C.

### 5.3.2.2. CO-Temperature Programmed Desorption (CO-TPD)

Figure 7 shows the CO-TPD profiles of Pt-Re/TiO<sub>2</sub> and Pt/TiO<sub>2</sub> catalysts. A broad CO desorption peak centered at temperature about 250°C corresponding to CO adsorbed on Pt was observed for both catalysts, however revealing a minor temperature decrease in the case of Pt-Re/TiO<sub>2</sub> (-10°C). The similar desorption temperature of CO and the similar peak areas, which also agrees well with the similar Pt dispersion (Table 2), confirm that Re is not significantly influencing the properties of the Pt particles.

### 5.3.2.3. IR spectra of CO adsorption

Figure 8 shows *in situ* FTIR spectra of adsorbed CO at 300°C on Pt/TiO<sub>2</sub> and Pt-Re/TiO<sub>2</sub> catalysts. CO adsorption on TiO<sub>2</sub> (Fig. 8a) showed no peaks and is used as reference for the experiments with Pt and Pt-Re catalysts. CO adsorbed on Pt/TiO<sub>2</sub> (Fig. 8b) showed a band at 2074 cm<sup>-1</sup> with a shoulder at 2060cm<sup>-1</sup>. These peaks have been assigned to linearly adsorbed CO on Pt [29,30]. The two different frequencies indicate different Pt adsorption sites, i.e., CO adsorbed on Pt atoms having different coordination numbers. CO adsorbed on Pt-Re/TiO<sub>2</sub> (Fig.8c) showed IR absorption bands at 2074cm<sup>-1</sup> with two shoulders at 2060 and 2040cm<sup>-1</sup> and a band at 1942cm<sup>-1</sup>. The observed two new bands at 2040 and 1942cm<sup>-1</sup> correspond to linearly adsorbed CO on Re and bridging CO on Re, respectively [29, 31].

The effect of Re addition on the peak position of CO adsorbed linearly on Pt, was analyzed by deconvoluting the spectra between 1970–2100cm<sup>-1</sup> for both catalysts, as shown in Fig. 9. Lorentzian peak-shape was assumed to fit the experimental data. In the fitting process, the peak widths was fixed while peak positions, heights and the number of peaks were optimized to obtain a good fit with the experimental data. In order to have an accurate comparison between Pt/TiO<sub>2</sub> and Pt-Re/TiO<sub>2</sub>, the deconvoluted bands for Pt/TiO<sub>2</sub> (Fig.9A), which represent linearly adsorbed CO on Pt, are considered as starting point for deconvoluting the spectra for adsorbed CO on Pt-Re/TiO<sub>2</sub>. However, Peak heights and peak positions were then optimized whenever necessary until having best fit

to the experimental data; also, additional peaks were added when necessary. The sum of the squared differences between the experimental data and the fitted spectrum is minimized in order to obtain the best fit.

In case of Pt/TiO<sub>2</sub> (Fig. 9 A), the measured spectrum is well described with 4 peaks at 2074, 2065, 2056, and 2045cm<sup>-1</sup>. It appears that just adding the CO on metal Re peak at 2039 cm<sup>-1</sup> [29, 31] is sufficient to account for the difference in peak shape between CO adsorbed on Pt/TiO<sub>2</sub> (Fig. 9A) versus that on Pt-Re/TiO<sub>2</sub> (Fig. 9B). Peak positions and ratios of the Pt-CO contributions do not significantly change, supporting the conclusions based on H<sub>2</sub>-TPR and CO-TPD, that any strong interaction between Pt and Re by alloy formation is absent in our catalysts.

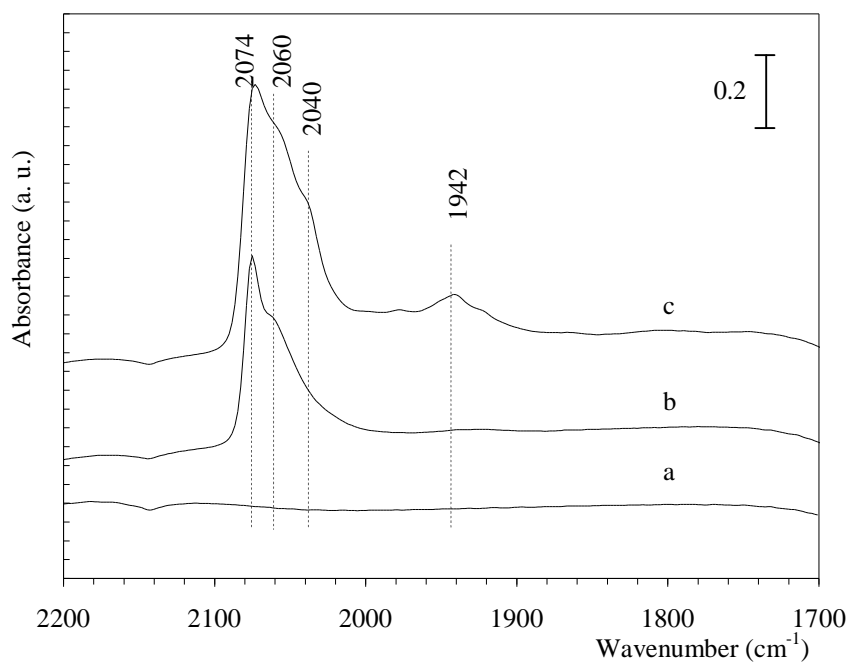


Fig. 8: *In situ* CO adsorption FTIR spectra at 300°C. (a) Blank experiment (b) on TiO<sub>2</sub> (c) on Pt/TiO<sub>2</sub>, (d) on Pt-Re/TiO<sub>2</sub>.

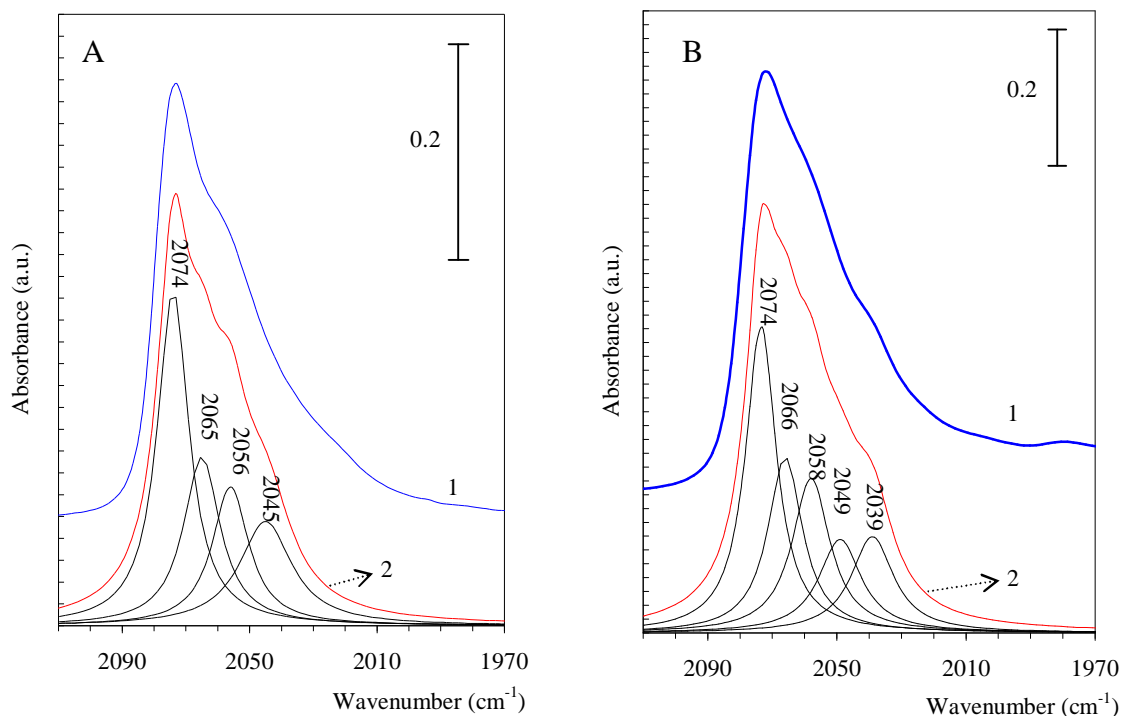


Fig. 9: Results of curve fitting the measured linear-CO spectra at 300°C of Pt/TiO<sub>2</sub> (A), and Pt-Re/TiO<sub>2</sub> (B). Curve 1 is the measured spectrum, and curve 2 is the sum of fitted spectra.

#### 5.3.2.4. IR spectra of *in situ* WGS reaction

Figure 10A shows the *in situ* FTIR spectra recorded under CO flow condition (spectrum a, identical to spectrum 8b) and under WGS reaction conditions (spectrum b) over Pt/TiO<sub>2</sub> catalyst. Comparing the two spectra, a new band at 1612 cm<sup>-1</sup> is observed, which is assigned to (weakly) adsorbed H<sub>2</sub>O on titania [32]. Figure 10 B represents the deconvolution of the CO-Pt band under *in situ* WGS conditions at 300°C on Pt/TiO<sub>2</sub>. The CO-Pt band deconvolution requires five peaks to obtain a good fit with the experimental spectrum, respectively at 2073, 2067, 2059, 2053, and 2047cm<sup>-1</sup>. The procedure here was identical to the procedure described in the previous paragraph: the four peaks according deconvolution of CO on Pt (Fig. 9A) were used as the starting point, varying the exact positions as well as intensity of these peaks and adding additional peak with low intensity at low wave number, in order to obtain a good fit with the experimental spectrum. The result is that a set of peaks at the same wave numbers is able to describe the experimental data (Fig. 10B), an additional peak with low intensity at low wave number was necessary.

However, the ratio of intensities of the CO-Pt peaks changed significantly, which is especially clear when comparing the intensity of the 2074-2073  $\text{cm}^{-1}$  peak versus the peak at 2066-2067  $\text{cm}^{-1}$ . The reason for this is not clear, but it may be speculated that the effect is caused by adsorbate –adsorbate interactions with reaction intermediates on the Pt surface, such as formate.

Figure 11A shows the FTIR spectra during CO flow (spectrum a) and during the WGS reaction (spectrum b) at 300°C over Pt-Re/TiO<sub>2</sub> catalyst. No CO peaks on Re at 1942 and 2040  $\text{cm}^{-1}$  were observed during WGS reaction. We showed in Chapter 3 [3] that Re/TiO<sub>2</sub> catalyst has no activity for WGS reaction, thus, we rule out the possibility that the absence of any CO-Re peak is due to high reactivity of CO-Re with H<sub>2</sub>O. Moreover, Sato *et al.* [16] reported using *in situ* XPS characterization, oxidation of Re to ReO<sub>x</sub> in Pt-Re/TiO<sub>2</sub> catalyst by H<sub>2</sub>O even at 100°C. Thus, water either influences the oxidation state of Re or competes with CO for the adsorption sites on Re. We will explain this in more details in Chapter 6.

Figure 11B shows the deconvolution of the CO-Pt band of Pt-Re/TiO<sub>2</sub> during *in situ* WGS reaction at 300°C, applying the same procedure as before. The measured spectrum requires also five peaks to obtain a good fit with the experimental spectrum, respectively at 2068, 2061, 2053, 2045 and 2037  $\text{cm}^{-1}$ . Comparing these peaks with the peaks from deconvolution of CO adsorption (Fig.9B), the CO-Pt peak on Pt-Re/TiO<sub>2</sub> under WGS conditions is shifting so strongly that the peak at 2074-2073  $\text{cm}^{-1}$  has disappeared completely. This is indicating a significant increase in CO adsorption strength, which we tentatively attribute to the influence of Re on Pt by forming an alloy under reaction conditions. A similar shift of CO-Pt bands on 2%Pt-3%Re/TiO<sub>2</sub> during WGS was also observed by Sato *et al.* [16]. A more detailed characterization of the catalyst after testing might give more details. However, Fung *et al.* [9] reported that Re undergoes complete oxidation at room temperature by comparing the TPR profiles of calcined and passivated samples of Re/Al<sub>2</sub>O<sub>3</sub>; therefore, it seems impossible to accurately characterize the Pt-Re/TiO<sub>2</sub> after catalytic testing unless exposure to ambient is prevented. An *in situ* XPS

characterization may be an excellent tool to give more details about the extent of interaction between Pt and Re and whether metal Re exists or not under WGS condition.

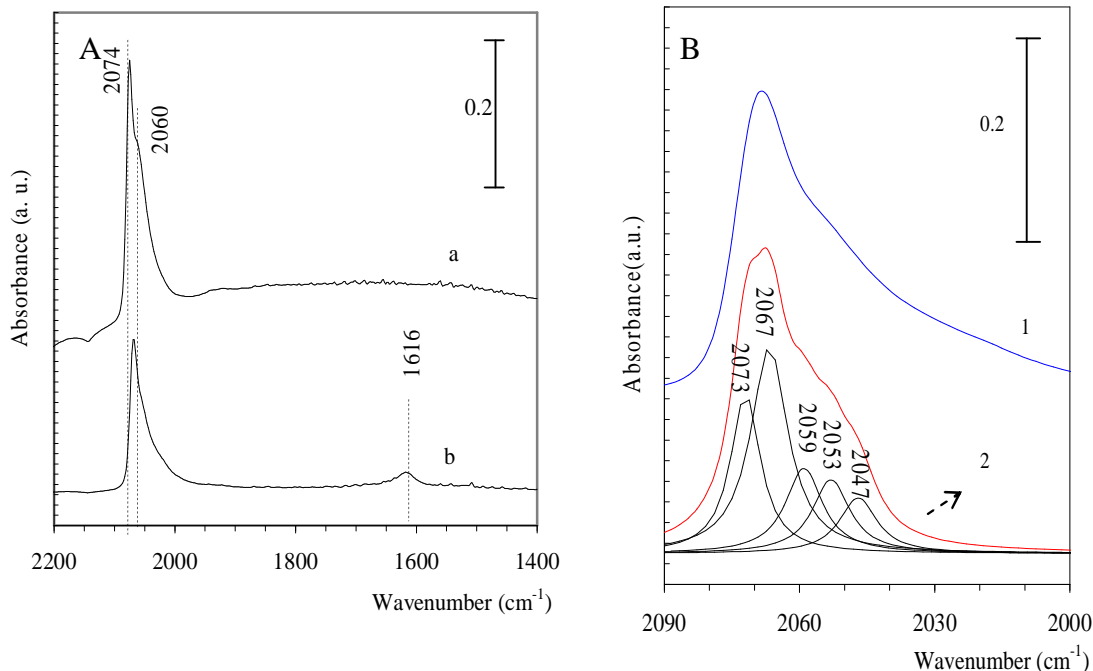


Fig.10A: *In situ* FTIR spectra at 300°C of Pt/TiO<sub>2</sub> catalyst; (a) 5% CO/He flow; (b) *In situ* WGS reaction 5%CO/10%H<sub>2</sub>O/He

Fig.10B: Curve fitting the measured *in situ* WGS reaction at 300°C of Pt/TiO<sub>2</sub>. Curve 1 is the measured spectrum, and curve 2 is the sum of fitted spectra.

To summarize, different characterization techniques (H<sub>2</sub>-TPR, CO-TPD, and *in situ* FTIR of CO adsorption and at WGS conditions) were used to study any possible interaction between Pt and Re in the optimal Pt-Re/TiO<sub>2</sub> catalyst developed in this study (unity Pt/Re molar ratio, 0.5wt% of each metal, and prepared by deposition Re precursor prior to Pt precursor without intermediate calcination/reduction). All characterization techniques, including IR under CO flow, indicate that the interaction between Pt and Re in the catalyst is not significant and give no evidence for any Pt-Re alloy formation. However, during WGS reaction, in the presence of CO, H<sub>2</sub>O, H<sub>2</sub>, and CO<sub>2</sub>, interaction between Pt and Re is more pronounced as observed by *in situ* FTIR.

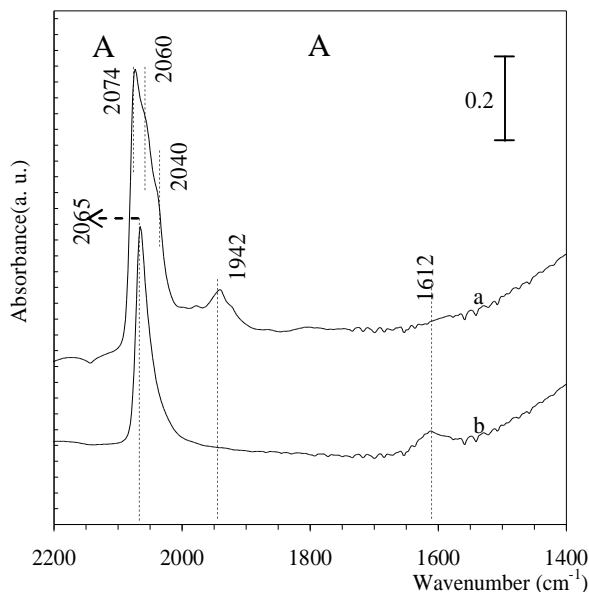


Fig.11A: *In situ* FTIR spectra at 300°C of Pt-Re/TiO<sub>2</sub> catalyst; (a) 5% CO/He flow; (b) *In situ* WGS reaction 5%CO/10%H<sub>2</sub>O/He

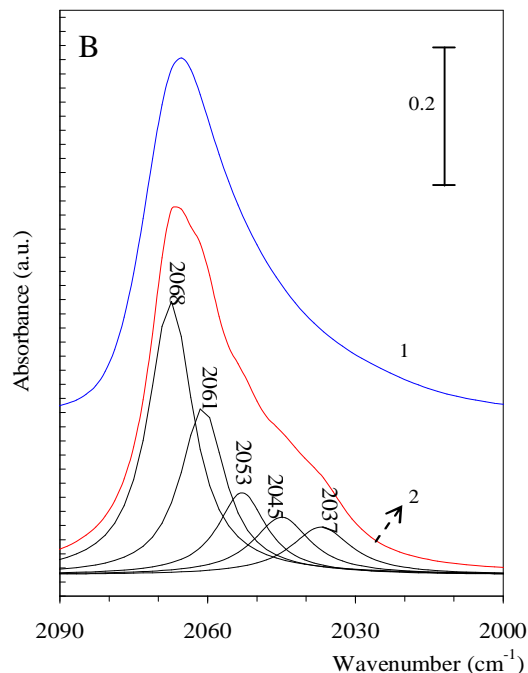


Fig.11B: Curve fitting the measured *in situ* WGS reaction at 300°C of Pt-Re/TiO<sub>2</sub>. Curve 1 is the measured spectrum, and curve 2 is the sum of fitted spectra.

Therefore, we propose that originally ReO<sub>x</sub> surrounds the Pt particles (see Fig. 11); these ReO<sub>x</sub> particles seem not to influence the properties of Pt particles significantly. Under WGS conditions, ReO<sub>x</sub> is undergoing red-ox cycles (as will be explained in Chapter 6), possibly resulting in the formation of Re-metal (Re<sup>0</sup>). It is well possible that a fraction of this reduced Re is diffusing into the Pt particles, forming a small amount of alloy, possibly exclusively in the periphery of the Pt particles. The exact nature of this interaction is unclear at this moment. Attempts with *ex situ* XPS, EXAFS, and EELS did not allow us to establish the nature of this interaction more specifically. This is due to inherent difficulty in the experimental techniques and to the very similar electronic structure of Pt and Re.

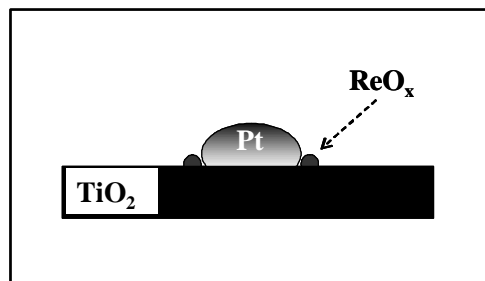


Fig.11: Schematic diagram showing a possible Pt and ReO<sub>x</sub> interactions

We have shown in Chapter 3 [3] that Re improved both activity and stability of Pt/TiO<sub>2</sub> catalyst. The role of ReO<sub>x</sub> in activating H<sub>2</sub>O (as will be explained in Chapter 6) has a strong influence on the catalyst activity. At this moment, however, it is not clear whether possible formation of Re metal during WGS reaction and its effect on the adsorption properties of Pt particles by forming a small amount of alloy (as indicated by IR) is relevant for improving the activity or not. Regarding catalyst stability, we speculate that decoration of Pt particles with highly stable ReO<sub>x</sub> particles is preventing sintering by anchoring the Pt particles (Fig. 11). Strong interaction of ReO<sub>x</sub> with TiO<sub>2</sub> is supported by TPR (Fig. 6). Anchoring small Pt particles, preventing migration on TiO<sub>2</sub> surface and resulting in improved catalyst stability, is in agreement with the suggestions of Iida and Igarashi for 3%Pt-2%Re/TiO<sub>2</sub> catalyst [15]. However, we can not rule out any role of possible alloy formation in the periphery of the Pt particles under WGS reaction conditions.

#### 5.4 Conclusions

Pt-Re/TiO<sub>2</sub> catalyst, having excellent catalytic activity and stability for WGS, was optimized by studying the influence of catalyst preparation strategy, Pt/Re molar ratio, and metal content. The optimum catalyst performance (stability and activity) was obtained when (i) impregnating the Re precursor prior to the Pt precursor without intermediate drying and calcination, (ii) using Pt/Re molar ratio of unity, and (iii) applying 0.5wt% content of each metal.

Characterization studies of the optimum catalyst with H<sub>2</sub>-TPR, CO-TPD, and *in situ* FTIR of CO adsorption and *in situ* WGS reaction, indicate absence of any significant interaction between Pt and ReO<sub>x</sub> before catalytic reaction. Under WGS conditions, however, interaction of Pt and Re seems to be significant, but the relevance for catalyst activity and stability remains uncertain at this point.

## 6. References

- [1] C.H. Bartolomew, R.J. Farrauto, in: *Fundamentals of industrial catalytic processes*, John Wiley & Sons, New Jersey, 2006, p. 909.
- [2] W. Ruettinger, O. Ilinich, R. J. Farrauto, *J. Power. Sour.* 118 (2003) 61.
- [3] K. G. Azzam, I.V. Babich, K. Seshan and L. Lefferts, *J. Catal.* 251 (2007) 163.
- [4] S. Hilaire, X. Wang, T. Luo, R.J. Gorte, J. Wagner, *Appl. Catal. A* 215 (2001) 271.
- [5] Q. Fu, H. Saltsburg, M. Flytzani-Stephanopoulos, *Sci.* 301 (2003) 935.
- [6] R. Radhakrishnan, R. R. Willigan, Z. Dardas, T. H. Vanderspurt, *Appl. Catal. B* 66 (2006) 23.
- [7] H. E. Klusdahl, Chevron, US Patent 3415737 (1968).
- [8] J. L. Margitfalvi, S. Gobolos, *Catal.* 17 (2004) 1.
- [9] S. Fung, M. R. McDeitt, P. A. Tooty, M. J. Kelley, D. C. Koningsberger, B. C. Gates, *J. Catal.* 140 (1993) 190.
- [10] C.L. Pieck, P. Marecot, C.A. Querini, J.M. Parera and J. Barbier, *Appl. Catal A* 133 (1995) 281.
- [11] L. S. Carvalho, C. L. Pieck, M. C. Rangel, N. S. Fígoli, J. M. Grau, P. Reyes, J. M. Parera, *Appl. Catal. A* 269 (2004) 91.
- [12] R. Prestvik, K. Moljord, K. Grande, A. Holmen, *J. Catal.* 174 (1998) 119.
- [13] M. Ronning, T. Gjervan, R. Prestvik, D. G. Nicholson, A. Holmen, *J. Catal.* 204 (2001) 292.
- [14] M. A. Vuurman, D. J. Stufkens, A. Oskam, *J. Mol. Catal.* 76 (1992) 263.
- [15] H. Iida, A. Igarashi, *Appl. Catal. A* 303 (2006) 192.
- [16] Y. Sato, K. Terada, S. Hasegawa, T. Miyao, S. Naito, *Appl. Catal. A: General* 296 (2005) 80.
- [17] S. Yu Choung, M. Ferrandon, T. Krause, *Catal. Today* 99 (2005) 257.
- [18] C. L. Pieck, C. R. Vera, J. M. Perera, G. N. Gimenez, L. R. Serra, L. S. Carvalho, M. C. Rangel, *Catal. Today* 107-108 (2005) 637.
- [19] H. Dexpert, P. Lagarde, *J. Mol. Catal.* 25 (1984) 347.
- [20] K. G. Azzam, I. V Babich, K. Seshan, L. Lefferts, *Appl. Catal. B* 80 (2008) 129.
- [21] P. Panagiotopoulou, D. I. Kondarides, *J. Catal* 225 (2004) 327.

- [22] X. Wang, R. J. Gorte, J. P. Wagner, *J. Catal.* 212 (2002) 225.
- [23] C. Zhang, H. He, K. Tanaka, *Appl. Catal. B*, 65 (2006) 37.
- [24] N.S. de Resende, J.-G. Eon, M. Schmal, *J. Catal.* 183 (1999) 6.
- [25] P. Arnoldy, O. S. L. Bruinsma, J. A. Moulijn, *J. Mol. Catal.* 30 (1985) 111.
- [26] J. H. Onuferko, *Appl. Surf. Sci.* 19 (1984) 227.
- [27] D. Hongzhang, W. Rongan, F. Lianqing, W. Haizen, L. Liwu, *Appl. Catal.* 78 (1991) 1.
- [28] Y.V. Guryev, I. I. Ivanova, V. V. Lunin, W. Grunert, M. W. E. van den Berg, *Appl. Catal. A* 329 (2007) 16.
- [29] H. Iida, A. Igarashi, *Appl. Catal. A* 303 (2006) 48.
- [30] P. Panagiotopoulou, A. Christodoulakis, D.I. Kondarides, S. Boghosian, *J. Catal.* 240 (2006) 114.
- [31] C. Bolivar, H. Charcosset, R. Frety, M. Primet, L. Tournayan, C. Betizeau, G. Leclercq, R. Maurel, *J. Catal.* 45 (1976) 163.
- [32] J. Steyn, G. Patrick, M. S. Scurrall, D. Hildebrandt, M. C. Raphulu, E. van der Lingen, *Catal. Today* 122 (2007) 254 and references therein.

# Chapter 6

## **Role of Re in Pt-Re/TiO<sub>2</sub> catalyst for Water Gas Shift reaction: A mechanistic and kinetic study.**

---

### ***Abstract***

*Transient kinetic studies and in situ FTIR spectroscopy were used to follow the reaction sequences that occur during Water Gas Shift reaction over Pt-Re/TiO<sub>2</sub> catalyst. Results pointed to contributions of an associative formate route with red-ox regeneration and two classical red-ox routes involving TiO<sub>2</sub> and ReO<sub>x</sub>, respectively. Under WGS reaction condition rhenium is present at least partly as ReO<sub>x</sub> providing an additional red-ox route for WGS reaction in which ReO<sub>x</sub> is reduced by CO generating CO<sub>2</sub> and re-oxidized by H<sub>2</sub>O forming H<sub>2</sub>. The overall reaction rate, based on steady state kinetics, was given by  $r_{H_2} = 0.075 \cdot e^{\frac{31kJ \cdot mol^{-1}}{RT}} \cdot p_{H_2O} \cdot p_{H_2}^{-0.5} (1 - \beta)$ , where  $\beta$  is the approach to equilibrium. Results obtained in the study indicated that the reaction between CO adsorbed on Pt and OH groups on titania is the rate determining step.*

**Keywords:** Water Gas Shift (WGS); Platinum; Rhenium; Titania; Kinetics; Reaction mechanism; Reaction orders

## 6.1. Introduction

Recently, there is a growing interest in onboard H<sub>2</sub> production for automobiles-fuel cells. Water Gas Shift (WGS) reaction,  $\text{CO} + \text{H}_2\text{O} \leftrightarrow \text{CO}_2 + \text{H}_2$ ,  $\Delta H = -41.1$  kJ/mol, is the critical step in maximizing H<sub>2</sub> yield from syngas, produced by steam reforming or partial oxidation of hydrocarbons [1].

Current commercial WGS technology involves multiple stages/catalysts, *i.e.*, (i) HTS (Fe<sub>2</sub>O<sub>3</sub>/Cr<sub>2</sub>O<sub>3</sub>) and (ii) LTS (Cu/ZnO/Al<sub>2</sub>O<sub>3</sub>). This is not suitable for mobile fuel cell applications because of its technical complexity, *e.g.*, sensitivity to startup – shutdown cycles [1-4]. There is thus tremendous interest in the development of a single stage WGS conversion. Precious metals, such as Au [5, 6], Pd [7, 8] or Pt [4,9-12] on different oxide supports, *e.g.*, CeO<sub>2</sub> [4, 6, 9, 11, 12], ZrO<sub>2</sub> [4, 10], TiO<sub>2</sub> [4, 8], Ce<sub>x</sub>Zr<sub>1-x</sub>O<sub>2</sub> [4, 13], Ti<sub>x</sub>Ce<sub>1-x</sub>O<sub>2</sub> [4] have been explored and reported to be effective for WGS. It is commonly agreed [4, 12-16] that these catalysts are bi-functional wherein noble metal sorbs/activates CO and the oxide supports activate H<sub>2</sub>O. Based on DRIFT measurements and SSITKA data, supporting evidence was obtained for the spillover mechanism of OH/H towards the noble metal and for the role of noble metal in chemisorption and activation of CO. We have shown earlier [4] that the oxide support strongly influences the catalyst performance in terms of activity and stability. For catalysts with the similar Pt loading/dispersion activity changes more than 5 times for different supports used. Among the catalysts tested in our study [4], Pt/TiO<sub>2</sub> showed the best intrinsic activity (TOF, s<sup>-1</sup>), however, it deactivated with time on stream. Pt sintering was the cause of deactivation [4]. Deactivation could be overcome by adding Re to the catalyst [4]. The developed Pt-Re/TiO<sub>2</sub> catalyst showed excellent activity, selectivity to H<sub>2</sub> and stability for WGS [4].

WGS reaction is reported to occur mainly through two reaction routes, *i.e.*, a red-ox [15,17,18] and an associative formate mechanism [16,19-22]. The red-ox mechanism involves successive reduction (by CO) and oxidation (by H<sub>2</sub>O) of the support, while the associative mechanism involves reaction through an adsorbed surface intermediate (formate species). We have reported [23], based on transient kinetics and *in situ* FTIR

studies, that WGS reaction mechanism is complex and depends strongly on the nature of the oxide supports and experimental conditions. An associative formate route with a red-ox regeneration of the oxide support was suggested as an additional possibility. The difference between this and the conventional “associative formate route” is that the conversion of surface formate to  $\text{H}_2$  and  $\text{CO}_2$  occurs using oxygen from titania in the former while it is from water in the latter. In the case of  $\text{Pt}/\text{TiO}_2$  (Fig. 1), we found that WGS reaction follows both (i) a red-ox and (ii) an associative formate with red-ox regeneration routes [23].

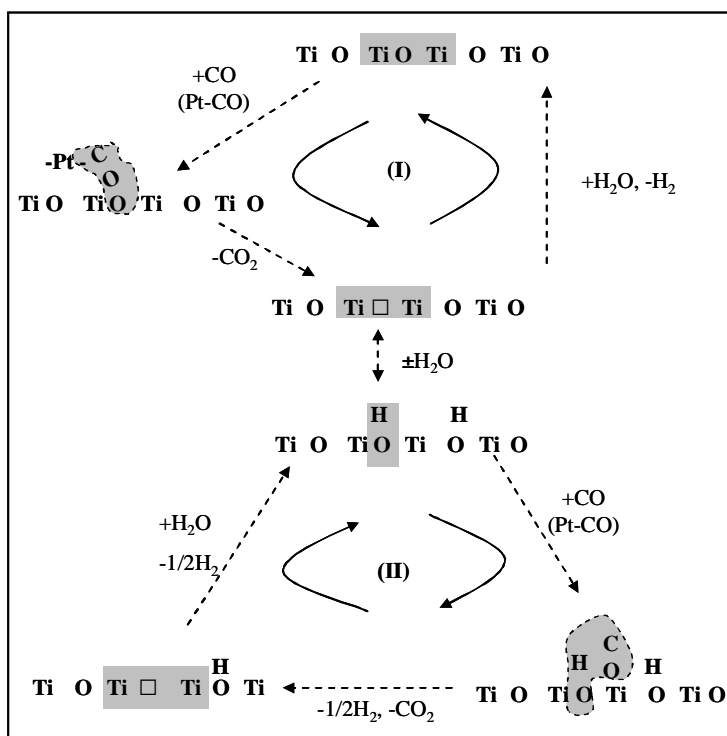


Fig. 1: WGS reaction pathways over  $\text{Pt}/\text{TiO}_2$  catalyst as proposed in [22]: (I) Red-ox cycle and (II) Formate with red-ox regeneration

It is generally accepted that addition of Re to  $\text{Pt}/\text{TiO}_2$  causes significant improvement in the catalytic activity [4, 8, 10, 24, 25]. However, there is still debate about the reason for the higher activity of  $\text{Pt-Re}/\text{TiO}_2$  compared to  $\text{Pt}/\text{TiO}_2$  despite the efforts by Iida *et al.* [10, 24] and Sato *et al.* [8, 25]. The objective of this study is to establish the reaction sequences that occur in presence of Re and to understand the role of Re in  $\text{Pt-Re}/\text{TiO}_2$  for WGS reaction.

## 6.2. Experimental

### 6.2.1. Catalyst preparation

Titania (P25, Degussa) supported Pt and Re catalysts (0.5wt% Pt/TiO<sub>2</sub>, 0.5wt% Re/TiO<sub>2</sub>, 0.5wt% Pt-0.5wt% Re/TiO<sub>2</sub> and 0.3wt% Pt-0.3wt% Re/TiO<sub>2</sub>) were prepared by wet impregnation, details of which are described elsewhere [4]. 5wt% Pt/Carbon (Activated Carbon, Norrit, ROX 0.8, 1100 m<sup>2</sup>.g<sup>-1</sup>) catalyst was prepared by wet impregnation of the carbon with aqueous solution of H<sub>2</sub>PtCl<sub>6</sub> (Aldrich). The bimetallic (5wt% of each) Pt-Re/C was prepared by sequential impregnation without intermediate drying or calcination. Carbon was first contacted with the required concentration of NH<sub>4</sub>ReO<sub>4</sub> (Aldrich) in water for 1 h with continuous stirring. Solution of H<sub>2</sub>PtCl<sub>6</sub> was then added and allowed to equilibrate for 1 h. Both catalysts (Pt/C and Pt-Re/C) were then dried at 75°C for 2 h under vacuum in a rotary evaporator. Subsequently, the catalysts were reduced in H<sub>2</sub> at 300°C (10% H<sub>2</sub>/Ar, heating rate 10°C min<sup>-1</sup>) for 4 h. For all of the experiments described below, the gases (He, H<sub>2</sub>, CO, and CO<sub>2</sub>) used were of >99.9% purity.

### 6.2.2. Characterization

Surface areas were measured with N<sub>2</sub> physisorption using a Micromeritics ASAP 2400 device and applying the BET method. Pt loading was determined using a Philips PW 1480 X-ray Fluorescence Spectrometer.

FTIR spectra were recorded on self-supported catalyst pellets (about 10 mg of the catalyst) under flow conditions (5% CO/He, 10 % H<sub>2</sub>O/He and (5% CO + 10% H<sub>2</sub>O)/He) at 300°C using a Bruker Vector 22 with MCT detector. Pulse experiments were mimicked by fast switching between He and a mixture of He containing CO or H<sub>2</sub>O. The catalyst pre-treatment was similar to catalytic test experiments. Spectra are presented in absorbance units. The empty IR cell was used as a background spectrum.

Pt dispersion was measured with CO chemisorption at room temperature using a Micromeritics Chemisorb 2750. The amount of sample used for each measurement was ~ 250 mg. Prior to measuring the CO uptake, the samples were reduced in pure H<sub>2</sub> (99.9%) from room temperature to 300°C at a rate of 10°C/min, flushed with He at 425°C for 1 h and then cooled to room temperature (25°C) in He. The CO uptake measurements were conducted at room temperature by injecting a series of pulses containing 1 mL of CO into a He stream flowing over the sample at a rate of 25 mL/min and measuring the amount of CO adsorbed per pulse. Our IR results on Pt-Re/TiO<sub>2</sub> showed, in agreement with finding of Peick *et al.* [26], that at room temperature, CO was only adsorbed on Pt.

### 6.2.3. Pulse experiments

Pulse transient experiments were performed at 300°C at atmospheric pressure using a fixed-bed reactor, details of which are described elsewhere [4, 22]. The catalyst (about 50 mg) was first reduced at 300°C in 10 vol% H<sub>2</sub>/He, 30 ml/min flow for 1 h. After this it was heated at 330°C in He (30 ml/min) for 30 min. After cooling down to 300°C the catalyst was contacted with fixed amounts of reactant gases using He as a carrier gas. Amount of CO in each pulse was 3.9 μmol. H<sub>2</sub>O (1.0 μl) was injected manually directly into the reactor using a microsyringe. Pulses were repeated until the responses for reactants and products no longer changed. To determine the products formed, the outlet of the reactor was directly connected to a Porapak column (5 m, 100°C) and a thermal conductivity detector (TCD). Downstream to the TCD detector, gases were analyzed by an online mass spectrometer (Balzers QMS 200 F). Quantitative determination of all gaseous products, except of H<sub>2</sub> and H<sub>2</sub>O, was obtained from TCD data with accuracy not below ±0.1 μmol/g<sub>cat</sub>. H<sub>2</sub> was detected by MS; the data for H<sub>2</sub> are semi quantitative and comparison in H<sub>2</sub> formation between catalysts is not applicable.

### 6.2.4. Catalytic test

Catalytic tests for WGS reaction were carried out in a fixed bed quartz tubular reactor (3 mm i.d.) under differential conditions, details of the setup used are described elsewhere

[4]. All catalysts were first reduced in 10% H<sub>2</sub> in N<sub>2</sub> (total flow was 100ml/min) for 30 min and subsequently purged with N<sub>2</sub> for another 30 min at 300°C. A gas mixture containing 3 vol. % CO, 7.5% H<sub>2</sub>O and N<sub>2</sub> balance was used for catalytic tests. The feed was adjusted in bypass mode to obtain constant CO/H<sub>2</sub>O/N<sub>2</sub> (=3/7.5/89.5 mol/mol%, N<sub>2</sub> as an internal standard) before the experiment. For kinetic measurements partial pressures of one of the reactants or products was varied while keeping concentrations of the other components constants (see Appendix A - Table A1). The partial pressures were selected taking into account application of the catalyst in a WGS-membrane reactor, removing H<sub>2</sub> and consequently increasing CO<sub>2</sub> concentration axially. The total flow rate of the feed gas into the reactor was kept at 350 ml/min using Brooks mass flow controllers. The inlet and outlet gases (CO, CO<sub>2</sub>, H<sub>2</sub>, H<sub>2</sub>O, and N<sub>2</sub>) were analyzed using Varian Micro GC (CP4900) using MS5 and PPQ columns. The conversion of CO was kept below 15% to be close to differential conditions.

### 6.3. Results

#### 6.3.1. Catalysts characterization and WGS reaction performance.

Table 1 gives details of the characteristics of the catalysts and their catalytic performance. BET surface areas were similar for all TiO<sub>2</sub>-based catalysts ( $48 \pm 1 \text{ m}^2/\text{g}$ ) indicating no effect of Pt or Re impregnation on the surface area of TiO<sub>2</sub>. The metal contents of the catalysts were close to the values expected from preparation procedures *i.e.*  $0.5 \pm 0.04 \text{ wt}\%$  for Pt/TiO<sub>2</sub>, Re/TiO<sub>2</sub>, and Pt-Re/TiO<sub>2</sub> catalysts. Both Pt/TiO<sub>2</sub> and Pt-Re/TiO<sub>2</sub> showed similar Pt dispersions ( $50 \pm 3\%$ ), no influence of the presence of Re on Pt dispersion was observed. For Pt/C and Pt-Re/C catalysts, the metal loadings (Pt, Re) were higher  $5 \pm 0.4 \text{ wt}\%$  (Table 1). We used higher loading of Pt and Re to increase catalyst activity and have an observable WGS rate in the case of Pt-Re/C, if any. Pt/C and Pt-Re/C catalyst showed Pt dispersion of about  $15 \pm 3\%$ .

It can be seen from Table 1 that Re/TiO<sub>2</sub> catalyst showed no activity in WGS reaction. However, Pt-Re/TiO<sub>2</sub> showed higher catalytic activity than Pt/TiO<sub>2</sub>; intrinsic activity for

H<sub>2</sub> formation (TOF<sub>300°C</sub> · s<sup>-1</sup>) increased from 10 s<sup>-1</sup> for Pt/TiO<sub>2</sub> to 15 s<sup>-1</sup> for Pt-Re/TiO<sub>2</sub>. The addition of Re to Pt/TiO<sub>2</sub> also improved the stability of the catalyst. Pt-Re/TiO<sub>2</sub> showed almost no deactivation; however, under identical conditions, Pt/TiO<sub>2</sub> lost about 40% of its initial activity after 20 h time on stream [4].

Table 1: Properties of the catalysts

| Catalyst               | BET (m <sup>2</sup> /g) | Pt/Re contents <sup>1</sup> (wt%) | Pt dispersion <sup>2</sup> (%) | TOF (s <sup>-1</sup> ) of H <sub>2</sub> formation at 300°C | TOF (s <sup>-1</sup> ) of H <sub>2</sub> formation at 280°C | Stability <sup>3</sup> |
|------------------------|-------------------------|-----------------------------------|--------------------------------|---|---|------------------------|
| Pt/TiO <sub>2</sub>    | 48                      | 0.49                              | 49                             | 10  | 8   | -                      |
| Pt-Re/TiO <sub>2</sub> | 49                      | 0.50/0.48                         | 50                             | 15  | 12  | +                      |
| Pt-Re/TiO <sub>2</sub> | n. m.                   | 0.34/0.26                         | 58                             | 16  | 13  | n. m.                  |
| Re/TiO <sub>2</sub>    | 48                      | 0.52                              | -                              | no activity   | no activity   | n. a.                  |
| Pt/C <sup>4</sup>      | n. m.                   | 5.2                               | 15                             | no activity   | no activity   | n. a.                  |
| Pt-Re/C <sup>4</sup>   | n. m.                   | 4.9/5.4                           | 18                             | n. m.   | n. m.   | n. m.                  |

<sup>1</sup> Measured by XRF

<sup>2</sup> Measured by CO chemisorption at 25°C

<sup>3</sup> Pt/TiO<sub>2</sub> lost 40% of initial activity in 20 h testing [4], n. a.: not applicable, n. m.: not measured

<sup>4</sup> Carbon surface area of 1100 m<sup>2</sup>g<sup>-1</sup>.

### 6.3.2. Transient pulse experiments over Pt-Re/TiO<sub>2</sub> catalytic system.

In order to investigate the reaction pathways and elementary steps of the WGS reaction over Pt-Re/TiO<sub>2</sub> catalyst, transient kinetic pulse studies were carried out. Figure 2 gives the details of the pulse experiments and the response from the GC (PPQ column)-MS system, for CO and H<sub>2</sub>O pulses over Pt-Re/TiO<sub>2</sub> catalyst at 300°C. Fig. 3 shows the cumulative amounts of CO consumed and CO<sub>2</sub> formed during the pulse experiments. Values for hydrogen are based on MS response and can only be used semi-quantitatively.

Contacting Pt-Re/TiO<sub>2</sub> with CO (Fig. 2) resulted in the simultaneous formation of CO<sub>2</sub> and H<sub>2</sub>. After 5 CO pulses, only traces of CO<sub>2</sub> and H<sub>2</sub> were observed and the amount of

CO detected in the outlet of the reactor (Fig. 3) was close to the amount of the pulse applied ( $\pm 0.1 \mu\text{mol}/\text{g}_{\text{cat}}$ ). During the CO pulse sequence, cumulatively  $88 \mu\text{moles g}^{-1}_{\text{cat}}$  CO was consumed and  $81 \mu\text{moles g}^{-1}_{\text{cat}}$   $\text{CO}_2$  was formed (Fig. 3). Thus,  $7 \mu\text{moles g}^{-1}_{\text{cat}}$  CO was retained on catalyst surface.

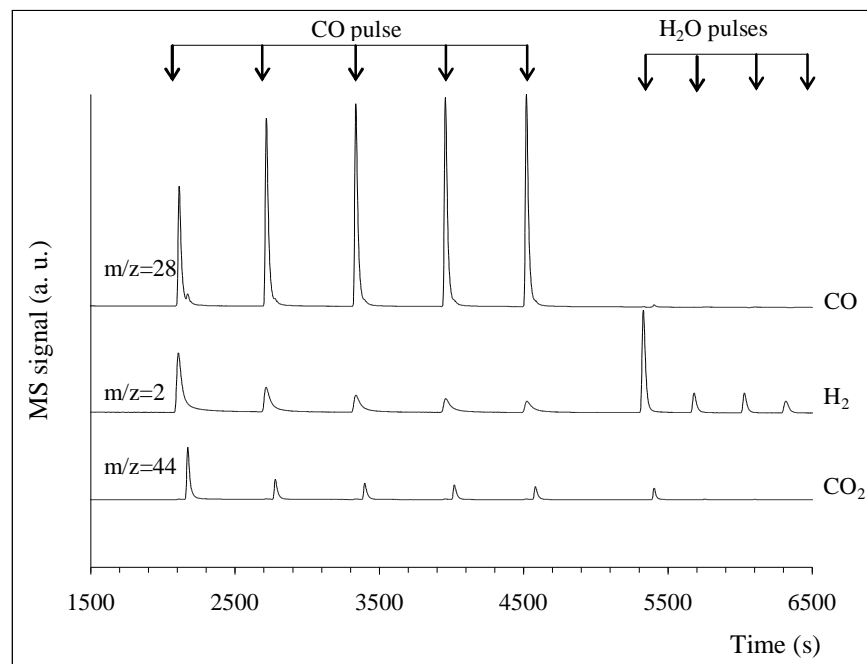


Fig. 2: MS response for pulse experiment over Pt-Re/TiO<sub>2</sub> catalyst reduced at 300°C in H<sub>2</sub>(10%)/He flow. Five pulses CO are followed with four pulses H<sub>2</sub>O. Difference in time between products detected is due to their separation with GC (porapak column).

After the CO pulse sequence, the catalyst was contacted with H<sub>2</sub>O pulses (see Fig. 2). Contacting Pt-Re/TiO<sub>2</sub> with H<sub>2</sub>O resulted in H<sub>2</sub> as the main product. The carbon balance of the cycle is excellent (97%, see Fig. 3) when taking into account the amounts of CO<sub>2</sub> formed ( $5 \mu\text{moles g}^{-1}_{\text{cat}}$  whereas  $7 \mu\text{moles g}^{-1}_{\text{cat}}$  of CO was retained on the catalyst during the CO experiment). Subsequent CO-H<sub>2</sub>O pulse cycles gave the same results.

Figure 4 shows the *in situ* FTIR spectra recorded under conditions identical to those during CO/H<sub>2</sub>O pulse experiments. Fig. 4a shows the IR spectra of the catalyst at 300°C in He, *in situ*, after reduction in H<sub>2</sub> at this temperature. After exposure to CO at 300°C (Fig. 4b), the band appearing at 2071 and the shoulder at 2060 cm<sup>-1</sup> represent linearly adsorbed CO on Pt [22, 23, 27]. The shoulder at 2038 cm<sup>-1</sup> corresponds to linearly

adsorbed CO on Re [10, 28, 29] and the band at  $1940\text{ cm}^{-1}$  indicates bridging CO on Re [10, 28, 29].

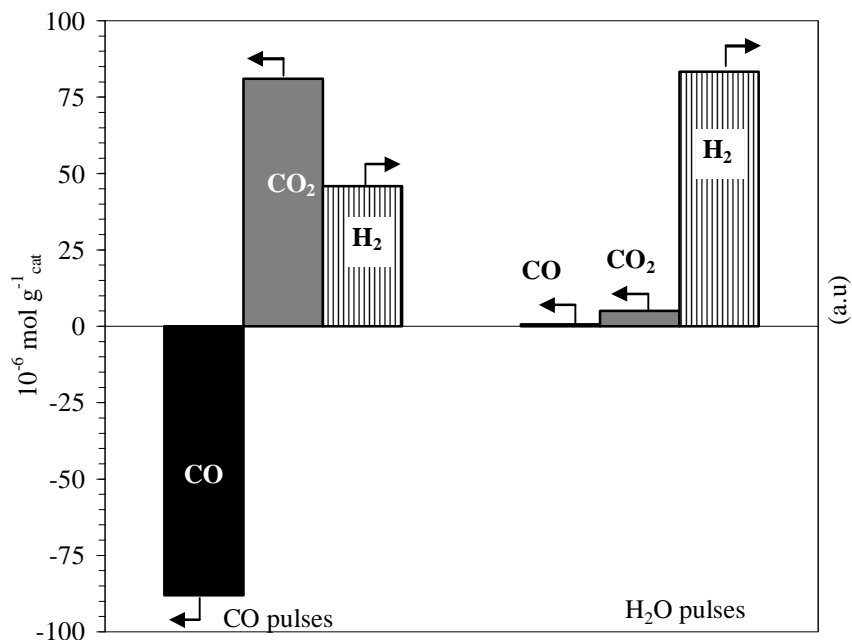


Fig. 3: Quantification of the CO and H<sub>2</sub>O pulse results over Pt-Re/TiO<sub>2</sub> catalyst at 300°C.

We have shown earlier that [4] rhenium is present in oxidised form (ReO<sub>x</sub>) in the fresh catalyst and it cannot be reduced completely to metal below 600°C. FTIR results indicate that rhenium is at least partially also present in metallic form after reduction at 300°C. Bands corresponding to adsorbed carbonates and/or formates [1200 – 1600  $\text{cm}^{-1}$ ] were not observed. FTIR spectra recorded after H<sub>2</sub>O pulses at 300°C (Fig. 4c), showed only one band at  $1612\text{ cm}^{-1}$ , which corresponds to (weakly) adsorbed H<sub>2</sub>O on titania [30]. Fig. 5 shows the *in situ* FTIR spectra recorded under steady-state WGS reaction conditions over Pt-Re/TiO<sub>2</sub> catalysts at 200 and 300°C. CO vibration region (2200 – 1800  $\text{cm}^{-1}$ ) looks very similar to spectra shown in Fig.4 and therefore is not reported here. In the region typical for C-H vibrations, the bands at 2885 and 2950  $\text{cm}^{-1}$  corresponding to the C-H stretching in formate were observed only at the lower temperature (200°C). The fact that these bands are absent at 300°C may indicate that formate decomposes rapidly at this temperature.

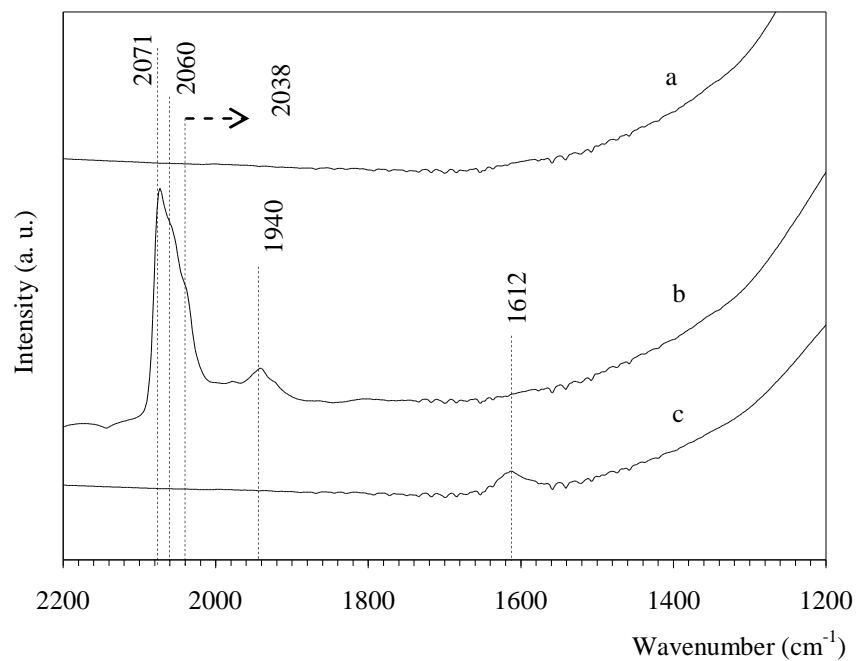


Fig. 4: *In situ* FTIR spectra at 300°C of Pt-Re/TiO<sub>2</sub> catalyst; (a) reduced in 10 vol% H<sub>2</sub>/He flow; (b) after CO pulses; (c) after H<sub>2</sub>O pulses.

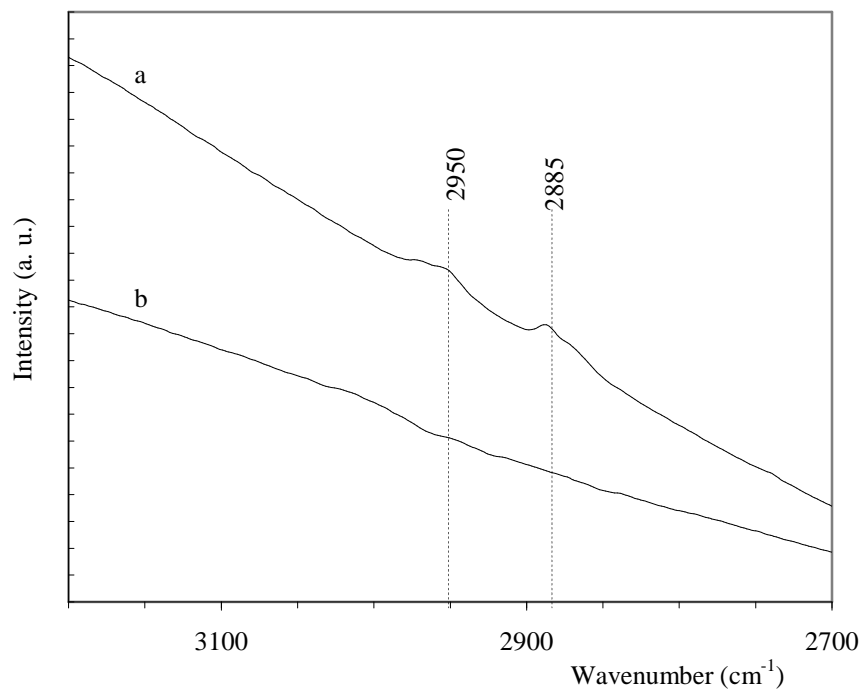


Fig. 5: *In situ* FTIR spectra of Pt-Re/TiO<sub>2</sub> catalyst in WGS conditions (5%CO, 10%H<sub>2</sub>O, 85%He), total pressure of 1 atm. (a) at 200°C and (b) at 300°C.

### 6.3.3. Transient pulse experiments over Pt/C and Pt-Re/C catalytic system.

Supported Pt catalysts for WGS reaction are reported to be bi-functional [4, 12-16] where CO activation occurs on Pt and an oxide support (*e.g.*, TiO<sub>2</sub>) is essential to sorb/activate water and the reaction follows Langmuir-Hinshelwood type kinetics. In order to exclude any contribution of the oxide support (TiO<sub>2</sub>) in the activation of water during WGS cycle, we have used carbon as support and prepared two catalysts, *i.e.*, Pt/C and Pt-Re/C. As we will show later, carbon used in this study is not an active support for WGS reaction.

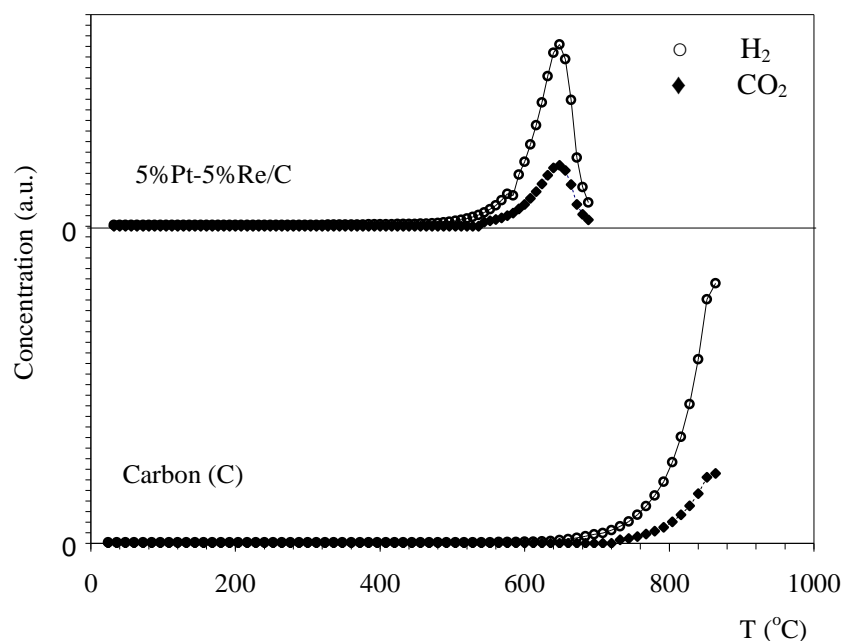


Fig. 6: GC concentration (a. u.) of H<sub>2</sub> and CO<sub>2</sub> during Temperature Programmed Reaction with H<sub>2</sub>O (5% H<sub>2</sub>O in N<sub>2</sub> flow) for carbon (C) and 5%Pt-5%Re/C. Lines are just to guide the eye.

Figure 6 shows the concentration (in a.u.) of H<sub>2</sub> and CO<sub>2</sub> formed during Temperature Programmed Reaction (oxidation) with water of carbon support and Pt-Re/C catalyst. The catalysts were heated in 5% H<sub>2</sub>O/N<sub>2</sub> stream from room temperature to 650°C for Pt-Re/C or to 850°C in case of carbon (heating rate 3°C min<sup>-1</sup>). The outlet of the reactor was analyzed every 2.5 min with a Micro-GC. The results show that, at temperatures below 700°C, the carbon support is stable in presence of water and no gasification took place

(formation of CO, CO<sub>2</sub> or H<sub>2</sub>). In the case of Pt-Re/C, H<sub>2</sub>O reacted with carbon forming CO<sub>2</sub> and H<sub>2</sub>, starting at 500°C. These results proof that pulsing of H<sub>2</sub>O at 300°C over the Pt-Re/C cannot affect the carbon support. The Pt/C and Pt-Re/C catalysts were first reduced in 10% H<sub>2</sub>/N<sub>2</sub> at 300°C for 1 h prior to the pulse experiments. Pt/C did not show any activity for WGS under our conditions and accordingly, we did not observe any product (CO<sub>2</sub>, H<sub>2</sub>) formation during CO and H<sub>2</sub>O pulsing. However, in the case of Pt-Re/C (Fig. 7), during the CO pulses, formation of CO<sub>2</sub> was observed. This is different from the case of Pt-Re/TiO<sub>2</sub> where we observed both CO<sub>2</sub> and H<sub>2</sub> during CO pulsing. When H<sub>2</sub>O was introduced, both H<sub>2</sub> and CO<sub>2</sub> were observed.

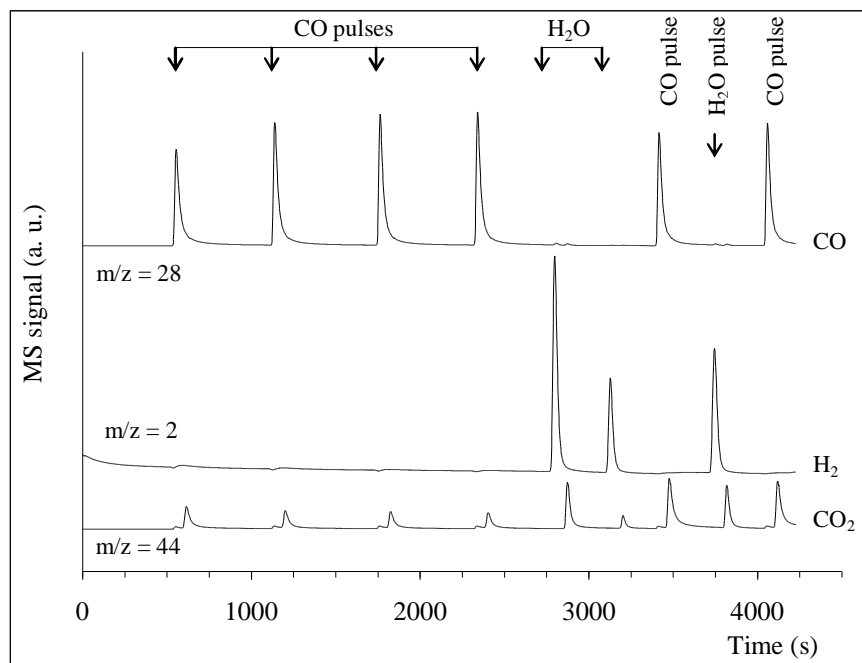


Fig. 7: MS response for pulse experiment over 5%Pt-5%Re/C catalyst reduced at 300°C. The catalyst was reduced in H<sub>2</sub>(10%)/He flow at 300°C prior to pulse experiments. Difference in time between products detected is due to their separation with GC (porapak column).

Additional experiments were performed with an inert support material. Pt-Re/C catalyst was first contacted with CO at 300°C and then heated to 400°C in a flow of He, in order to desorb CO completely from both Pt [31, 32] as well as Re (separate *in situ* IR measurements showed that CO desorption on Pt-Re/TiO<sub>2</sub> was complete at 390°C). After this, pulsing H<sub>2</sub>O resulted in formation of H<sub>2</sub> exclusively (Fig. 8). Furthermore, subsequently pulsing with CO resulted in CO<sub>2</sub> formation.

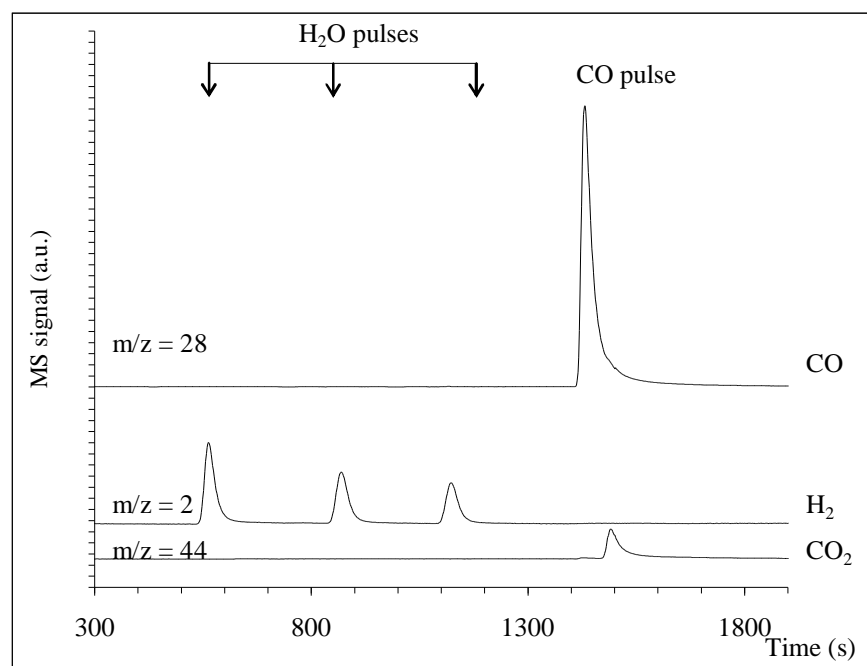


Fig. 8: MS response for pulse experiment over 5%Pt-5%Re/C catalyst. The catalyst was heated in He stream to 400°C after CO pulses then cooled down to 300°C prior to H<sub>2</sub>O pulses.

#### 6.3.4. Kinetic studies for Pt-Re/TiO<sub>2</sub> catalytic system.

Kinetic measurements were carried out according to the procedure given in the experimental section. The complete data set of concentrations are summarized in Appendix A (Table A1). Absence of heat and mass transfer limitation were checked using the Madon – Boudart test [33]. Specifically, two catalysts with different (i) Pt, Re loadings (0.5%Pt-0.48%Re/TiO<sub>2</sub> and 0.3%Pt-0.3%Re/TiO<sub>2</sub>) and (ii) comparable Pt dispersions, 50% and 58% respectively), gave identical rates for two different temperatures (TOF  $15 \pm 1 \text{ s}^{-1}$  at 300°C and  $12 \pm 1 \text{ s}^{-1}$  at 280°C for both catalysts, see Table 1). Based on these data we can exclude heat and mass transfer limitations in WGS reaction under selected conditions.

Dependence of reaction rates on the partial pressures of reactants and products, at 300°C and 2 atm. are shown in Fig. 9. These kinetic data were fitted to the power rate law

expression below, to determine the apparent reaction orders with respect to reactants and products.

$$r_{\text{H}_2} = k_f p^a_{\text{CO}} p^b_{\text{H}_2\text{O}} p^c_{\text{H}_2} p^d_{\text{CO}_2} (1-\beta) \quad (1)$$

In this equation,  $r_{\text{H}_2}$  is the rate of  $\text{H}_2$  formation,  $k_f$  is the forward rate constant,  $a$ ,  $b$ ,  $c$  and  $d$  are the apparent reaction orders and  $\beta$  is the approach to equilibrium ( $\beta = p_{\text{CO}_2} p_{\text{H}_2} / K_{\text{eq}} p_{\text{CO}} p_{\text{H}_2\text{O}}$ ). The reverse reactions could be neglected (*i.e.*,  $\beta \sim 0$ ) as conversion was 15% maximum and thus far from equilibrium (95% conversion). The experimentally determined reaction orders are presented in Tables 2 and 3. Data in Table 2 corresponds to high CO and low  $\text{CO}_2$  concentrations and Table 3, *vice versa*.

Table 2: Reaction orders of CO,  $\text{H}_2\text{O}$ ,  $\text{CO}_2$  and  $\text{H}_2$  calculated from Fig. 9 (high CO concentration).

| High CO and low $\text{CO}_2$ concentrations |                                      |                               |                              |
|--|--------------------------------------|-------------------------------|------------------------------|
| $\text{CO}^a$ ( $\pm 0.1$ )                  | $\text{H}_2\text{O}^b$ ( $\pm 0.1$ ) | $\text{CO}_2^c$ ( $\pm 0.1$ ) | $\text{H}_2^d$ ( $\pm 0.1$ ) |
| 0.0  | 0.8                                  | 0.0                           | -0.5                         |

<sup>a</sup> Concentration range: 3 – 12 vol%, 18%  $\text{H}_2\text{O}$ , 10%  $\text{H}_2$ , 6%  $\text{CO}_2$  and balance  $\text{N}_2$ .

<sup>b</sup> Concentration range: 12 – 26 vol%, 12% CO, 10%  $\text{H}_2$ , 6%  $\text{CO}_2$  and balance  $\text{N}_2$ .

<sup>c</sup> Concentration range: 6 – 24 vol%, 12% CO, 18%  $\text{H}_2\text{O}$ , 10%  $\text{H}_2$  and balance  $\text{N}_2$ .

<sup>d</sup> Concentration range: 3 – 15 vol%, 12% CO, 18%  $\text{H}_2\text{O}$ , 6%  $\text{CO}_2$  and balance  $\text{N}_2$ .

Table 3: Reaction order of CO,  $\text{H}_2\text{O}$ ,  $\text{CO}_2$  and  $\text{H}_2$  (low CO and high  $\text{CO}_2$  concentration).

| High CO and low $\text{CO}_2$ concentrations |                                      |                               |                              |
|--|--------------------------------------|-------------------------------|------------------------------|
| $\text{CO}^a$ ( $\pm 0.1$ )                  | $\text{H}_2\text{O}^b$ ( $\pm 0.1$ ) | $\text{CO}_2^c$ ( $\pm 0.1$ ) | $\text{H}_2^d$ ( $\pm 0.1$ ) |
| 0.4  | 0.7                                  | 0.0                           | -0.4                         |

<sup>a</sup> Concentration range: 1 – 4 vol%, 23%  $\text{H}_2\text{O}$ , 2%  $\text{H}_2$ , 20%  $\text{CO}_2$  and balance  $\text{N}_2$ .

<sup>b</sup> Concentration range: 14 – 23 vol%, 2% CO, 2%  $\text{H}_2$ , 20%  $\text{CO}_2$  and balance  $\text{N}_2$ .

<sup>c</sup> Concentration range: 8– 20 vol%, 2% CO, 23%  $\text{H}_2\text{O}$ , 2%  $\text{H}_2$  and balance  $\text{N}_2$ .

<sup>d</sup> Concentration range: 2– 8 vol%, 2% CO, 23%  $\text{H}_2\text{O}$ , 20%  $\text{CO}_2$  and balance  $\text{N}_2$ .

At the higher CO concentrations (Table 2), the rate was close to zero order in CO. However, at lower CO concentrations (Table 3), the reaction order of CO showed positive values (0.4). Further, the reaction was close to first order in water. Reaction rates were independent of  $\text{CO}_2$  concentrations showing zero order kinetics. Hydrogen inhibited the reaction, showing a fractional negative order (-0.5) for the rates.

Figure 10 shows Arrhenius plots for Pt/TiO<sub>2</sub> and Pt-Re/TiO<sub>2</sub>. The apparent activation energies calculated were similar in both the cases (30 ± 1, kJ/mol).

#### 6.4. Discussions

There is consensus that supported noble metal catalysts (*e.g.* Pt) are bifunctional in WGS, *i.e.*, both Pt and the oxide support has roles in the catalytic sequence [4, 12-16]. We have shown earlier [23], based on transient kinetic and *in situ* FTIR spectroscopic studies that on Pt/TiO<sub>2</sub>, WGS reaction proceeds *via* two routes (i) a classical red-ox sequence in which CO reduces the oxide support and water re-oxidizes it and (ii) an associative formate route with red-ox regeneration. In both cases, Pt assists in the sorption/activation of CO. The reaction sequences are shown in Fig.1.

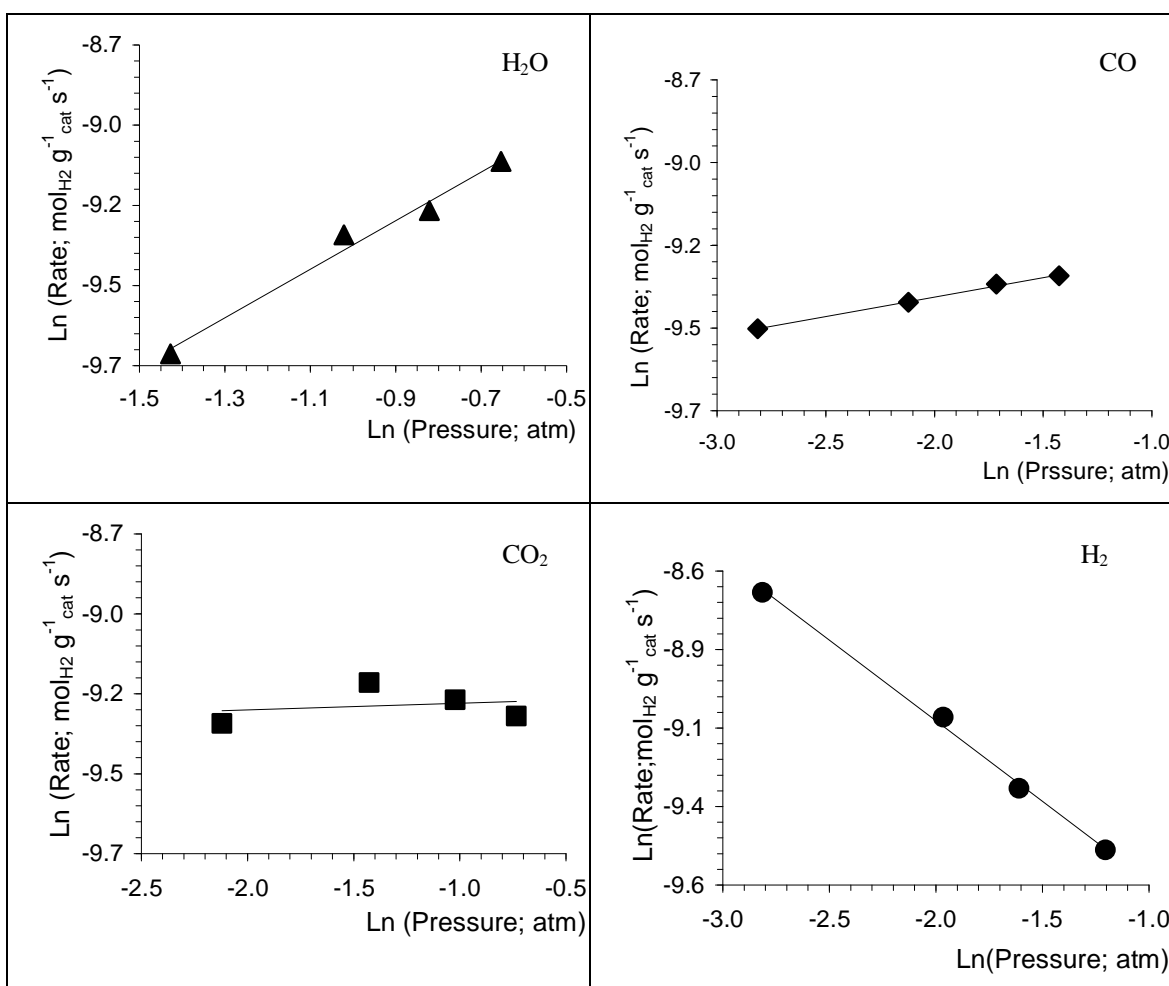


Fig. 9: Determination of power-rate law orders (WGS reaction) for Pt-Re/TiO<sub>2</sub> catalyst at 300°C and 2 atm. Variation of rates with partial pressures of components (see Table A1).

Since addition of Re to Pt/TiO<sub>2</sub> enhances catalyst activity (Table 1), it is interesting to know how Re influences the reaction sequences. The results of CO and H<sub>2</sub>O pulses (Figs. 2 and 3) over Pt-Re/TiO<sub>2</sub> indicate that, as in the case of Pt/TiO<sub>2</sub>, both (i) the classical red-ox and (ii) associative formate route with red-ox regeneration are taking place. For example, formation of H<sub>2</sub> and CO<sub>2</sub> during CO pulses indicates the reaction of CO with the hydroxyl groups from the catalyst surface (Eqn. (1)). Using *in situ* IR spectroscopy, we observed (Fig. 5) presence of formate type intermediates on the surface of TiO<sub>2</sub> during WGS reaction at 200°C. Sato *et al.* [8] also observed formate intermediate on Pt-Re/TiO<sub>2</sub> catalyst, using *in situ* IR spectroscopy during WGS reaction, but at lower temperatures (100°C). Moreover, Iida *et al.* [10,24] suggested that WGS occurred *via* formate intermediates over Pt/TiO<sub>2</sub> and Pt-Re/TiO<sub>2</sub> catalysts. Their conclusion was based on data of *in situ* IR spectroscopy at 250°C. Even though we did not see surface formate at our reaction conditions (300°C), we speculate that such intermediates are still relevant, in agreement with Sato *et al.* [8,25] and Iida and Igrashi [10,24]. The fact that contacting the catalyst with CO results in H<sub>2</sub> and CO<sub>2</sub>, implies a reaction between CO and hydroxyl groups on the oxide surface, which stoichiometrically should lead to ‘formate type’ species. We suggest that these formates decompose rapidly (based on our observations that the catalyst is active and contains formates during WGS at 200°C) to H<sub>2</sub> and CO<sub>2</sub> (Eq. (2)), reducing the catalyst. Formation of hydrogen during subsequent contact with water shows oxidative regeneration of TiO<sub>2</sub> (Eq. (3)).



The facts that CO<sub>2</sub> is produced during CO pulses and hydrogen is formed in the subsequent contact with water make it impossible to exclude that the classical red-ox cycle contributes (Fig. 1, Eqs. (4) and (5)). Thus, the reaction sequence seems to be similar to that for Pt/TiO<sub>2</sub>, as shown in Fig. 1. Therefore, the results of pulse studies over Pt-Re/TiO<sub>2</sub> indicate that the reaction mechanism is comparable with what we proposed [23] earlier for Pt/TiO<sub>2</sub> (Eqs. (2) – (5), and Fig.1). Interestingly, activation energies calculated from kinetic experiments (Fig. 10) showed very similar values for both catalysts *i.e.*, 29 kJ.mol<sup>-1</sup> for Pt/TiO<sub>2</sub> and 31 kJ.mol<sup>-1</sup> for Pt-Re/TiO<sub>2</sub>.



In spite of the similarity in the mechanistic reaction sequences over the two catalysts, *i.e.*, Pt/TiO<sub>2</sub> and Pt-Re/TiO<sub>2</sub>, the latter showed higher WGS activity (Table 1). There is still debate in the literature about the reason for the higher activity of Pt-Re/TiO<sub>2</sub> compared to Pt/TiO<sub>2</sub> [8, 10, 24, 25]. Iida and Igrashi [10, 24] explain the higher activity of Pt-Re/TiO<sub>2</sub> catalyst due to an increase of Pt dispersion resulting from the presence of rhenium. In our case, however, Pt-Re/TiO<sub>2</sub> showed higher activity than Pt/TiO<sub>2</sub> in spite of the identical Pt dispersions (50±3%) in both catalysts and identical catalyst total surface areas (Table 1). This may indicate another role for rhenium in our case. It has to be stated that (i) the Pt and Re loadings as well as (ii) Pt/Re molar ratios were different in the two studies. It is reported elsewhere [34, 35] that both these factors can influence catalytic characteristics (*e.g.*, Pt dispersion) and catalytic performance.

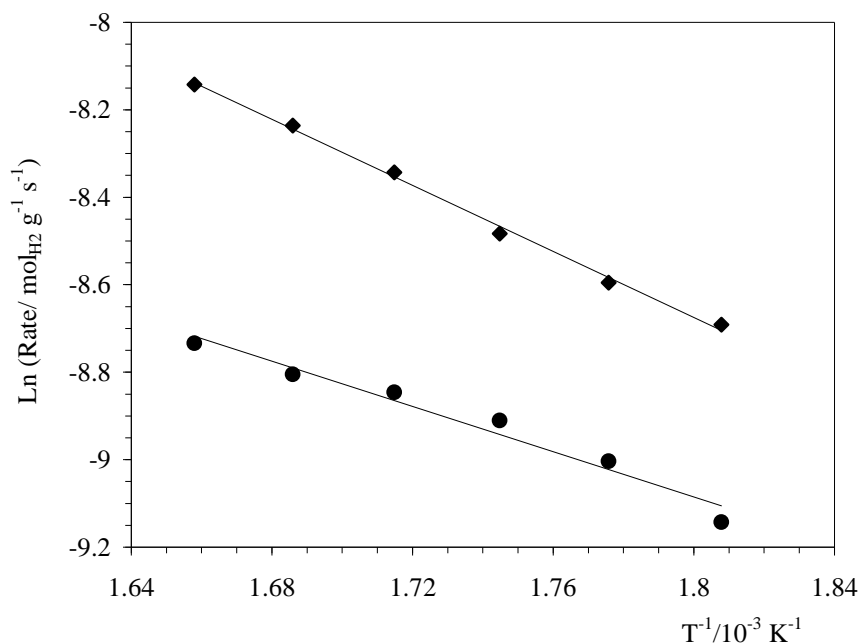


Fig. 10: Arhenius plot for the WGS reaction on 0.5%Pt-0.48%Re/TiO<sub>2</sub> (♦) and 0.5%Pt/TiO<sub>2</sub> (●). Conditions of at 1 atm. total pressure and 3% CO, 7.5% H<sub>2</sub>O and 89.5vol% N<sub>2</sub>.

Alternatively, Sato *et al.* [8, 25], based on IR results at 200°C, attributed the enhanced activity of Pt-Re/TiO<sub>2</sub> to a variety of factors, *viz.*, (i) alloy formation between Pt and Re,

(ii) role of Re in stabilizing the formate and its facile transformation to H<sub>2</sub> and CO<sub>2</sub>. EXAFS studies on our catalysts were inconclusive regarding Pt-Re alloy formation. Detailed studies based on (i) CO sorption and (ii) EELS to explore interaction between Re and Pt are in progress. At this moment, based on our knowledge, we cannot exclude alloy formation (Pt-Re) and its effect on catalytic activity.

Discussions below, based on our own results, consider yet another possibility for the positive influence of the presence of rhenium on catalyst activity. During CO pulses over the two catalysts, we observed higher CO<sub>2</sub> production in the case of Pt-Re/TiO<sub>2</sub> (81 and 51 μmoles g<sup>-1</sup><sub>cat</sub> CO for Pt-Re/TiO<sub>2</sub> and Pt/TiO<sub>2</sub> [23], respectively). This indicates availability of extra oxygen in Pt-Re/TiO<sub>2</sub> catalyst.

Our XPS results in chapter 3 [4] and that of Iida *et al.* [10] showed that rhenium is present in oxidized form (ReO<sub>x</sub>) in the Pt-Re/TiO<sub>2</sub> catalyst at ambient conditions. Temperature programmed reduction using hydrogen [4] showed that (ReO<sub>x</sub>) could not be reduced completely below 600°C. Since WGS is carried out at 300°C in the current study, at least part of the rhenium should be present in oxidized form in our working catalyst. Therefore it is reasonable to consider the possibility that oxygen from ReO<sub>x</sub> is involved in the oxidation of CO, which can be replenished by oxygen from water, as in a re-oxidation step.

In order to establish the role, if any, of ReO<sub>x</sub> in the Pt-Re/TiO<sub>2</sub> catalyst, it is necessary to exclude the role of TiO<sub>2</sub> (where ‘red-ox’ normally occurs during WGS cycle). Thus, CO and H<sub>2</sub>O pulse experiments were carried out over Pt-Re/C catalyst. Since Pt/C showed no WGS shift activity (see Fig. 7a) we exclude any catalytic role for carbon in the Pt-Re/C catalyst. During CO pulses (Fig. 7b), only CO<sub>2</sub> was observed and as expected no hydrogen was formed. The only source available for oxygen is then ReO<sub>x</sub>, and oxidation of CO must be by oxygen from ReO<sub>x</sub>, (Eq. (6)). The amount of oxygen consumed to make CO<sub>2</sub> was less than 2% of the total oxygen available in ReO<sub>x</sub>, assuming the stoichiometry to be ReO<sub>2</sub>.



Contacting this catalyst subsequently with H<sub>2</sub>O resulted in the formation of H<sub>2</sub> and CO<sub>2</sub> (Fig. 7b). H<sub>2</sub> formation would correspond to re-oxidation of ReO<sub>x-1</sub> by H<sub>2</sub>O (Eq. (7)). This is indeed confirmed by Sato *et al.* [8] who reported, using *in situ* XPS characterization, the oxidation of reduced ReO<sub>x</sub> in Pt-Re/TiO<sub>2</sub> catalyst by H<sub>2</sub>O even at 100°C.

The following arguments clarify why CO<sub>2</sub> was formed during H<sub>2</sub>O pulse. It is important to recall that neither carbonate nor formate were stable on Pt-Re/TiO<sub>2</sub> catalyst at 300°C (see Fig. 4). Thus, during the H<sub>2</sub>O pulses, re-oxidation of ReO<sub>x-1</sub> occurs and the CO sorbed on Pt can react with oxygen from ReO<sub>x</sub> to form CO<sub>2</sub>. To establish this, the catalyst was contacted with CO at 300°C and then heated to 400°C in He for 1 h. This allowed desorption of all CO sorbed on the catalyst [31, 32]. Subsequent contact with H<sub>2</sub>O at 300°C, as in the earlier case, resulted in H<sub>2</sub> formation only (Fig. 8). The next CO pulse led to only CO<sub>2</sub>, as expected from a classical red-ox cycle *via* ReO<sub>x</sub> (Eqs (6) and (7)). Repeated cycles of CO and H<sub>2</sub>O pulses (Fig.7b), subsequently, led to the same product distribution compared with the first cycle indicating the reduction and re-oxidation of ReO<sub>x</sub> in the Pt-Re/C catalyst.

To summarize, we observe that the addition of Re to Pt/TiO<sub>2</sub> catalyst (i) does not influence the reaction sequences (ii) at least part of the rhenium is present as ReO<sub>x</sub> and it can not be reduced completely under at the WGS conditions used in this study and (iii) ReO<sub>x</sub> provides an additional red-ox route to the reaction sequences (reduction by CO and re-oxidation by H<sub>2</sub>O). We propose this additional red-ox activity to be the reason for the enhanced catalytic activity observed for Pt-Re/TiO<sub>2</sub>. Thus, WGS on Pt-Re/TiO<sub>2</sub> catalyst follows the mechanistic sequence of an associative formate with red-ox regeneration (Eqs. (2) and (3)) and two classical red-ox routes *i.e.*, involving TiO<sub>2</sub> (Eqs. (4) and (5)) and ReO<sub>x</sub> (Eqs. (6) and (7)) respectively.

Accurate description of the reaction rates with help of empirical kinetic expressions (*e.g.* power rate law) is essential for reactor design. Moreover, kinetic descriptions can serve as an indication of the prevalent reaction mechanism and sometimes specific mechanisms can be rejected. In this study, two data sets have been selected (Table 2 and 3 and Figs. 9 and 10) for further discussion below.

To recall, the reaction rate was not influenced by CO<sub>2</sub> and CO (at high CO concentration), depended linearly on p<sub>H<sub>2</sub>O</sub> and influenced negatively (-0.5 order) by p<sub>H<sub>2</sub></sub>. Zero order in CO implies that, at the temperature and pressure used in this study, the CO sorption is facile and CO coverage on Pt is close to complete ( $\phi_{\text{CO}} \sim 1$ ). This is fully in agreement with previous work on Pt/CeO<sub>2</sub> [12, 36], Pd/CeO<sub>2</sub> [17], Rh/CeO<sub>2</sub> [12], Pt/Ce<sub>0.58</sub>Zr<sub>0.42</sub>O<sub>2</sub> [37], and Pt/Al<sub>2</sub>O<sub>3</sub> [36] all reporting zero order in CO. Therefore, CO adsorption can be ruled out as the rate determining step. In the case of low CO concentrations, reaction order in CO becomes positive (Table 3). This is also typical for zero order reactions that tend to first order at low reactant concentrations. In agreement with that, Jacobs *et al.* [38] also reported the increase of CO reaction order from zero to one over Pt/CeO<sub>2</sub> catalyst when using lower CO concentrations.

Zero order kinetics observed for CO<sub>2</sub> indicates that desorption of CO<sub>2</sub> from TiO<sub>2</sub>, where it is formed, is fast (Pt does not adsorb CO<sub>2</sub> at this temperature). We have shown earlier, based on kinetic pulse transient and *in situ* IR studies [23], that carbonates are unstable on TiO<sub>2</sub> at the reaction temperature (300°C) used. Wang *et al.* [39] also reported, using TPD measurements, the instability of carbonate on TiO<sub>2</sub> surface above 250°C. Therefore desorption of CO<sub>2</sub> can be ruled out as rate limiting step.

The reaction order in H<sub>2</sub>O was close to unity (0.8) independent of CO and CO<sub>2</sub> pressure. Water is the most difficult molecule to activate in WGS since the reaction involves splitting an extremely stable O-H bond and therefore a positive order is not surprising. Bunluesin *et al.* (Pt/CeO<sub>2</sub>) [12], Phatak *et al.* (Pt/CeO<sub>2</sub> and Pt/Al<sub>2</sub>O<sub>3</sub>) [36], and Radhakrishnan *et al.* [37], (Pt-Re/Ce<sub>0.58</sub>Zr<sub>0.42</sub>O<sub>2</sub>) also reported a first order dependence of the WGS rate on p<sub>H<sub>2</sub>O</sub>. These arguments suggest that the rate determining step may

involve water, *i.e.*, re-oxidation of the support. The first order in  $p_{\text{H}_2\text{O}}$  might indicate that the rate is limited by re-oxidation of  $\text{TiO}_2$  (Eqs. (3) and (5)) and/or  $\text{ReO}_x$  (Eq. (7)) by water.

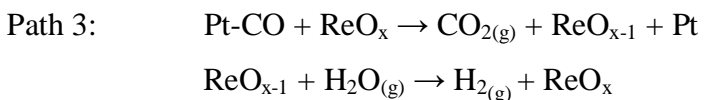
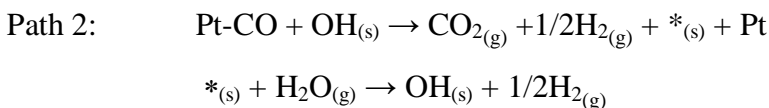
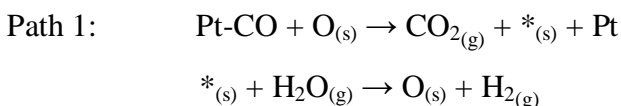
WGS reaction inhibition by hydrogen, (the reaction order is -0.5) is more difficult to understand. However, the observation of a negative order in  $\text{H}_2$  implies that application of a hydrogen-selective-membrane reactor, in order to remove hydrogen from the reaction mixture, would not only drive the conversion above the maximum conversion according thermodynamic equilibrium, but it would also enhance reaction rates. Therefore, the proposition of a hydrogen-selective-membrane reactor is a promising concept for WGS. Half order in hydrogen indicates dissociation of  $\text{H}_2$ . In principle, this impedance by hydrogen can occur at the Pt or support sites during reaction. We do not think that the rate inhibition is due to competitive adsorption between “H” and CO on Pt surface, in disagreement with Phatak *et al.* [36], because CO adsorption is known to be much more facile than “H” on Pt [40], *e.g.*, CO is a strong poison for (de)hydrogenation reactions on Pt. Moreover, the zero order in CO excludes the possibility of significant competition between “H” and CO on Pt. The role, if any, for Pt (in case of hydrogen) will be to catalyze associative desorption (as  $\text{H}_2$ ) of any hydrogen formed. Radhakrishnan *et al.* [37] also reported a negative order (-0.3) in  $\text{H}_2$  for WGS over Pt-Re/Ce<sub>0.58</sub>Zr<sub>0.42</sub>O<sub>2</sub> catalyst, however, no explanation was given.

Steam reforming and WGS are typical reactions involving water as a reactant. In the case of steam reforming on oxide supported nickel catalysts, water activation is reported to occur on both nickel and the support oxide (MgO-Al<sub>2</sub>O<sub>3</sub>) [41-43]. It has been reported that hydrogen can influence the reaction rate negatively (reaction order of (-1)), during steam reforming of hydrocarbons, by suppressing  $\text{H}_2\text{O}$  activation [41-43]. It is important to recall that bi-functional catalysis is suggested for Pt based steam reforming catalysts, in which the support plays a role in activating water [44, 45]. Activation of  $\text{H}_2\text{O}$  is not thermodynamically favorable on Pt [46].

Therefore, over Pt-Re/TiO<sub>2</sub> catalyst, the influence of H<sub>2</sub> must be *via* the support (TiO<sub>2</sub>) and/or *via* ReO<sub>x</sub>. A separate kinetic study on Pt/TiO<sub>2</sub> (without Re) catalyst also showed negative order in H<sub>2</sub> (reaction order of -0.4). We therefore conclude that the negative influence of H<sub>2</sub> concentration is in suppressing activation of H<sub>2</sub>O on TiO<sub>2</sub> *via* reactions (3) and/or (5) as explained below.

It has been suggested [47-49] that oxygen defect vacancies, in reducible oxides such as titania, can act as specific sites for H<sub>2</sub> activation. This results in trapped ionic hydrogen (Ti<sup>4+</sup>-H<sup>-</sup>) species [47-49]. As we showed in our reaction scheme, Fig. 1, such oxygen vacancies are necessary for the activation of water, it is thus also possible that the presence of hydrogen at these vacant oxygen sites hinders activation of H<sub>2</sub>O on these defect sites of TiO<sub>2</sub> *via* influencing the formation of OH<sup>-1</sup> and/or O<sup>-2</sup> (Eqs. (3) and (5)). Since this is reported to occur at lower temperatures (75°C), we can neither confirm nor exclude this possibility.

According to the reaction mechanism proposed in the beginning of this section, however, three different reaction paths may contribute. We have used kinetic modeling of our experimental results over Pt-Re/TiO<sub>2</sub> to validate these reaction sequences.



We have derived the rate equation for each of these paths and then simplified the rate equation by assuming rate limiting steps for each case. This allowed us to calculate the

resulting apparent reaction orders and to determine which path is the dominant. Appendix B gives the details of the kinetic analyses.

Based on these analyses, in the case of the reactions occurring in Path 2, we observe convergence with experimentally observed orders. Interestingly, in this situation we also find a (-0.5) order in hydrogen and (+1) order in water. Thus, the kinetic analysis indicates that during the WGS reaction at 300°C over Pt-Re/TiO<sub>2</sub> catalyst (i) Path 2 seems to be the dominant, (ii) the reaction of OH groups from TiO<sub>2</sub> support with CO adsorbed on Pt ( $\text{Pt-CO} + \text{OH}_{(s)} \rightarrow \text{CO}_{2(g)} + 1/2\text{H}_{2(g)} + *_{(s)} + \text{Pt}$ ) is the rate determining, and (iii) hydrogen inhibits the activation of H<sub>2</sub>O by suppressing the formation of OH groups on TiO<sub>2</sub>, either by shifting the equilibrium ( $*_{(s)} + \text{H}_2\text{O}_{(g)} \leftrightarrow \text{OH}_{(s)} + 1/2\text{H}_{2(g)}$ ) or by interaction of hydrogen with vacancies as discussed earlier.

## 6.5. Conclusions

In the Pt-Re/TiO<sub>2</sub> catalyst, rhenium is present at least partly as ReO<sub>x</sub>, providing an additional red-ox route for WGS reaction in which ReO<sub>x</sub> is reduced by CO generating CO<sub>2</sub> and re-oxidized by H<sub>2</sub>O forming H<sub>2</sub>. Thus, under the experimental conditions of this work, an associative formate route with red-ox regeneration (*via* TiO<sub>2</sub>) as well as two classical red-ox routes involving both TiO<sub>2</sub> and ReO<sub>x</sub> are possible reaction routes for WGS reaction.

We propose that the formate route with red-ox regeneration on TiO<sub>2</sub> is the dominant pathway and that the reaction of adsorbed CO on Pt with OH groups on TiO<sub>2</sub> is rate determining. Hydrogen inhibits the WGS rate by suppressing the formation of OH groups. Removing H<sub>2</sub> from the reaction mixture by using a hydrogen-selective-membrane reactor is promising strategy for practical applications.

**6.6. References**

- [1] C.H. Bartolomew, R.J. Farrauto, in: *Fundamentals of industrial catalytic processes*, John Wiley & Sons, New Jersey, 2006, p. 909.
- [2] W. Ruettinger, O. Ilinich, R. J. Farrauto, *J. Power. Sour.* 118 (2003) 61.
- [3] S. David, *Catal. Rev. – Sci. Eng.* 21 (1980) 275.
- [4] K. G. Azzam, I.V. Babich, K. Seshan, L. Lefferts, *J. Catal.* 251 (2007) 163.
- [5] T. Tabakova, V. Idakiev, D. Andreeva, I. Mitov, *Appl. Catal. A: General* 222 (2000) 91.
- [6] Q. Fu, H. Saltsburg, M. Flytzani-Stephanopoulos, *Science* 301 (2003) 935.
- [7] X. Wang, R. J. Gorte, *Appl. Catal. A: General* 247 (2003) 157.
- [8] Y. Sato, K. Terada, S. Hasegawa, T. Miyao, S. Naito, *Appl. Catal. A: General* 296 (2005) 80.
- [9] G. Jacobs, L. Williams, U. Graham, D. Sparks, B. Davis, *J. Phys. Chem. B* 107 (2003) 10398.
- [10] H. Iida, A. Igarashi, *Appl. Catal. A: General* 303 (2006) 48.
- [11] F. C. Meunier, D. Tibiletti, A. Goguet, D. Reid, R. Burch, *Appl. Catal. A: General* 289 (2006) 104.
- [12] T. Bunluesin, R. J. Gorte, G. W. Graham, *Appl. Catal. B: Environmental* 15 (1998) 107.
- [13] S. Yu Choung, M. Ferrandon, T. Karause, *Catal. Today* 99 (2005) 257.
- [14] D. C. Grenoble, M. M. Estadt, D. F. Ollis, *J. Catal.* 67 (1981) 90.
- [15] R. J. Gorte, S. Zhao, *Catal. Today* 104 (2005) 18.
- [16] G. G. Olympiou, C. M. Kalamaras, C. D. Zeinalipour-Yazdi, A. M. Efstathiou, *Catal. Today* 127 (2007) 304.
- [17] S. Hilaire, X. Wang, T. Luo, R.J. Gorte, J. Wagner, *Appl. Catal. A: General* 215 (2001) 271.
- [18] Y. Li, Q. Fu, M. Flytzani-Stephanopoulos, *Appl. Catal. B: Environmental* 27 (2000) 179.
- [19] G. Jacobs, U. M. Graham, E. Chenu, P. M. Patterson, A. Dozier, B. H. Davis, *J. Catal.* 229 (2005) 499.

- [20] A. Goguet, S. O. Shekhtman, R. Burch, C. Hardcare, F. C. Meunier, G. S. Yablonsky, *J. Catal.* 237 (2006) 102.
- [21] S. Y. Choung, M. Ferrandon, T. Krause, *Catal. Today* 99 (2005) 257.
- [22] P. Panagiotopoulou, A. Christodoulakis, D. I. Kondarides, S. Boghosian, *J. Catal.* 240 (2006) 114.
- [23] K. G. Azzam, I.V. Babich, K. Seshan, L. Lefferts, *J. Catal.* 251 (2007) 153.
- [24] H. Iida, A. Igrashi, *Appl. Catal. A: General* 303 (2006) 192.
- [25] Y. Sato, K. Terada, Y. Soma, T. Miyao, S. Naito, *Catal. Comm.* 7 (2006) 91.
- [26] C. L. Pieck, C. R. Vera, J. M. Perera, G. N. Gimenez, L. R. Serra, L. S. Carvalho, M. C. Rangel, *Catal. Today* 107-108 (2005) 637.
- [27] Holmgren, B. Andersson, D. Duprez, *Appl. Catal. B* 22 (1999) 215.
- [28] C. Bolivar, H. Charcosset, R. Frety, M. Primet, L. Tournayan, C. Betizeau, G. Leclercq, R. Maurel, *J. Catal.* 45 (1976) 163.
- [29] J. B. Peri, *J. Catal.* 52 (1978) 144.
- [30] J. Steyn , G. Patrick, M. S. Scurrall, D. Hildebrandt, M. C. Raphulu, E. van der Lingen, *Catal. Today* 122 (2007) 254 and references therein.
- [31] P. Loof, B. Kasemo, S. Andersson, A. Frestad, *J. Catal.* 130 (1991) 181.
- [32] B. N. Racine, M. J. Sally, B. Wade, R. K. Herz, *J. Catal.* 127 (1991) 307.
- [33] R. Madon and M. Boudart, *Ind. Eng. Chem. Fundm.* 21 (1982) 438.
- [34] J. L. Margitfalvi, S. Gobolos, *Catalysis* 17 (2004) 1.
- [35] A. S. Fung, M. R. Mcdevitt, P. A. Tooley, M. J. Kelley, D. C. Koningsberger, B. C. Gates, *J. Catal.* 140 (1993) 190.
- [36] A. A. Phatak , N. Koryabkina, S. Rai, J. L. Ratts, W. Ruettinger, R.J. Farrauto, G. E. Blau, W. N. Delgass, F. H. Ribeiro, *Catal. Today* 123 (2007) 224.
- [37] R. Radhakrishnan, R. R. Willigan, Z. Dardas, T. H. Vanderspurt, *Appl. Catal. B: Environmental* 66 (2006) 23.
- [38] G. Jacobs, L. Williams, U. Graham, G. A. Thomas, D. E. Sparks, B. H. Davis, *Appl. Catal. A: General* 252 (2003) 107.
- [39] J. A. Wang, A. Cuan, J. Salamones, N. Nava, S. Castillo, M. Moran-Pineda, F. Rojas, *Appl. Surf. Sci.* 230 (2004) 94.

- [40] N. V. Pavlenko, N. I. O'chenko, Yu. I. Pyatnitskii, *Theoretical and Experimental Chemistry*, 33 no.5 (1997) 254.
- [41] R. Rostrup-Nielsen, in: J.R. Anderson and M. Boudart (Eds), *Catalysis, Science and Technology*, Springer-Verlag, Berlin, 1984, Vol 5, p. 50.
- [42] I. M. Bodrov, L. O. Apel'baum, M. I. Temkin, *Kinet. Catal.* 5 (1964) 696.
- [43] I. M. Bodrov, L. O. Apel'baum, M. I. Temkin, *Kinet. Catal.* 9 (1968) 1065.
- [44] K. Takanabe; K. Aika, K Seshan, and L. Lefferts *J. Catal.*, 227 (2004) 101.
- [45] K. Takanabe, K. Aika, K. Inazu, T. Baba, K. Seshan, L. Lefferts, *J. Catal.* 243 (2006) 263.
- [46] M. A. Henderson, *Surf. Sci. Rep.* 46 (2002) 1.
- [47] W. Gopel, G. Rocker, *Phys. Rev. B*, 28 (1983) 3427.
- [48] M. Calatayud, A. Markovits, C. Minot, *Surf. Sci.* 524 (2003) 49.
- [49] J. Leconte, A. Markovits, M. K. Skalli, C. Minot, A. Belmajdoub, *Surf. Sci.* 497 (2002) 194.

## Appendix A

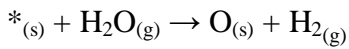
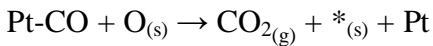
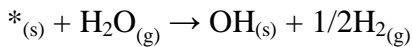
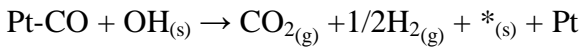
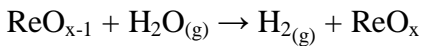
See Table A1.

Table A1: kinetic data used for reaction order calculation in the case of high CO concentration (Fig. 9).

| $p_{\text{CO}}$ (bar)       | $p_{\text{H}_2}$ (bar) | $p_{\text{H}_2\text{O}}$ (bar) | $p_{\text{CO}_2}$ (bar) | $p_{\text{N}_2}$ (bar) | Rate ( $\mu\text{molH}_2 \text{ g}^{-1} \text{ s}^{-1}$ ) |
|-----------------------------|------------------------|--------------------------------|-------------------------|------------------------|---|
| <b>H<sub>2</sub> order</b>  |                        |                                |                         |                        |   |
| 0.247                       | 0.066                  | 0.355                          | 0.120                   | 1.211                  | 172.0   |
| 0.241                       | 0.142                  | 0.362                          | 0.119                   | 1.138                  | 116.0   |
| 0.241                       | 0.198                  | 0.370                          | 0.112                   | 1.081                  | 92.1  |
| 0.240                       | 0.291                  | 0.380                          | 0.120                   | 0.989                  | 75.7  |
| <b>CO order</b>             |                        |                                |                         |                        |   |
| 0.241                       | 0.198                  | 0.370                          | 0.112                   | 1.081                  | 92.1  |
| 0.173                       | 0.192                  | 0.360                          | 0.122                   | 1.153                  | 89.8  |
| 0.115                       | 0.192                  | 0.363                          | 0.121                   | 1.211                  | 85.1  |
| 0.057                       | 0.191                  | 0.366                          | 0.120                   | 1.267                  | 78.5  |
| <b>CO<sub>2</sub> order</b> |                        |                                |                         |                        |   |
| 0.241                       | 0.198                  | 0.370                          | 0.112                   | 1.081                  | 92.1  |
| 0.240                       | 0.196                  | 0.360                          | 0.243                   | 0.961                  | 104.7   |
| 0.238                       | 0.195                  | 0.358                          | 0.367                   | 0.840                  | 99.2  |
| 0.237                       | 0.194                  | 0.365                          | 0.493                   | 0.716                  | 94.3  |
| <b>H<sub>2</sub>O order</b> |                        |                                |                         |                        |   |
| 0.242                       | 0.200                  | 0.234                          | 0.121                   | 1.20                   | 63.6  |
| 0.241                       | 0.198                  | 0.370                          | 0.112                   | 1.081                  | 92.1  |
| 0.232                       | 0.191                  | 0.444                          | 0.122                   | 1.016                  | 99.4  |
| 0.232                       | 0.190                  | 0.522                          | 0.120                   | 0.936                  | 119.1   |

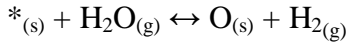
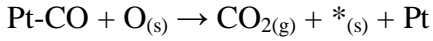
**Appendix B. Mathematical derivation of rate equation for WGS over Pt-Re/TiO<sub>2</sub> catalyst**

Based on the proposed reaction mechanism in this paper, three reaction sequences have been suggested.

**Path 1 (over TiO<sub>2</sub>):****Path 2 (over TiO<sub>2</sub>):****Path 3 (over ReO<sub>x</sub>):**

From the kinetic study, we found that, in the case of high CO and low CO<sub>2</sub> concentrations, the reaction orders were zero order in both CO and CO<sub>2</sub>, linear in H<sub>2</sub>O and (-0.5) in H<sub>2</sub> concentrations). In the other case (low CO and high CO<sub>2</sub> concentrations) only the reaction order of CO is influenced (increased to 0.4) however, no significant changes occur to the reaction order of the other gases. In the comparison between the experimental data and rate derived from modeling, we will consider the reaction orders of 0, 0, 1, and -0.5 for CO, CO<sub>2</sub>, H<sub>2</sub>O, and H<sub>2</sub>, respectively.

**B.1. If Path 1 is the dominant:****B.1.1. CO reaction with O<sub>(s)</sub> is r. d. s.:**



$$r_1 = k_1 \Phi_{\text{CO}} \theta_{\text{O}_s}$$

Where  $k_1$  is the forward rate constant,  $\Phi_{\text{CO}}$  is the coverage of CO, and  $\theta_{\text{O}_s}$  is the coverage of oxygen on  $\text{TiO}_2$  surface.

$$\text{Rate is zero order in CO} \rightarrow \Phi_{\text{CO}} = 1 \rightarrow r_1 = k_1 \theta_{\text{O}_s}$$

$$k_2 \theta_* p_{\text{H}_2\text{O}} - k_{-2} \theta_{\text{O}_s} p_{\text{H}_2} = 0$$

$\theta_{\text{O}_s} = K_2 \theta_* p_{\text{H}_2\text{O}} / p_{\text{H}_2}$ , where  $K_2$  is the equilibrium constant of dissociative adsorptions of  $\text{H}_2\text{O}$  in the vacant sites of  $\text{TiO}_2$  surface as  $\text{O}_{(s)}$  and  $\text{H}_{2(g)}$ .

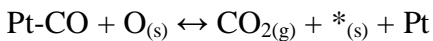
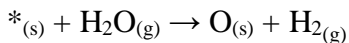
$$\theta_* + \theta_{\text{O}_s} = 1 \rightarrow \theta_* = 1 - \theta_{\text{O}_s}$$

$$\theta_{\text{O}_s} = K_2 (1 - \theta_{\text{O}_s}) p_{\text{H}_2\text{O}} / p_{\text{H}_2} \rightarrow \theta_{\text{O}_s} = K_2 p_{\text{H}_2\text{O}} / (p_{\text{H}_2} + K_2 p_{\text{H}_2\text{O}})$$

$$r_1 = k_1 \frac{K_2 p_{\text{H}_2\text{O}}}{p_{\text{H}_2} + K_2 p_{\text{H}_2\text{O}}}$$

If  $K_2 p_{\text{H}_2\text{O}} \gg p_{\text{H}_2} \rightarrow r_1 = \text{constant}$  (disagree with kinetic results). If  $p_{\text{H}_2} \gg K_2 p_{\text{H}_2\text{O}} \rightarrow r_1 = K_2 p_{\text{H}_2\text{O}} / p_{\text{H}_2}$  (-1 order in  $\text{H}_2$  concentrations, disagree with kinetic results) therefore, at this both extreme situation, the reaction of CO with  $\text{O}_s$  can not be r. d. s. It is not possible to look mathematically at intermediate situations from the current data.

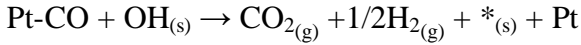
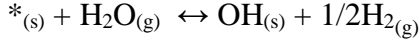
### B.1.2. If the reaction of $\text{H}_2\text{O}$ with $*_{(s)}$ is the r. d. s.



$$r_1 = k_1 \theta_* p_{\text{H}_2\text{O}}$$

$k_3 \Phi_{\text{CO}} \theta_{\text{O}_s} - k_{-3} p_{\text{CO}_2} \theta_* \Phi_* = 0 \rightarrow \theta_* \neq f(\text{H}_2)$ , where  $K_3$  is equilibrium reaction constant of the reaction of adsorbed CO on Pt with oxygen from  $\text{TiO}_2$  surface.

This means  $r_1 \neq f(\text{H}_2)$  and thus order zero in  $\text{H}_2$  (which is in disagreement with kinetic results)

**B.2. If Path 2 is the dominant:****B.2.1. If CO reaction with OH<sub>(s)</sub> (r. d. s.)**

$$r_1 = k_1 \Phi_{\text{CO}} \theta_{\text{OHs}}$$

$$\text{Rate is zero order in CO} \rightarrow \Phi_{\text{CO}} = 1 \rightarrow r_1 = k_1 \theta_{\text{OHs}}$$

$$k_4 \theta^* p_{\text{H}_2\text{O}} - k_{-4} \theta_{\text{OHs}} \sqrt{p_{\text{H}_2}} = 0$$

$\theta^* = \theta_{\text{OHs}} \sqrt{p_{\text{H}_2}} / K_4 p_{\text{H}_2\text{O}}$ , where  $K_4$  is the equilibrium constant of dissociative adsorptions of H<sub>2</sub>O to hydroxyls in the vacant sites of TiO<sub>2</sub> surface

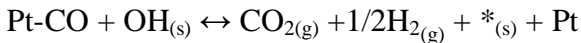
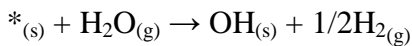
$$\theta^* + \theta_{\text{OHs}} = 1 \rightarrow \theta_{\text{OHs}} = 1 - \theta^* = 1 - \theta_{\text{OHs}} \sqrt{p_{\text{H}_2}} / K_4 p_{\text{H}_2\text{O}}$$

$$\theta_{\text{OHs}} = \frac{K_4 \frac{p_{\text{H}_2\text{O}}}{\sqrt{p_{\text{H}_2}}}}{1 + K_4 \frac{p_{\text{H}_2\text{O}}}{\sqrt{p_{\text{H}_2}}}}$$

$$r_1 = k_1 \frac{K_4 \frac{p_{\text{H}_2\text{O}}}{\sqrt{p_{\text{H}_2}}}}{1 + K_4 \frac{p_{\text{H}_2\text{O}}}{\sqrt{p_{\text{H}_2}}}}$$

$$\text{If } 1 \gg K_4 p_{\text{H}_2\text{O}} / \sqrt{p_{\text{H}_2}}, \text{ then } r_1 = k_1 K_4 \frac{p_{\text{H}_2\text{O}}}{\sqrt{p_{\text{H}_2}}}$$

*This rate is linear in H<sub>2</sub>O and -0.5 in H<sub>2</sub> concentration (in agreement with kinetic results)*

**B.2.2. If the H<sub>2</sub>O reaction with oxygen vacant site is the r. d. s.**

$$r_1 = k_1 \theta_* p_{\text{H}_2\text{O}}$$

$$k_5 \Phi_{\text{CO}} \theta_{\text{OHs}} - k_{-5} p_{\text{CO}_2} \sqrt{p_{\text{H}_2}} \theta_* = 0, \text{ where } \Phi_{\text{CO}}=1$$

$\theta_* = K_5 \theta_{\text{OHs}} / \sqrt{p_{\text{H}_2}} p_{\text{CO}_2}$ , where  $K_5$  is the equilibrium reaction constant of the reaction of adsorbed CO on Pt with OH groups from  $\text{TiO}_2$  surface.

$$\text{But: } \theta_* + \theta_{\text{OHs}} = 1 \rightarrow \theta_{\text{OHs}} = 1 - \theta_*$$

$$\theta_* = K_5 (1 - \theta_*) / \sqrt{p_{\text{H}_2}} p_{\text{CO}_2} \rightarrow \theta_* = K_5 / (1 + K_5 / \sqrt{p_{\text{H}_2}} p_{\text{CO}_2})$$

Then:

$$r_1 = k_1 K_5 p_{\text{H}_2\text{O}} / (1 + K_5 / \sqrt{p_{\text{H}_2}} p_{\text{CO}_2})$$

If  $1 \gg K_5 / \sqrt{p_{\text{H}_2}} p_{\text{CO}_2} \rightarrow r_1 = k_1 K_5 p_{\text{H}_2\text{O}}$  (disagree with kinetic data)

If  $1 \ll K_5 / \sqrt{p_{\text{H}_2}} p_{\text{CO}_2} \rightarrow r_1 = k_1 p_{\text{H}_2\text{O}} p_{\text{CO}_2} \sqrt{p_{\text{H}_2}}$  (this rate is linearly positive in  $\text{H}_2\text{O}$  and  $\text{CO}_2$ , and also positive (0.5) in  $\text{H}_2$ , which is also in disagreement with kinetic data)

### B.3. If Path 3 is the dominant

The rate derivation of this path is comparable with the results of path 1; however, the oxygen here is involved from  $\text{ReO}_x$  instead of  $\text{TiO}_2$ . Details are thus not repeated.

This path can be ruled out as a dominant reaction path since a separate kinetic study on Pt/ $\text{TiO}_2$  catalyst showed a -0.5 reaction order in  $\text{H}_2$ . In addition, in the case of Re-Pt/ $\text{TiO}_2$  the rate of  $\text{H}_2$  formation increases with 50 % only compared to the activity of Pt/ $\text{TiO}_2$ . Note that the number of Pt and Re atoms is of the same order. Thus the red-ox route via  $\text{ReO}_x$  does significantly contribute, but is still not the main pathway.

### B.4. Conclusion

From this modeling, path 2 seems to be the dominant path and the reaction of adsorbed CO (CO-Pt) with OH groups from  $\text{TiO}_2$  seems to be the rate determining. The rate equation, which is derived based on this assumption, matches with experimental kinetic data.

# Chapter 7

## Outlook and recommendations for future work

---

The research presented in this thesis has provided information about the development of efficient single-stage water gas shift (WGS) catalyst that shows promise for H<sub>2</sub> production in fuel cell applications. The information includes (i) the influence of catalyst support on WGS reaction sequences (reaction mechanism), selectivity, activity, and stability. (ii) Detailed deactivation mechanism of Pt/TiO<sub>2</sub> catalyst in WGS reaction. (iii) Development of the efficient WGS catalyst (Pt-Re/TiO<sub>2</sub>). (iv) Optimization, characterization, kinetic and mechanistic studies on Pt-Re/TiO<sub>2</sub> catalyst in WGS reaction.

### 7.1. Water Gas Shift reaction mechanism

The work described in this thesis (Chapter 2 [1]) revealed that the reaction mechanism for WGS is complex and strongly depends on the nature of the oxide support used. The two reaction mechanisms proposed in literature, *i.e.* red-ox and associative formate mechanisms, do not cover all possible WGS routes over Pt based catalysts. In this thesis, an associative formate route with a red-ox regeneration of the oxide support was suggested as an additional possibility. The difference between this and the conventional “associative formate route” is that the conversion of surface formate to H<sub>2</sub> and CO<sub>2</sub> occurs using oxygen from the support in the former while it is from water in the latter. Further, WGS follows the classical associative formate mechanism over Pt/CeO<sub>2</sub>; on the other hand, both classical red-ox and associative formate with red-ox regeneration are relevant for Pt/TiO<sub>2</sub>.

It is clear from all the proposed WGS mechanisms that the activation of H<sub>2</sub>O molecule is the key to understand the reaction sequence/mechanism. A thorough understanding of the way how H<sub>2</sub>O splits (activation) on the catalyst support to O<sub>s</sub>, OH<sub>s</sub>, or its direct activation with the intermediates (e.g. formate) formed on the catalyst surface during the reaction, will lead to a breakthrough in understanding the exact WGS reaction mechanism, thus helping development of more efficient catalysts. To achieve this, we recommend the following pulse characterization technique using D<sub>2</sub>O<sup>18</sup> and CO gases in which the outlet gases should be measured with Mass Spectrometer (MS) and Gas Chromatography (GC). It is essential that the choice of GC columns must allow quantification of H<sub>2</sub>, CO, and CO<sub>2</sub> gases. The principle of this technique is to clean first the active O<sub>s</sub> and OH<sub>s</sub> groups from the catalyst surface by pulsing CO gas at the reaction temperature (e.g. 300°C). When no CO is consumed any more by pulsing CO, the temperature can be raised (e.g. 400°C) in order to desorb CO from the Pt surface. In this case; the catalyst surface will be free of CO, contains no reactive hydroxyls, and has oxygen vacancies. Next, pulsing D<sub>2</sub>O<sup>18</sup> will give valuable information about the way of activation of H<sub>2</sub>O molecules on Pt based catalysts: (a) if no gas is formed, then D<sub>2</sub>O<sup>18</sup> is apparently activated on the catalyst as O<sup>18</sup>D (water activation via forming hydroxyls), (b) if only D<sub>2</sub> is formed and D<sub>2</sub> mass balance is close to 1, then water apparently splits to H<sub>2</sub>(g) and O<sub>s</sub> (classical red-ox route of H<sub>2</sub>O), (c) if only D<sub>2</sub> is formed and D<sub>2</sub> mass balance < 1, then water can be spiltted to H<sub>2</sub>(g), O<sub>s</sub>, and OH<sub>s</sub> over such a catalyst, (d) if DH is also formed in combination with D<sub>2</sub>, then possible D-H exchange between D<sub>2</sub>O<sup>18</sup> and OH or between DH and OH groups far from Pt active sites occur.

After completing the D<sub>2</sub>O<sup>18</sup> pulses, the oxygen vacancies of the catalysts surface are expected to be completely filled with O<sup>18</sup> and/or O<sup>18</sup>D, depending on the oxide supports of the catalysts used. The next CO pulses will conclude the different methods of H<sub>2</sub>O activation and the role of OH and/or oxygen diffusion from the surface or the bulk of the catalysts to Pt active sites. Different observations could lead to different conclusions: (a) if only CO<sup>16</sup>O<sup>18</sup> is produced and carbon mass balance is close to unity, then: (i) the catalyst split H<sub>2</sub>O molecules to H<sub>2</sub>(g) and O<sub>s</sub> (classical red-ox), (ii) the role of oxygen diffusion (from surface and/or bulk) to Pt active sites can be neglected as factor

influencing catalyst performance; (b) if  $\text{CO}^{16}\text{O}^{18}$  and  $\text{CO}^{16}\text{O}^{16}$  are produced (carbon mass balance close to 1), then: (i) the catalyst split  $\text{H}_2\text{O}$  molecules to  $\text{H}_2(\text{g})$  and  $\text{O}_s$  and (ii) oxygen diffusion (from surface and/or bulk) may play a role in catalyst performance. The ratio of the surface area from the MS peaks will indicate if diffusion effect is significant or not. (c) if  $\text{CO}^{16}\text{O}^{18}$  and  $\text{D}_2$  (and/or  $\text{DH}$ ) are produced in which carbon balance close to unity and  $\text{D}_2$  balance from both  $\text{CO}$  and  $\text{D}_2\text{O}^{18}$  pulses is also close to unity, then  $\text{H}_2\text{O}$  is activated via  $\text{OH}_s + 1/2\text{H}_2(\text{g})$ . (d) If no gases are formed or  $\text{CO}^{16}\text{O}^{18}$  and  $\text{D}_2$  are produced with carbon balance  $< 1$  and/or  $\text{D}_2$  balance  $< 1$ , then this is complex case and no solid conclusion can be drawn.

## 7.2. Development of an efficient catalyst for WGS

The nature of the oxide support has strong influence on the performance of Pt based catalysts in the WGS reaction. Besides the effect of the oxide supports on the WGS reaction routes (Chapter 2 [1]), supports also strongly influence activity and stability of Pt based catalysts (see Chapters 3 and 4 [2,3]). Among the catalysts studied in this work,  $\text{TiO}_2$  (Degussa P25, 40% rutile and 60% anatase) supporting Pt was the most active catalyst; however, it deactivated with time on stream. Pt/ $\text{TiO}_2$  deactivation was caused by loss of active surface Pt (sintering). This deactivation problem was overcome by adding second metal (Re) to Pt/ $\text{TiO}_2$ . The developed catalyst (Pt-Re/ $\text{TiO}_2$ ) in this work has excellent stability and even higher activity than monometallic Pt/ $\text{TiO}_2$ .

Crystallite phases of titanium (IV) oxide ( $\text{TiO}_2$ ) are known to have strong influence on the performance of  $\text{TiO}_2$ -based catalysts. Ding *et al.* [4] reported that the ratio of anatase to rutile has a strong effect on the photo catalytic activity in oxidation reaction of phenol. Recently, Iida and Igarashi [5] reported that Pt supported on  $\text{TiO}_2$  – Rutile (R) is more active than that of supported on  $\text{TiO}_2$  – Anatase (A) for WGS reaction. The reason of higher activity was claimed to be due to the higher Pt dispersion when it was supported on rutile titania. In order to check the influence of  $\text{TiO}_2$  phase and surface area, we have prepared and tested several Pt/ $\text{TiO}_2$  catalysts with different surface areas and different

titania phases, results are shown in Table 7.1. These catalysts were prepared using the same preparation procedure that is described in Chapter 3 [2].

Table 7.1: Influence of TiO<sub>2</sub> phase and surface area on Pt/tiO<sub>2</sub> catalyst intrinsic activity

| # | Catalyst – producer (phase)                    | S <sub>BET</sub><br>(m <sup>2</sup> /g) | H/Pt<br>(%) | Rate (μmol H <sub>2</sub> g <sup>-1</sup> <sub>cat</sub> s <sup>-1</sup> )<br>at 300°C | TOF<br>(s <sup>-1</sup> ) |
|---|--|---|-------------|--|---------------------------|
| 1 | 0.5Pt/TiO <sub>2</sub> - Ishihara Sangyo (A)   | 12                                      | 35          | 23   | 3                         |
| 2 | 0.5Pt/TiO <sub>2</sub> - Ishihara Sangyo (R)   | 1.5                                     | 15          | 2  | 0.5                       |
| 3 | 0.5Pt/TiO <sub>2</sub> – Degusa (A+R)          | 48                                      | 55          | 135  | 10                        |
| 4 | 0.5Pt/TiO <sub>2</sub> – Sachtleben chemie (A) | 117                                     | 45          | 97   | 8                         |

The results seem to indicate that both surface area and TiO<sub>2</sub> phases influence the intrinsic WGS activity over Pt/TiO<sub>2</sub>. The catalyst with a mixture of rutile and anatase (# 3) showed better performance than that of pure anatase phase (# 1 or 4) or pure rutile phase (# 2). Moreover, the catalyst with higher surface area, in case of pure anatase (# 4), showed more activity than that with lower surface area (#1). It is clear that the existence of both rutile and anatase is important for the higher activity of the catalyst; however, an optimization study for the exact ratio is essential. A detailed study on the influence of anatase to rutile ratio and catalyst surface area on the performance of Pt/TiO<sub>2</sub> catalyst is highly recommended.

### 7.3. Optimization of Pt-Re/TiO<sub>2</sub> catalyst

An optimization study on the preparation strategy, Pt/Re molar ratios, and Pt/Re metal contents on the performance of Pt-Re/TiO<sub>2</sub> in WGS reaction is discussed in Chapter 5 [6]. This study showed that impregnating Re precursor prior to Pt precursor without intermediate drying and calcination, using Pt/Re molar ratio of unity, and a 0.5wt% content of each metal give the best catalyst performance (activity and stability).

Both platinum and rhenium are expensive materials, so reducing the metals contents to less than 0.1wt % each and in combination with high performance of the catalyst (activity and stability) may result in a breakthrough in WGS reaction technology. Therefore, we

highly recommend more optimization research on the influence of starting precursor materials employed (Pt and Re precursors), preparation methods and conditions, pretreatment conditions (calcination and reduction), and the effect of chlorine contents on the degree of interaction between Pt and Re in order to enhance the activity of Pt-Re/TiO<sub>2</sub> catalyst. This optimization study in combination with the effect of rutile to anatase ratio recommended above may result in decreasing the contents of the active metals and still having an efficient catalyst activity for WGS.

#### **7.4. References**

- [1] K. G. Azzam, I. V. Babich, K. Seshan, L. Lefferts, *J. Catal.* 251 (2007) 153.
- [2] K. G. Azzam, I. V. Babich, K. Seshan, L. Lefferts, *J. Catal.* 251 (2007) 163.
- [3] K. G. Azzam, I. V. Babich, K. Seshan, L. Lefferts, *Appl. Catal. A*, 338 (2008) 66.
- [4] Z. Ding, G. Q. Lu, P. F. Greenfield, *J. Phys. Chem. B*, 104 (2000) 4815.
- [5] H. Iida, A. Igarashi, *Appl. Catal. A* 298 (2006) 152.
- [6] K. G. Azzam, I. V. Babich, K. Seshan, L. Lefferts, *Appl. Catal. B*, 80 (2008) 129.

# Acknowledgment

---

Appreciation is due to many people who have helped, often without knowing they were doing so, for inspiration, exhortation, and supports throughout the four years it has taken to create this work.

I am especially grateful to my promoter Leon Lefferts for hosting me in his group as an AIO. His supervision and continuous support stimulated tremendously in my research work. Through rewarding discussions with him, I have gained much more knowledge. His kind help in all aspects has made the past four years an ever-good memory in my life. I also deeply thank my mentor K. Seshan who guided me through the field of catalysis. His constant guidance and encouragement as well as many opportunities he gave me to practice have stimulated many of my interests and enabled me to gain more experience in research.

I am highly grateful to the promotion committee members who proofed this work.

I am very grateful to Igor Babich who works as postdoc in the project. Thanks Igor for the great inputs in this work. I will never forget your especial advice to me that I should be good in explaining (why) as well as finding (what).

I should not forget to thank the students who worked and take part in this work: Nuria, Angel, and Dennis.

I owe special thank to all my CPM colleagues and friends who met during the four years PhD. Leon, Seshan, Jan, Barbara, Lianne, Bert, Igor, Karin, Jeroen, Louise, Nabeel, Cristiano, Dejan, Sune, Berta, Gassia, Iris, Kumer, Vijay, Patrick, Hans, Davide, Sergio, Daryl, Kazu, Zhu, Jiang, Salim, Valer, and Locu: I would like to thank you all for the enjoyable time during work, coffee breaks, and weekly borrels.

I am very grateful to Sander van Bergen, Ralf Knibbeler, and Martin de Boer for their efforts in translating the summary of my thesis to Dutch language. Thank you all very much.

Personal thanks to all Arabic friends that I met during my PhD: Mousa Al-Tarazi, Ayser Oqlat, Khalid Al-Batyneh, Yahya Banat, Mohamad AboZahra, Mohamad Alhalaby, Ahmad Rawashdeh, Wael, Abdalla, salah, and Ziad.

Most importantly, special thanks to those dear ones whose input and contributions I can not even find suitable words to acknowledge: **my parents, my wife (Ola), my sisters, and my brothers** (*especially Nedhal who financially supported me during my bachelor and master studies*), for their continuous supports through the years. I would like to thank you all for the love, patients, and encouragements that enabled me to complete this work.

# Publications

---

## Articles

**Bifunctional catalysts for single-stage water–gas shift reaction in fuel cell applications. Part 1: Effect of the support on the reaction sequence.**

K. G. Azzam, I. Babich, K. Seshan, L. Lefferts

Journal of Catalysis 257 (2007) 153-162.

**A bifunctional catalyst for the single-stage water–gas shift reaction in fuel cell applications. Part 2: Roles of the support and promoter on catalyst activity and stability**

K. G. Azzam, I. Babich, K. Seshan, L. Lefferts

Journal of Catalysis 257 (2007) 163-171.

**Role of Re in Pt–Re/TiO<sub>2</sub> catalyst for water gas shift reaction: A mechanistic and kinetic study.**

K. G. Azzam, I. Babich, K. Seshan, L. Lefferts

Applied Catalysis B: 80 (2008) 129-140.

**Single stage Water Gas Shift conversion over Pt/TiO<sub>2</sub> - Problem of catalyst deactivation.**

K. G. Azzam, I. Babich, K. Seshan, L. Lefferts

Applied Catalysis A 338 (2008) 66-71.

**Precipitation of CuS and ZnS in a bubble column reactor.**

K. Azzam, M. O. Azzam, M. Al-Tarazi, A. Heesink, G. Versteeg.

AICHE Journal, vol. 51. no. 1, p. 235 (2005).

**Single stage Water Gas Shift conversion over Pt-Re/TiO<sub>2</sub> – Optimization and characterization.**

K. G. Azzam, I. Babich, K. Seshan, L. Lefferts

In preperation.

**Oral presentations**

**Development of Active, Selective and Stable Catalyst for Water-Gas-Shift Reaction.**

K. Azzam, I.V. Babich, K. Seshan, L. Lefferts

6<sup>th</sup> Netherlands' Catalysis and Chemistry Conference (NCCC VII), Noordwijkerhout, The Netherlands, March 6, 2006.

**Development of Active, Selective and Stable Catalyst for Water-Gas-Shift Reaction.**

K. Azzam, I.V. Babich, K. Seshan, L. Lefferts

American Chemical Society Meeting & Exposition (ACS), Atlanta, GA, USA, March 26, 2006.

**Water-Gas-Shift Reaction: Role of the Support in the Reaction Pathways.**

K. Azzam, I.V. Babich, K. Seshan, L. Lefferts

7<sup>th</sup> Netherlands' Catalysis and Chemistry Conference (NCCC VIII), Noordwijkerhout, The Netherlands, March 5, 2007.

**Efficient Bi-Functional Catalysts for Single Stage Water Gas Shift Conversion.**

K. Azzam, I.V. Babich, K. Seshan, L. Lefferts

8<sup>th</sup> Natural Gas Conversion Symposium (8<sup>th</sup> NGCS), Natal, Brazil May 27, 2007.

**Single Stage Bi-metallic Water Gas Shift Conversion Catalysts for Fuel Cell Applications**

K. Azzam, I.V. Babich, K. Seshan, L. Lefferts

American Chemical Society Meeting & Exposition (235<sup>th</sup> ACS), New Orleans, USA, April 6, 2008.

**Efficient Bi-functional Catalyst for Single Stage Water Gas Shift Conversion for Fuel Cell Applications**

K. Azzam, I.V. Babich, K. Seshan, L. Lefferts

International Conference on Communications (ICC 2008), Beijing, China, accepted- May 19, 2008.

**Poster presentations**

**Efficient Bi-functional Catalyst for Single Stage Water Gas Shift Conversion for Fuel Cell Applications.**

K. Azzam, I.V. Babich, K. Seshan, L. Lefferts

20<sup>th</sup> North American Catalysis Society (20<sup>th</sup> NACS), Houston, Tx, USA, June 17, 2007.

**Efficient Bi-functional Catalyst for Single Stage Water Gas Shift Conversion for Fuel Cell Applications.**

K. Azzam, I.V. Babich, K. Seshan, L. Lefferts

Europacat VIII, Turko/Abo, Finland, August 26, 2007.



ISBN 978-90-365-2644-9



9 789036 526449